

Electronic Theses and Dissertations, 2004-2019

2008

Finite Element Modeling Of Tides And Currents Of The Pascagoula River

Qing Wang
University of Central Florida

 Part of the [Civil Engineering Commons](#)
Find similar works at: <https://stars.library.ucf.edu/etd>
University of Central Florida Libraries <http://library.ucf.edu>

This Masters Thesis (Open Access) is brought to you for free and open access by STARS. It has been accepted for inclusion in Electronic Theses and Dissertations, 2004-2019 by an authorized administrator of STARS. For more information, please contact STARS@ucf.edu.

STARS Citation

Wang, Qing, "Finite Element Modeling Of Tides And Currents Of The Pascagoula River" (2008). *Electronic Theses and Dissertations, 2004-2019*. 3477.
<https://stars.library.ucf.edu/etd/3477>

FINITE ELEMENT MODELING OF TIDES AND CURRENTS
OF THE PASCAGOULA RIVER

by

QING WANG

B.S. Hohai University, 2003

M.S. Delft University of Technology, 2006

A thesis submitted in partial fulfillment of the requirements
for the degree of Master of Science
in the Department of Civil, Environmental and Construction Engineering
in the College of Engineering and Computer Science
at the University of Central Florida
Orlando, Florida

Summer Term
2008

© 2008 Qing Wang

ABSTRACT

This thesis focuses on the simulation of astronomic tides of the Pascagoula River. The work is comprised of five steps: 1) Production of a digital elevation model describing the entire Pascagoula River system; 2) Development of an inlet-based, unstructured mesh for inbank flow to better understand the basis of the hydrodynamics within the Pascagoula riverine system. In order to assist in the mesh development, a toolbox was constructed to implement one-dimensional river cross sections into the two-dimensional model; 3) Implementation of a sensitivity analysis of the Pascagoula River two inlet system to examine the inlet effects on tidal propagation; 4) Improvement of the inlet-based model by performing a preliminary assessment of a spatially varied bottom friction; 5) Implementation of an advection analysis to reveal its influence on the flow velocity and water elevation within the domain.

The hydrodynamic model employed for calculating tides is ADCIRC-2DDI (ADvanced CIRCulation Model for Shelves, Coasts and Estuaries, Two-Dimensional Depth Integrated). This finite element based model solves the shallow water equations in their full nonlinear form. Boundary conditions including water surface elevation at the off-shore boundary and tidal potential terms allow the full simulation of astronomic tides.

The improved astronomic tide model showed strong agreement with the historical data at seven water level monitoring gauge stations. The main conclusions of this research are: 1) The western

inlet of the Pascagoula River is more dominant than the eastern inlet; however, it is necessary to include both inlets in the model. 2) Although advection plays a significant role in velocity simulation, water elevations are insensitive to advection. 3) The astronomic model is sensitive to bottom friction (both global and spatial variations); therefore, a spatially varied bottom friction coefficient is suggested. As a result of this successful effort to produce an astronomic tide model of the Pascagoula River, a comprehensive storm surge model can be developed. With the addition of inundation areas the surge model can be expected to accurately predict storm tides generated by hurricanes along the Gulf Coast.

ACKNOWLEDGMENTS

This thesis is the result of my two-year study in the Coastal Hydroscience Analysis, Modeling & Predictive Simulations (CHAMPS) Lab in University of Central Florida whereby I have been accompanied and supported by many people. It is my pleasure that I now have the opportunity to express my gratitude for all of them. First and foremost I wish to thank my advisor, Dr. Scott C. Hagen, for offering me the opportunity to pursue graduate work under his guidance and supporting me throughout my study with his patience and knowledge. I would also like to thank Drs. Manoj Chopra and Gour-Tsyh Yeh for agreeing to serve on my committee; my lab mate, Naeko Takahashi, for working very closely with me on the Pascagoula River project and providing me the joyfulness of our teamwork. I have really enjoyed working with them and their efforts to this study helped me tremendously to achieve my goal.

Further, I would like to show my appreciation to all the members in CHAMPS lab. Thanks to all of them for encouragement and assistance to me during my program of study. Besides Naeko, Pete Bacopoulos is always ready to help me and Naeko solve most of the technical problems we met (especially his contribution in developing the Toolbox); Stephen Medeiros helped me correct grammar mistakes in my thesis very carefully and he suggested insightful improvements as well; other current lab members David Coggin, Derek Giardino, Alfredo Ruiz, Hitoshi Tamura are all very nice persons and I do enjoy the communication with them; former lab members Yuji

Funakoshi, Michael Parrish have been generous with their time and insights to give me valuable advices. It is indeed not sufficient to express my gratitude with only a few words.

Moreover, I would like to thank Mr. David Welch, Mr. Dave Reed and Mr. Dave Ramirez in Lower Mississippi River Forecast Center for their hospitality during our visit to LMRFC and collecting and compiling the cross section data for this project efficiently and professionally. Their corporation made my work much easier.

Last but not least, none of this would have been possible without the love and patience from my family; my friends in UCF also have brought the colorfulness to my memory.

This research was funded in part by award NA04NWS4620013 from the National Oceanic and Atmospheric Administration (NOAA), U.S. Department of Commerce. The statements, findings, conclusions and recommendations are those of the author and do not necessarily reflect those of the NOAA, the Department of Commerce and its affiliates.

TABLE OF CONTENTS

| | |
|---|-----|
| LIST OF FIGURES | ix |
| LIST OF TABLES | xiv |
| LIST OF ABBREVIATIONS..... | xv |
| CHAPTER 1. INTRODUCTION..... | 1 |
| 1.1 Description of the Study Area..... | 1 |
| 1.2 Research Objectives..... | 5 |
| CHAPTER 2. LITERATURE REVIEW | 8 |
| 2.1 Tides and Tidal Analysis | 8 |
| 2.2 Numerical Modeling of Tides..... | 13 |
| 2.3 Numerical Modeling in Estuarine Study..... | 17 |
| 2.4 Previous Modeling Studies for the Pascagoula River..... | 20 |
| CHAPTER 3. NUMERICAL MODEL DESCRIPTIONS | 22 |
| 3.1 ADCIRC Model Background | 22 |
| 3.2 Governing Equations | 23 |
| 3.3 Bottom Friction in ADCIRC..... | 28 |
| 3.4 Possible Error Sources | 31 |
| CHAPTER 4. PRELIMINARY ASTRONOMIC TIDE MODEL DEVELOPMENT FOR THE PASCAGOULA RIVER..... | 33 |
| 4.1 Preliminary Mesh Generation..... | 33 |
| 4.2 Mesh Adaptation and Variation..... | 43 |

| | |
|---|-----|
| 4.3 Model Setup | 48 |
| 4.4 Preliminary Model Results | 51 |
| 4.5 Model Domain Verification | 58 |
| CHAPTER 5. BATHYMETRY IMPROVEMENTS TO THE ASTRONOMIC TIDE MODEL FOR THE PASCAGOULA RIVER | 62 |
| 5.1 Description of Bathymetry Data | 63 |
| 5.2 Cross Section Interpolation Toolbox | 68 |
| 5.3 Cross Section Interpolation Toolbox Applications on the Pascagoula River | 80 |
| 5.4 Model Setup and Results | 83 |
| CHAPTER 6. MODEL SENSITIVITY ANALYSES | 89 |
| 6.1 A Preliminary Sensitivity Analysis on Bottom Friction | 89 |
| 6.2 Advection Effect on Velocity Residuals and Tidal Elevation | 97 |
| CHAPTER 7. CONCLUSIONS AND FUTURE WORK | 103 |
| 7.1 Conclusions | 103 |
| 7.2 Future Work | 105 |
| APPENDIX A. ADCIRC-2DDI INPUT FILE: MESH DESCRIPTION (Bathymetry Improved Model) | 107 |
| APPENDIX B. ADCIRC-2DDI INPUT FILE: MODEL PARAMETER | 109 |
| APPENDIX C. TIDAL CONSTITUENTS FOR HARMONIC ANALYSIS | 113 |
| APPENDIX D. CROSS SECTION INTERPOLATION TOOLBOX (FORTRAN CODE) | 118 |
| REFERENCES | 123 |

LIST OF FIGURES

| | |
|--|----|
| Figure 1.1 Map of the Pascagoula River drainage basin (The area of study is shown in the red box) (Mossa and Coley, 2004)..... | 2 |
| Figure 1.2 Map of the area of study: the lower Pascagoula River, and its principal tributaries including Black Creek, Red Creek, Escatawpa River and Big Creek. | 3 |
| Figure 2.1 The Moon's gravity differential field at the surface of the earth. | 8 |
| Figure 2.2: (a) Conditions for spring tides at new and full moon (syzygy). (b) Conditions for neap tides at quarter moons (also called lunar quadrature) (Pugh, 2004)..... | 9 |
| Figure 2.3 The unstructured, 53K finite element mesh for the WNAT model domain..... | 17 |
| Figure 3.1 Variation in C_f with bathymetric depth for various values of H-Break, $C_{fmin} = 0.0025$, $\theta = 10$ and $\lambda = 1/3$. (Murray, 2003)..... | 30 |
| Figure 4.1 Mesh Generation Step 1 & 2 - digitized boundary and 2D mesh: (a) (b) Pascagoula River with erosion and deposition areas; (c) (d) Heavily forested reach in Big Creek, showing the minimum element size. | 36 |
| Figure 4.2 Mesh Generation Step 1 & 2 - digitized boundary and 2D mesh: (a) (b) Pascagoula River near Poticaw Landing, splitting into East Pascagoula River and West Pascagoula River; (c) (d) East Pascagoula River Inlet (The Port of Pascagoula)..... | 37 |

| | |
|--|----|
| Figure 4.3 SL15 mesh (FEMA Southern Louisiana Gulf Coast Mesh) zoom into the Pascagoula River region (boundary showed in red). | 38 |
| Figure 4.4 Mesh Comparison at the East Pascagoula River inlet (Left) and Cumbest Bluff, MS (Right): (a) SL15 mesh; (b) the preliminary comprehensive Pascagoula River mesh; (c) the location within the Pascagoula River model; (d) mesh bathymetry interpolated from the SL15. 40 | |
| Figure 4.5 The comprehensive Pascagoula River mesh displayed on Google Earth (Version 4.3) | 41 |
| Figure 4.6 The preliminary comprehensive Pascagoula River mesh with 136,676 computational points and 211,312 triangular elements. | 42 |
| Figure 4.7 Mesh adaptation of the comprehensive Pascagoula River inlet-based mesh | 44 |
| Figure 4.8 Zoom into the marsh area located near the Pascagoula inlets | 46 |
| Figure 4.9 Variations of the Pascagoula River inlet-based meshes | 47 |
| Figure 4.10 Open boundary assignment (Left: 53K WNAT model; Right: Open water boundary of the inlet-based Pascagoula River models) | 49 |
| Figure 4.11 The historical gauge stations within the Pascagoula River model domain | 52 |
| Figure 4.12 Resyntheses of historical and model tidal constituents, corresponding to the stations located at Pascagoula, MS and Pascagoula Point, Mississippi Sound, MS. | 54 |
| Figure 4.13 Resyntheses of historical and model tidal constituents, corresponding to the stations located at West Pascagoula at Gautier, MS and Pascagoula River Mile 1, MS. | 55 |
| Figure 4.14 Resyntheses of historical and model tidal constituents, corresponding to the stations at Pascagoula River at Cumbest Bluff and Graham Ferry, MS. | 56 |

| | |
|--|----|
| Figure 4.15 Resyntheses of historical and model tidal constituents, corresponding to the station located at Escatawpa River at I-10 near Orange Grove, MS..... | 57 |
| Figure 4.16 Finite element mesh of the WNAT + Pascagoula model, compared to the Original 53K WNAT model domain..... | 59 |
| Figure 4.17 Tidal resynthesis analysis plots at two Pascagoula stations, comparing the WNAT + Pascagoula model and the Model A..... | 60 |
| Figure 4.18 Tidal resynthesis analysis plots at two Pascagoula stations, comparing the WNAT + Pascagoula model and the Model A..... | 61 |
| | |
| Figure 5.1 Cross section comparison between USGS survey data and Mobile hydrographic survey at East Pascagoula River and Lower Escatawpa River..... | 66 |
| Figure 5.2 Bathymetric data coverage of USGS Survey and Mobile Hydrographic Survey | 67 |
| Figure 5.3 Triangulation and the ineffective interpolation in SMS..... | 69 |
| Figure 5.4 Triangulation and correct interpolation in SMS using the Cross Section Interpolation Toolbox..... | 69 |
| Figure 5.5 Cross Section Interpolation Toolbox Workflow | 72 |
| Figure 5.6 The steps executed by the Toolbox code - An example of simple river reach bathymetry interpolation..... | 74 |
| Figure 5.7 A river reach in the Loxahatchee River..... | 75 |
| Figure 5.8 Two cross sections for one river reach (A: upstream, B: downstream) | 75 |
| Figure 5.9 The methodology of the Cross Section Interpolation Toolbox applied to an example channel in the Loxahatchee River, FL. | 77 |

| | |
|--|----|
| Figure 5.10 Demonstration of bathymetric point adjustment when two cross sections have different numbers of bathymetric points (Original points in diamond shape; modified points in cross shape)..... | 79 |
| Figure 5.11 Plots of model bathymetry in lower Pascagoula River region (Left: bathymetry from the preliminary model; Right: Updated bathymetry)..... | 81 |
| Figure 5.12 An example of the Toolbox application on West Pascagoula River: (a) Reach location; (b) Surveyed cross sections and cross sections applied to model; (c) Bathymetry before update; (d) Bathymetry after update. | 82 |
| Figure 5.13 Resynthesis of historical and two models' tidal constituents, corresponding to the stations at Pascagoula, MS and Pascagoula Point, Mississippi Sound, MS | 85 |
| Figure 5.14 Resynthesis of historical and two models' tidal constituents, corresponding to the stations at West Pascagoula at Gautier, MS and Pascagoula River Mile 1, MS..... | 86 |
| Figure 5.15 Resynthesis of historical and two models' tidal constituents, corresponding to the stations at Pascagoula River at Cumbest Bluff and Graham Ferry, MS..... | 87 |
| Figure 5.16 Resynthesis of historical and two models' tidal constituents, corresponding to the station at Escatawpa River at I-10 near Orange Grove, MS | 88 |
| | |
| Figure 6.1 Division of sub-domains: applying spatially varied C_{fmin} on the Pascagoula River model. (a) Domain Division 1, (b) Domain Division 2. | 92 |
| Figure 6.2 Tidal resynthesis analysis plots at upstream station-Graham Ferry, comparing C_{fmin} equals 0.0025 and 0.0040. Higher value 0.0040 fits better with historical record. | 94 |

Figure 6.3 Computed velocity residuals at the Pascagoula River inlets: (a) (b) vector and magnitude plots (advection enabled), (c) (d) vector and magnitude plots (advection disabled) .. 99

Figure 6.4 Computed velocity residuals at the Escatawpa River near the Beardslee Lake and Roberson Lake: (a) (b) vector and magnitude plots (advection enabled), (c) (d) vector and magnitude plots (advection disabled) 100

Figure 6.5 Tidal resynthesis plots at selected stations, comparing advection enabled and disabled 101

Figure 6.6 Tidal resynthesis plots at randomly selected locations, comparing advection enabled and disabled 102

LIST OF TABLES

| | |
|--|-----|
| Table 2.1 Some principal tidal constituents (Wright, 2000)..... | 12 |
| Table 4.1 Summary of the streams in the comprehensive Pascagoula River mesh..... | 34 |
| Table 4.2 Tidal Constituents used to force the ADCIRC model | 49 |
| Table 5.1 Summary of the Pascagoula River bathymetric data sets..... | 63 |
| Table 5.2 The format of Cross Section Interpolation Toolbox input files..... | 76 |
| Table 6.1 Summary of the assigned spatially-varying C_{fmin} | 92 |
| Table 6.2 RMS errors associated with model sensitivity analyses on uniform minimum bottom friction factor, C_{fmin} | 96 |
| Table 6.3 RMS errors associated with model sensitivity analyses on spatially varied minimum bottom friction factor, C_{fmin} | 96 |
| Table C.1 23 tidal constituents applied in ADCIRC harmonic analysis..... | 114 |
| Table C.2 37 tidal constituents used in the resynthesis of the historical tidal records for the NOS stations. | 115 |
| Table C.3 35 tidal constituents at the USGS stations extracted by T_TIDE | 117 |

LIST OF ABBREVIATIONS

| | |
|-------------|--|
| 1D | One Dimensional |
| 2D | Two Dimensional |
| ADCIRC-2DDI | Advanced Circulation Model for Oceanic, Coastal, and Estuarine Waters (Two-Dimensional, Depth-Integrated Option) |
| ATC | Average Tidal Cycle |
| CPP | Carte Parallelogrammatique Project |
| DEM | Digital Elevation Model |
| FEMA | Federal Emergency Management Agency |
| GIS | Geographic Information System |
| GPS | Global Positioning System |
| GWCE | Generalized Wave Continuity Equation |
| LMRFC | Lower Mississippi River Forecast Center |
| NAVD 88 | North American Vertical Datum of 1988 |
| NOS | National Ocean Service |
| RMS | Root Mean Square |
| ROMS | Regional Ocean Modeling System |
| SMS | Surface-water Modeling System |
| USGS | United States Geological Survey |

CHAPTER 1. INTRODUCTION

1.1 Description of the Study Area

The Pascagoula River basin encompasses most of southeastern Mississippi and a small part of southwestern Alabama, draining an area of approximately 9,700 square miles (Oldham and Rushing, 1970). As Mississippi's second largest basin, the Pascagoula River basin has an elliptical shape with a maximum length of 164 miles and a maximum width of 84 miles. The Pascagoula River itself is located in the lower Pascagoula River basin. It is formed by its two confluences: the Leaf River and the Chickasawhay River. From the confluence, the Pascagoula River flows southward for about 80 miles before emptying into the Gulf of Mexico through the Pascagoula Inlet.

The study area for this thesis covers the Pascagoula River below Merrill (in George County, MS, the junction of the Leaf and Chickasawhay Rivers), and four principal tributaries within the lower Pascagoula River basin: Black Creek, Red Creek, Escatawpa River and Big Creek. The normal water surface of the Pascagoula River ranges from sea level to about 85 feet above (0 to 26 meters), producing an average fall of 0.4 feet per mile in the lower basin (U.S. Army Corps of Engineers, 1968). The topography of the Pascagoula basin is generally rolling to hilly with low to moderate relief. Near the coast, there are low-lying flatlands and marshlands. At about 17 river miles from the mouth, the Pascagoula River splits into the East Pascagoula River and the West

Pascagoula River, both of which meander through the marshlands and eventually flow into the ocean, only three miles apart.

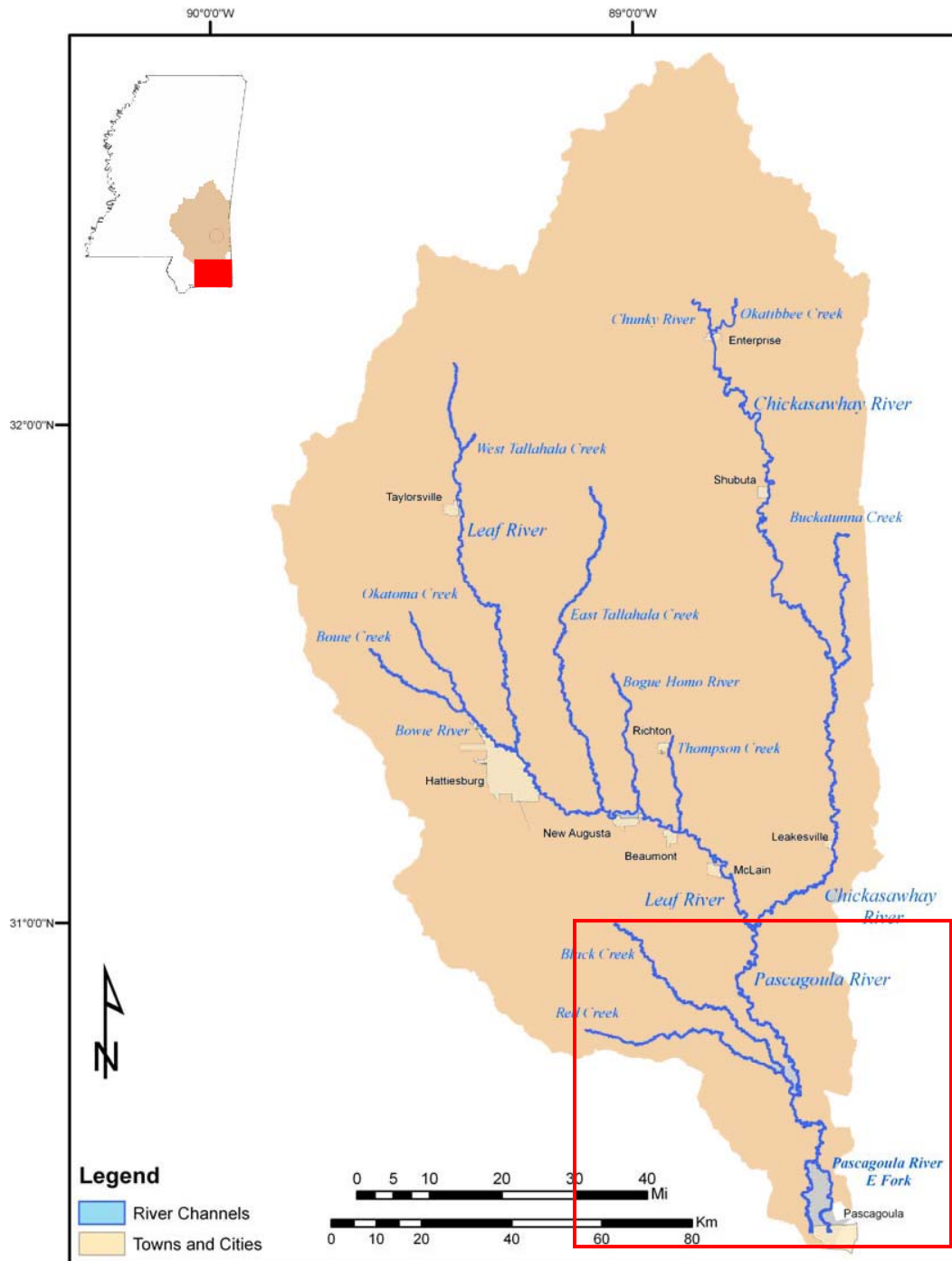


Figure 1.1 Map of the Pascagoula River drainage basin (The area of study is shown in the red box) (Mossa and Coley, 2004)

Figure 1.1 – 1.2 displays the area of study – the Pascagoula River and its main tributaries, as well as its location within the entire Pascagoula River drainage basin.



Figure 1.2 Map of the area of study: the lower Pascagoula River, and its principal tributaries including Black Creek, Red Creek, Escatawpa River and Big Creek.

As a part of the national comprehensive river basin planning program, the US Army Corps of Engineers developed a basin study of the Pascagoula River in the 1970s (U.S. Army Corps of Engineers, 1968). Several important stream characteristics were defined within that study: First, the streams of the Pascagoula River and its tributaries start with relatively steep slopes and narrow valleys in the hilly region upstream, and then develop into the more moderate streams further downstream. Such drainage characteristics are typical in the rivers of the southern United States. Second, the Pascagoula River main channel is relative flat and influenced by tides to some extent. The study indicates that tidal effects during low water are felt upstream from the mouth for a distance of about 42 miles, which is two miles downstream from the confluence point of the Black Creek and the Red Creek. Third, the width of the stream varies from wide to narrow and then expands to wide again as the river flows from Merrill to the inlets.

Although the Pascagoula River region has maintained its rural nature over the years, human activities have gradually altered the natural drainage system. In particular, the Pascagoula Port Project has significantly impacted the region. In the 1830's, the East Pascagoula River inlet was dredged to begin the Port of Pascagoula. Then, from 1913 to 1965, the Pascagoula Port Project built a dredging channel system from Mobile Bay to the lower Escatawpa River. The project included: an entrance channel from the Gulf of Mexico through Horn Island Pass; a channel in Mississippi Sound and Pascagoula River to the railroad bridge at Pascagoula; a channel from the railroad bridge to the Escatawpa River at the Highway 613 bridge; and an extended channel from the Highway 613 bridge, via Robertson and Bounds Lakes, to mile 6 on the Escatawpa River (Pascagoula Harbor, 1997). Currently, the Pascagoula River west harbor has a 38-foot deep

channel and a 940 feet wide turning basin (The Port of Pascagoula, 2008). Recently, an intention to widen and deepen these existing channels has been highlighted by the federal government due to the need for economic development and the environmental impacts (Department of the Army; U.S. Army Corps of Engineers, 2007).

1.2 Research Objectives

The Pascagoula River basin, the second largest in Mississippi, plays an important role in the region's water resource management. Accurate forecasts of the river flows and floods are required due to the development of this area. The Lower Mississippi River Forecast Center (LMRFC), as the regional forecast center located in Slidell, Louisiana, collects, processes, and provides water resource information and forecasts for the Pascagoula River. Currently, its forecasting area covers from the upstream Pascagoula basin to Graham Ferry (about 34.5 river miles to the mouth). However, there is no tidal station in the lower Pascagoula River area, even though occasional high water levels or small floods have been reported.

According to the situation and demand, the University of Central Florida is cooperating with the Hydrology Laboratory of the National Weather Service Office of Hydrologic Development and the LMRFC to implement a two-dimensional storm tide model on the lower Pascagoula River. The astronomical and meteorological tides are computed by the ADCIRC-2DDI (Advanced Circulation Two Dimensional DePTH Integrated) hydrodynamic circulation model. This finite element based model solves the shallow water equations in their full nonlinear forms. In addition, dynamic wind fields for a given hurricane or storm event (e.g. Hurricane Katrina) are converted

to spatially variable and time-independent wind surface stresses. They are then incorporated into the ADCIRC-2DDI model along with atmospheric pressure variations to permit the simulation of a storm tide. Eventually, an operational ADCIRC-2DDI storm tide model of the Pascagoula River will be built for the LMRFC to provide stage and flow forecasts, as well as to address some water quality issues. Simultaneously, the LMRFC is working on developing a one-dimensional HEC-RAS model for the Pascagoula River in order to provide forecasts of stages and flows.

The major objectives of the overall research are: 1) To develop a basis model by incorporating the Pascagoula River into an existing Western North Atlantic Tidal (WNAT) modeling domain, such that astronomic tides and storm surge can be accurately modeled. 2) To develop a continental shelf-based model for the Pascagoula River that will produce results comparable to the large-scale domain from Objective 1).

This thesis serves as the first report of this project, mainly focusing on the astronomical and meteorological tides simulation and the preliminary ADCIRC model development. As a result, six accomplished tasks are presented: 1) An inlet-based comprehensive mesh model for inbank flow has been produced. 2) A sensitivity analysis based on the inlet-based model is performed to examine the effect of the western inlet and eastern inlet of Pascagoula River. 3) A sensitivity analysis on advection is applied to investigate its influence on the flow velocity and water elevation within the domain. 4) The inlet-based mesh is incorporated into the existing unstructured, finite element mesh for the WNAT (Western North Atlantic Tidal) model domain.

5) A cross section toolbox is developed in order to update the channel bathymetry. 6) Model calibration follows with adjustments in bottom friction parameterization.

The thesis is presented as follows: First, a literature review of tides and their numerical modeling is given in Chapter 2. Second, the theory description of the numerical codes ADCIRC-2DDI is provided in Chapter 3. Third, Chapter 4 discusses the preliminary model development of the Pascagoula River, as well as the model results. Chapter 5 presents an improved astronomic tides model, whose bathymetry has been updated by the Cross Section Interpolation Toolbox. In Chapter 6, the improved astronomic tides model is further examined by model sensitivity analyses on bottom friction and advection effects. Finally, the conclusions and some suggested future work are discussed in Chapter 7.

CHAPTER 2. LITERATURE REVIEW

2.1 Tides and Tidal Analysis

Tides are defined as the regular rising and falling of the ocean surface, due to the gravitational attractions of the Moon and the Sun (Darwin, 1911). The primary mechanism of the tides can be explained by the physics of their generating force. Figure 2.1 shows a simplified model of the Moon's gravity differential field at the surface of the earth: On the side of the Earth nearest the Moon, the water is pulled towards the Moon more than the solid Earth. Similarly, the water is left behind more than the solid Earth on the side of the Earth furthest from the Moon. As a result, two tidal water bulges are produced for each rotation of the Earth, which also means that a given point on the Earth surface will experience two high and two low tides for each Earth's daily rotation (Hartel, 2000). However, local tidal pattern varies and it is significantly influenced by the Earth's land distribution (Kapoulitsas, 1985).

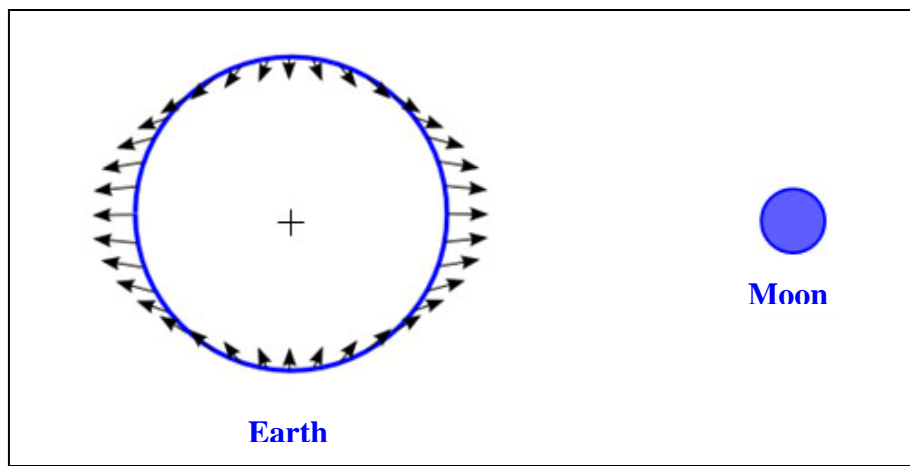


Figure 2.1 The Moon's gravity differential field at the surface of the earth.

In the sun-earth system, although the gravitational attraction of the sun is not as significant as the one of the moon, it can still cause the tidal range variations known as springs and neaps. When the moon is at the first or third quarter, the forces from the moon and the sun are partially cancelled by each other producing a low tide called neap tide. When the moon is at the new and full moon (known as syzygy), the fields from the sun and the moon are combined and a spring tide occurs (Figure 2.2). The height ratio of spring to neap tides is about 2.7:1 (Hicks, 2006; Griffin, 2008).

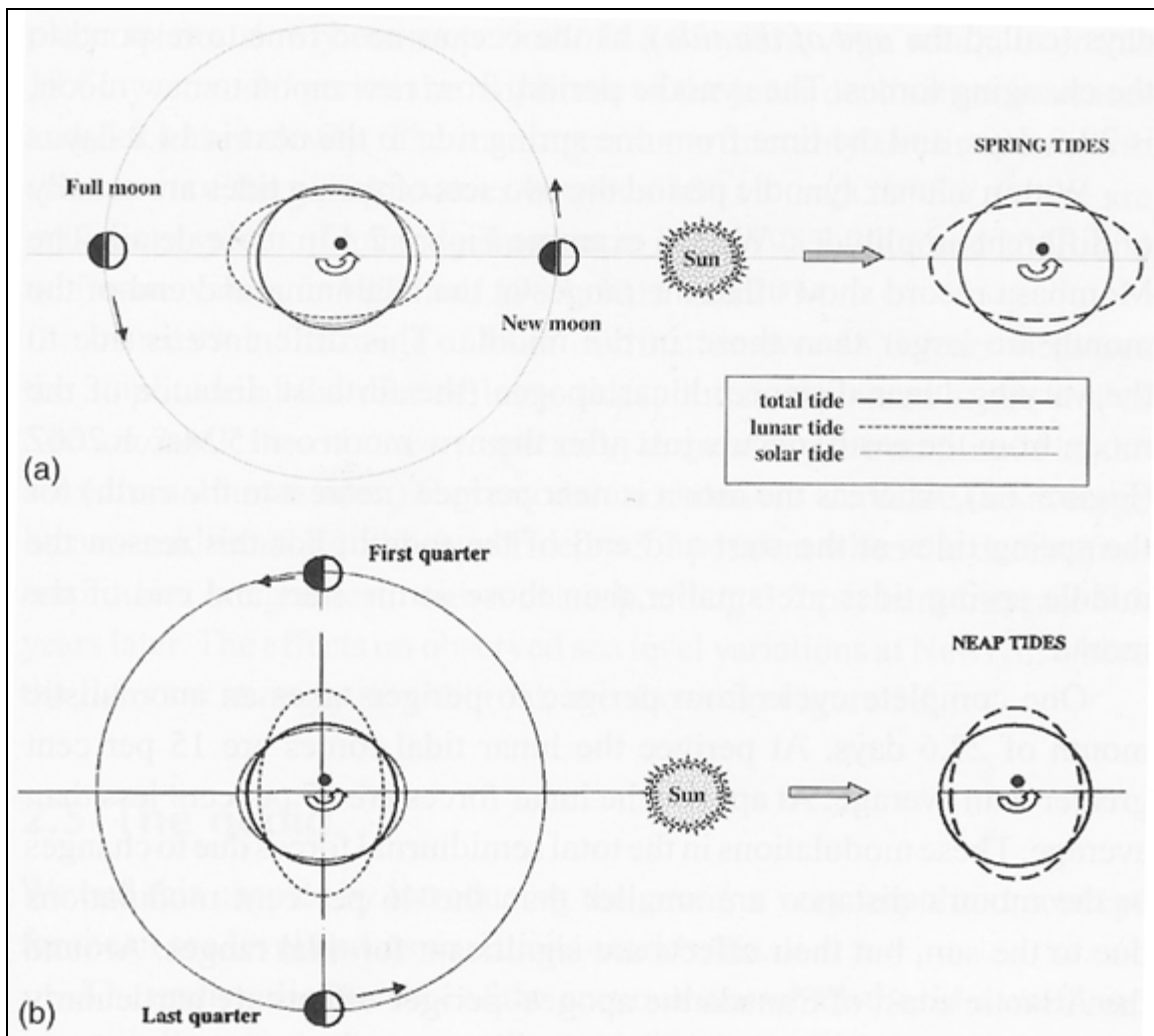


Figure 2.2: (a) Conditions for spring tides at new and full moon (syzygy). (b) Conditions for neap tides at quarter moons (also called lunar quadrature) (Pugh, 2004).

The tidal analysis begins by extracting tidal information from sea level records, understanding that tides can be defined as periodic movements that directly correspond to amplitude and phase of some periodic geophysical force. One of the most common methods for tidal analysis is the harmonic analysis method. The purpose of harmonic analysis is to determine the amplitude and phase of the individual cosine curves (or called partial tides), each representing a tidal constituent identified by its period in mean solar hours or, alternately, its speed in degrees per mean solar hour (speed = $360^\circ/T$ where T = period). The basis of harmonic analysis is the assumption that tidal variations can be represented by a number of harmonic terms of the form (Cartwright and Taylor, 1971):

$$H_n \cos(\omega_n t - g_n) \dots\dots\dots (2.1)$$

where n = component index; H_n = component amplitude; ω_n = component angular speed = $2\pi/T_n$; T_n = component period; g_n = component phase lag relative to some defined time zero (commonly taken as the phase lag on the equilibrium tide phase at the Prime Meridian, in which case it is called G_n); t = time.

Finding the tidal harmonic constants at one location allows one to predict tides at that location. Given the general form of Equation (2.1), an application of harmonic analysis is to select proper harmonic constituents to fit sea level observations. A more applicable tidal function $T(t)$ is used to fit the sea level records:

$$T(t) = Z_0 + \sum_N H_n f_n \cos[\omega_n t - g_n + (V_n + u_n)] \dots\dots\dots (2.2)$$

where the unknown parameters are Z_0 and the series of tidal constituent amplitudes and phases (H_n, g_n). Z_0 is included here as a variable to be fitted in the analysis, but it commonly represents local mean sea level (MSL) and is therefore a known parameter. The nodal adjustment factors are given as f_n and u_n and the terms $\omega_n t$ and V_n together determine the phase angle of the equilibrium tidal constituent. V_n is the equilibrium phase angle for the tidal constituent at the arbitrary time origin. The accepted convention is to use V_n as for the Prime Meridian and t in the standard time zone of the observation station (Pugh, 2004).

For any coastal location, each partial tide has a particular amplitude and phase. In order to make accurate tidal predictions for a location, it is important to identify the local tidal constituents (the amplitude and phase of partial tides) properly. In fact, as many as 390 harmonic constituents have been extracted or derived from the observed tidal records over the years (Darwin, 1911; Doodson, 1928; Horn, 1960). Recently, more attempts have been made to evaluate the contribution of non-tidal effects in the observation records in order to provide a quantitative estimate of the variability in the tidal record (Munk and Cartwright, 1966). Table 2.1 lists the nine most important harmonic constituents in three main classes: semi-diurnal constituents, diurnal constituents and long-period constituents. However, tidal constituents vary slightly among different analyses of data from different times at the same location. This is due to the inconsistency of measurement instruction, the interference of non-tidal energy at tidal frequencies, and so on. So far, the knowledge of tidal constituents is still under development due to the complexity of the sun-earth-moon geometry system.

The rise and fall of tide is accompanied by horizontal movement of the water called tidal current. In general, tidal currents are more variable than tidal heights, both in space and time. The current has both a magnitude and a direction, and can vary substantially over a short distance due to local bathymetry and horizontal geometry, introducing difficulty in collecting and analyzing the tidal current. It is also found that the amplitude of tidal current decreases with the water depth, slowly at top and then more rapidly as approaching the bottom. The phase also varies with depth, as it is earlier near the bottom than it is at the surface. Such variations in the currents are due to the stress arising from bottom friction, which can be derived from the dynamical equations (Bowden, 1983). The observation and prediction of tidal currents is more important in the offshore area and estuaries, since the effects of tidal currents on the movement of water in and out of bays and channels can be substantial.

Table 2.1 Some principal tidal constituents (Wright, 2000).

| <i>Name of tidal component</i> | <i>Symbol</i> | <i>Period in solar hours</i> | <i>Coefficient ratio* (M₂=100)</i> |
|--------------------------------|----------------|------------------------------|---|
| <i>Semi-diurnal:</i> | | | |
| Principal lunar | M ₂ | 12.42 | 100 |
| Principal solar | S ₂ | 12.00 | 46.6 |
| Larger lunar elliptic | N ₂ | 12.66 | 19.2 |
| Luni-solar | K ₂ | 11.97 | 12.7 |
| <i>Diurnal:</i> | | | |
| Luni-solar | K ₁ | 23.93 | 58.4 |
| Principal lunar | O ₁ | 25.82 | 41.5 |
| Principal solar | P ₁ | 24.07 | 19.4 |
| <i>Longer Period:</i> | | | |
| Lunar fortnightly | M _f | 327.86 | 17.2 |
| Lunar monthly | M _m | 661.30 | 9.1 |

*The coefficient ratio is the ratio of the amplitude of the tidal component to that of M₂.

2.2 Numerical Modeling of Tides

Due to the economic importance of the shipping and fishing industries, the prediction of tidal heights and currents has been studied for many years. At the beginning, physical models were used, especially in rivers and estuaries. These models can be hydraulic or electric analogue models. Hydraulic models have difficulties in representing a large area as the Coriolis effects are hard to include. Electric analogue models are able to simulate tides and storm surges including the effect of the Coriolis force and friction; however, the size of the modeled area is still limited (Ishiguro, 1972). Currently, the most efficient way to model tides is to solve the basic governing equations numerically using high performance computers. Two-dimensional depth-integrated models are widely used. Recently, three-dimensional models have been developed in order to investigate the effects of wind stress on the ocean surface, the variation of currents, and the density distribution of arising from the fresh water inflows.

The major approaches to tidal simulation include the finite difference method, the finite element method and the finite volume method. These methods are all based on solving a system of equations that account for mass and momentum by different computational techniques. Teubner et. al. developed a two-dimensional finite difference model for the Persian Gulf in Australia, using the dynamic nesting technique. This technique allows the model to increase mesh resolution at certain designated areas within a coarse grid. Thus, the computation accuracy and efficiency have been improved (Teubner, Najafi et al., 1999). Three-dimensional finite difference models have been developed to simulate the tides, especially tidal currents in coastal

areas (Tsvetsinsky, Arkhipov et al., 1998; Lewis and Noye, 1999; Noye, Nixon et al., 1999). The finite volume method is able to solve the partial differential equations for discrete areas on a meshed geometry without the requirement of a structured mesh (in contrast to the finite difference method). Hu et al. (1997) simulated tidal flows, wave propagation and wave-driven sediment transport by developing a high-resolution finite volume hydrodynamic solver. According to their methodology, the finite volume model grid is not required to be regular and orthogonal, which enables easy boundary fitting. Reggio and his colleagues have created a 3-D multiple-layer finite volume model based on Roe's Flux Difference-Splitting (FDS) method. The model is validated by several examples, such as a simple tidal wave propagation given a fixed open boundary in a rectangular domain; tidal constituent evolution for the St. Lawrence estuary (Reggio, Hess et al., 2002).

However, the finite element method is more popular in numerical modeling because it can be easily adapted to problems of great complexity and unusual geometry. With regard to tidal simulations, Hagen and his students of the University of Central Florida have been successfully using ADCIRC-2DDI, a finite element coastal circulation model, in their extensive hydrodynamic researches, e.g. unstructured mesh generation, tidal inlets and estuaries (Hagen, Westerink et al., 2001; Jones and Davies, 2005; Bacopoulos, 2006; Parrish and Hagen, 2007; Salisbury and Hagen, 2007). More details about ADCIRC model formulation and application are discussed in Chapter 3. Given the fact that these numerical methods are all applicable to coastal hydrodynamic problems, scientists have compared different methods of numerically modeling tides and tidal currents. (Jones and Davies, 2005) did an internal comparison between finite

difference and finite element (TELEMAC) approaches to model tides on west coast of Britain. Grenier et. al. have used the ADCIRC model, either two-dimensional depth integrated (2DDI) or three-dimensional local (3DL) to determine if wave-current interaction in the bottom boundary layer is an important factor affecting circulation in the Bight of Abaco. The simulation results revealed that the wave-current does not influence the overall circulation in the bight, due to the large bottom friction and depth limited wave height and period (Grenier, Luettich et al., 1993; Grenier, 1994).

For tidal computations, the shape of the shoreline and the ocean floor alter the way that tides propagate; therefore, coastal characteristics, such as underwater topography and coastline shape, need to be taken into account when forecasting tides. The effects of coastal morphology on tidal flow have been discussed in many references. One solution to this is to apply a large tidal model domain, which could significantly simplify the task of boundary condition specification. The advantage of forcing the open tides in deep waters has been demonstrated and is attributed to the fact that tides vary more gradually and nonlinear constituents are much smaller than on the continental shelf (Westerink, Luettich et al., 1994). By this conclusion, the Western North Atlantic Tidal (WNAT) model domain, encompassing the Gulf of Mexico, the Caribbean Sea, and the entire North Atlantic Ocean found west of the 60° west meridian (Figure 2.3) is constructed. Fine mesh elements are placed along the southeastern coast of the United States (a 30km wide band) and the continental shelf in order to accurately describe the detailed bathymetry (Parrish, 2001). Fine mesh elements are also necessary on the continental shelf (Westerink, Luettich et al., 1994; Hagen, Westerink et al., 2000; Hagen and Parrish, 2004), since

the wave dispersion occurring as the waves travel from the deep ocean to the continental shelf can be captured more accurately. A relatively coarse WNAT mesh (WNAT-53K) was developed from the existing high resolution WNAT mesh (WNAT-333K) by using an automated procedure. A localized truncation error analysis was performed using results from the highly resolved WNAT-333K as a guideline for internal element sizing (Hagen, Zundel et al., 2006).

The WNAT-53K model domain contains 52,774 computational nodes and 98,365 triangular elements, covering an area of approximately $8,347 \times 10^6 \text{ km}^2$. The new Pascagoula tidal model is developed by integrating this WNAT-53K mesh into a local Pascagoula mesh (For details, see Chapter 4). There are two major purposes for this domain: first, it can be used as a basis model for local tides and storm surge models and second, it will provide open water boundary conditions for shelf-based models.

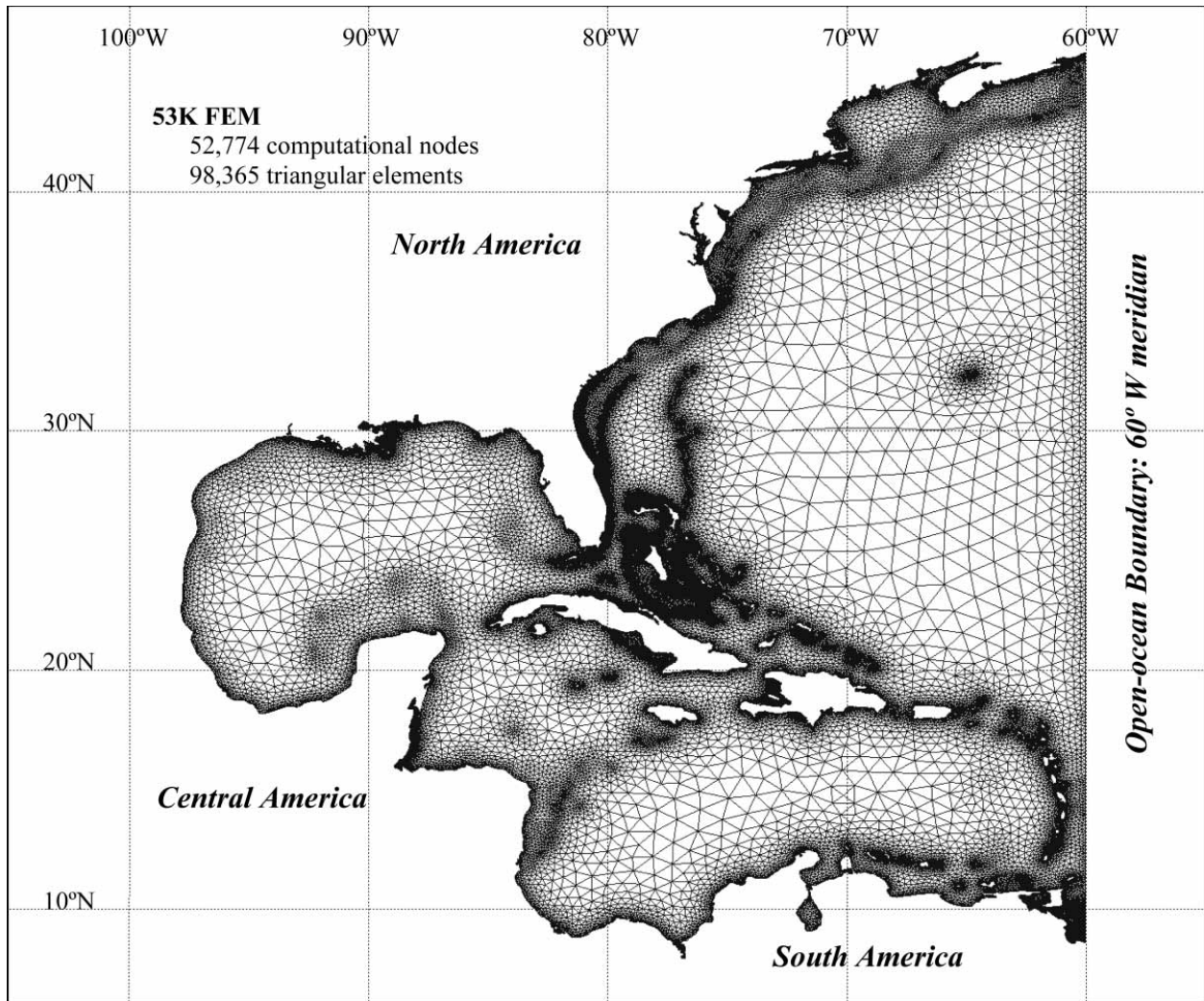


Figure 2.3 The unstructured, 53K finite element mesh for the WNAT model domain

2.3 Numerical Modeling in Estuarine Study

Tidal propagation in estuaries has been a popular topic for hydrologists over the years. It is a complicated physical and ecological system involving channel slope and depth variation, channel bed friction, freshwater discharge, surface water circulation and so on (Godin, 1991; 1999). Different numerical techniques have been developed to meet the various needs of human

activities in river estuaries. This section discusses these numerical estuary models with a main focus on tidal propagation and tidal currents.

Hamilton (1990) did a review on tidal currents and salinity in the Columbia River Estuary. A multi-channel, laterally averaged estuary model was used for simulating the estuary during low flow period and extreme low flow period. Water elevation, current and salinity in time series were compared with historical observations. By applying a finite-difference method on the advection terms, the model shows that the circulation processes, in particular the tidal advection of salt by the vertically sheared tidal currents, is the dominant mechanism. The results also reveal that large river flows have the capability of maintaining the salinity intrusion.

A tidal and storm surge model of Bristol Channel, UK is developed by applying the Incremental Differential Quadrature Method (IDQM) (Hashemi, Abedini et al., In Press). As an implementation of the method, the one-dimensional tidal elevation and surge model for channels has the advantage of using a small number of nodes to obtain reasonable results. Due to the easier boundary specification and the model efficiency, the timescale of the morphological simulations can be more than 10 years. The model gives reasonable results on tide simulation, although the peak magnitude during the surge event was under-predicted.

Walters and Cheng (1979) wrote an article on a two-dimensional hydrodynamic model for the tidal estuary. This finite element model computes the tidal and residual currents in an estuary (San Francisco Bay), using Galerkin finite element formulation. One of the specific interests of

this research is the mixed interpolation: quadratic functions for velocity and linear functions for water elevation.

Another two-dimensional hydrodynamic model is used to generate overtides and compound tides in the Amazon estuary (Gallo and Vinzon, 2005). The influences of the main estuarine harmonics M_4 , M_2 , S_2 and M_{sf} are discussed based on historical data and numerical results. It was determined that the tidal harmonic components prevail near the river mouth and over the continental shelf, but degrade when tides propagate to the upstream. The freshwater discharge plays an important role in the horizontal tidal flow; however, it does not have an effect on the water level asymmetry in Amazon River.

Warner and his colleagues (2005) modeled the Hudson River estuary with a three-dimensional model called Regional Ocean Modeling System (ROMS). This estuary model is able to reproduce the variation of salinity and currents including tides and freshwater discharge. One of their goals was to investigate the importance of salinity transport influenced by the tides propagating from the deep ocean. A discrepancy between the model and the data was found in the vertical salinity structure.

Bacopoulos (2006) has produced a ADCIRC-2DDI hydrodynamic tidal model of the Loxahatchee River estuary in Southeastern Florida. Several mesh variations have been built to detect the extent of tidal propagation between the Loxahatchee River and the Atlantic Intracoastal Waterway. Both the tidal constituents (include phase and amplitude) and velocity residuals were

computed and examined over the whole estuary. The net circulation patterns demonstrate the importance of including the Atlantic Intracoastal Waterway into the Loxahatchee River model, due to the interactions between the two systems.

2.4 Previous Modeling Studies for the Pascagoula River

As one of the major river basins in Mississippi, the Pascagoula River is well known for its high-quality habitats and wildlife. The majority of the basin area is still preserved with limited human activities. The Pascagoula River is the last free-flowing river in the contiguous United States, since there are no obstructions by dams or weirs (Droppo, 2003). As a result, the majority of the scientific work on the Pascagoula River has focused on wildlife management. The yellow-blotched map turtle habit study is a good example of Pascagoula wildlife researches (Moore and Seigel, 2006). In the 1970s, the U.S. Army Corps of Engineers in Mobile, AL, did a comprehensive basin study of the Pascagoula River. In this report, an early-action program for the next 15 to 20 years and a framework for future planning was suggested. This report was more from a strategy point of view, offering nonstructural measurements such as flood plain regulation, water hygiene maintenance and navigation improvement (Oldham and Rushing, 1970). Mossa and Coley (2004) at the University of Florida did a geomorphic assessment on the instability of the Pascagoula River and its tributaries, using varied sources of GIS data. Since some of the Pascagoula streams have been involved in considerable historical and recent mining activities, the study aims to quantify the effect on channel change or stability. The number of erosion and deposition areas reveals that the Pascagoula River, especially the lower Pascagoula River, is the

most stable channel among the three major rivers in the basin (the Leaf River, the Chickaswhay River and the Pascagoula River).

With regard to the numerical modeling of the Pascagoula River, there are few published researches. So far as the writer knows, the LMRFC (Lower Mississippi River Forecast Center) has developed a forecasting model for the Pascagoula River, although their model has not included the lower Pascagoula River (starting from Graham Ferry to the river mouth). However, the tidal impact on the water elevation can be critical in that area. As a result, the lack of tidal researches focused on the lower Pascagoula region is a main motivation of this presented research.

CHAPTER 3. NUMERICAL MODEL DESCRIPTIONS

3.1 ADCIRC Model Background

Advanced Circulation model (ADCIRC, v42.06), was used in this research to compute astronomical and meteorological tides. It is a numerical finite element hydrodynamic model program for shelves, coasts, and estuaries. Barotropic hydrodynamics were examined and density gradients were assumed to be relatively small, since these conditions are common near tidal inlets. These assumptions facilitate the use of the ADCIRC-2DDI (Advanced Circulation model for Oceanic, Coastal, and Estuarine Waters, Two-Dimensional Depth-Integrated) model.

In ADCIRC-2DDI, both finite element and finite difference methods have been applied in the spatial and time domains, providing an effective way to discretize the continuous shallow water equations and implement numerical modeling. ADCIRC also integrates a variety of boundary conditions, e.g. specified elevation/flow, surface stress, velocity conditions, atmospheric pressure. Five main forcings can be selected in ADCIRC based on different modeling objectives: elevation boundary conditions, normal flow boundary conditions, surface stress boundary conditions, tidal potential, and earth load/self attraction tide. Multiple choices are provided in ADCIRC post analysis. For example, harmonic constituents for elevation and depth averaged velocity during the course of the simulation; the deviation from mean sea level in time series for any locations in the domain (Luettich and Westerink, 2000). Because of its flexibility, ADCIRC-2DDI can be

used to accurately and efficiently produce tidal hydrographs and simulate storm surge. Further, the wetting and drying algorithm in ADCIRC-2DDI model allows the simulation of flood inundation and recession near shore and inland elements. All of these facts illustrate that ADCIRC-2DDI is a suitable and powerful simulation tool in this Pascagoula River study.

3.2 Governing Equations

The computations presented in this thesis have been performed using ADCIRC-2DDI code. ADCIRC-2DDI applies the depth-integrated equations of mass and momentum, ruled by the hydrostatic assumption and the Boussinesq approximation (Westerink, Blain et al., 1994). Using the hybrid bottom friction formulation and neglecting baroclinic terms and lateral diffusion/dispersion effects leads to the following set of equations in primitive non-conservative form, expressed in a spherical coordinate system (Kolar, Gray et al., 1994):

$$\frac{\partial \zeta}{\partial t} + \frac{1}{R \cos \phi} \left(\frac{\partial UH}{\partial \lambda} + \frac{\partial (VH \cos \phi)}{\partial \phi} \right) = 0 \dots\dots\dots (3.1)$$

$$\begin{aligned} & \underbrace{\frac{\partial U}{\partial t}}_{(1)} + \underbrace{\frac{1}{R \cos \phi} U \frac{\partial U}{\partial \lambda}}_{(2)} + \underbrace{\frac{1}{R} V \frac{\partial U}{\partial \phi}}_{(3)} - \left(\frac{\tan \phi}{R} U + f \right) V \\ & = - \underbrace{\frac{1}{R \cos \phi}}_{(4)} \frac{\partial}{\partial \lambda} \left[\underbrace{\frac{p_s}{\rho_0}}_{(5)} + \underbrace{g(\zeta - \eta)}_{(6)} \right] + \underbrace{\frac{\tau_{s\lambda}}{\rho_0 H}}_{(7)} - \underbrace{\tau_* U}_{(8)} \dots\dots\dots (3.2) \end{aligned}$$

$$\begin{aligned}
& \underbrace{\frac{\partial V}{\partial t}}_{(1)} + \underbrace{\frac{1}{R \cos \phi} U \frac{\partial V}{\partial \lambda}}_{(2)} + \underbrace{\frac{1}{R} V \frac{\partial V}{\partial \phi}}_{(3)} - \underbrace{\left(\frac{\tan \phi}{R} U + f \right)}_{(3)} U \\
& = - \underbrace{\frac{1}{R} \frac{\partial}{\partial \phi}}_{(4)} \left[\underbrace{\frac{p_s}{\rho_0}}_{(4)} + \underbrace{g(\zeta - \eta)}_{(5)(6)} \right] + \underbrace{\frac{\tau_{s\phi}}{\rho_0 H}}_{(7)} - \underbrace{\tau_* V}_{(8)} \dots \dots \dots (3.3)
\end{aligned}$$

where:

- | | |
|---|---|
| t = time; | g = acceleration due to gravity; |
| ζ = free surface elevation relative to the geoid; | U, V = depth-averaged horizontal velocities; |
| H = $\zeta + h$ = total height of the water column; | h = bathymetric depth relative to the geoid; |
| $f = 2 \Omega \sin \phi$ = Coriolis parameter; | ϕ = degrees latitude; |
| p_s = atmospheric pressure at the free surface; | g = acceleration due to gravity; |
| η = Newtonian equilibrium tide potential; | a = effective Earth elasticity factor; |
| ρ_0 = reference density of water; | τ_{sx}, τ_{sy} = applied free surface stress; |
| $\tau_* = C_f \frac{(U^2 + V^2)^{1/2}}{H}$, quadratic bottom stress (See Chapter 3.3); | |

R = radius of the earth.

Terms 1 through 8 are identified as follows:

- | | |
|-------------------------|-----------------------------|
| ① Local accumulation; | ⑤ Pressure force; |
| ② Advection; | ⑥ Tidal potential; |
| ③ Coriolis force; | ⑦ Surface wind stress; |
| ④ Atmospheric pressure; | ⑧ Bottom frictional stress. |

A practical expression for the effective Newtonian equilibrium tide potential η is given by Reid (1990):

$$\eta(\lambda, \phi, t) = \sum_{n,j} \alpha_{jn} C_{jn} f_{jn}(t_0) L_j(\phi) \cos \left[\frac{2\pi(t-t_0)}{T_{jn}} + j\lambda + \nu_{jn}(t_0) \right] \dots \dots \dots (3.4)$$

where

α_{jn} = the effective earth elasticity factor for tidal constituent n of species j ;

C_{jn} = a constant characterizing the amplitude of tidal constituent n of species j ;

f_{jn} = the time-dependent nodal factor;

$L_j(\phi)$ = the latitude-dependent functions of species j ;

t_0 = the reference time;

ν_{jn} = the time-dependent nodal argument ($j = 0$, declinational; $j = 1$, diurnal; $j = 2$, semi-diurnal);

T_{jn} = the period of constituent n of species j ;

The latitude-dependent functions, $L_j(\phi)$, for the tidal species j ($j = 0$, declinational; $j = 1$, diurnal; $j = 2$, semi-diurnal) are given by: $L_0 = 3 \sin^2 \phi - 1$, $L_1 = \sin(2\phi)$, and $L_2 = \cos^2 \phi$.

Reid (1990) suggests the values for C_{jn} . A typical value of 0.69 for the effective earth elasticity factor α is suggested for all the tidal constituents, although it is proved to be slightly constituent dependent (Schwidorski, 1980; Hendershott, 1981; Wahr, 1981).

ADCIRC-2DDI does not solve the shallow-water equations in primitive form, because of the spurious oscillations led by a continuous Galerkin finite element formulation. Alternatively, ADCIRC utilizes the Generalized Wave Continuity Equation (GWCE) formulation to replace the primitive continuity equation (Kinnmark, 1985; Kolar, Westerink et al., 1994). There are three steps to formulate the GWCE. First, apply time differentiation on the depth integrated primitive continuity equation. Second, implement spatial differentiation on the depth integrated primitive momentum equations. Last, combine the two sets of equations and add to the primitive continuity equation, with a weighting factor, G . As a result, the GWCE together with the two momentum conservation equations are set up into the ADCIRC-2DDI code in order to solve hydrodynamic problems and thus finally describe shallow water tidal flow. ADCIRC-2DDI is implemented using linear triangular elements for elevation, velocity and depth. The elevation and velocity solutions are computed by the equal order finite element interpolating functions.

The GWCE in a spherical coordinate system can be presented as:

$$\begin{aligned}
& \frac{\partial^2 \zeta}{\partial t^2} + \tau_0 \frac{\partial \zeta}{\partial t} - \frac{1}{R \cos \phi} \frac{\partial}{\partial \lambda} \left\{ \frac{1}{R \cos \phi} \left(\frac{\partial U U H}{\partial \lambda} + \frac{\partial U V H}{\partial \phi} \right) - \left(\frac{\tan \phi}{R} U + f \right) V H \right. \\
& \quad \left. - \frac{H}{R \cos \phi} \frac{\partial}{\partial \lambda} \left[\frac{p_s}{\rho_0} + g(\zeta - \alpha \eta) \right] + \frac{E_{h_2}}{R \cos \phi} \frac{\partial^2 \zeta}{\partial \lambda \partial t} + \frac{\tau_{s\lambda}}{\rho_0} - (\tau_* - \tau_0) U H \right\} \\
& - \frac{1}{R} \frac{\partial}{\partial \phi} \left\{ \frac{1}{R \cos \phi} \left[\frac{\partial H U V}{\partial \lambda} + \frac{\partial H V V \cos \phi}{\partial \phi} \right] + \left(\frac{\tan \phi}{R} U + f \right) U H - \frac{H}{R} \frac{\partial}{\partial \phi} \left[\frac{p_s}{\rho_0} + g(\zeta - \alpha \eta) \right] \right. \\
& \quad \left. + \frac{E_{h_2}}{R} \frac{\partial^2 \zeta}{\partial \phi \partial t} + \frac{\tau_{s\phi}}{\rho_0} - (\tau_* - \tau_0) V H \right\} - \frac{\tan \phi}{R} \left(\frac{\partial V H}{\partial t} + \tau_0 V H \right) = 0 \dots\dots\dots (3.5)
\end{aligned}$$

In order to facilitate a finite element solution to the governing equations, a Carte Parallelogrammatique Projection (CPP) (Kolar, Gray et al., 1994) is used to project Equation (3.1) – (3.3) from spherical coordinate system into a rectilinear coordinate system. The rectilinear coordinate system (x', y') is centered in longitude and latitude at (λ_0, ϕ_0) :

$$x' = R(\lambda - \lambda_0) \cos \phi_0$$

$$y' = R\phi$$

By using CPP projection equations, the shallow water equations in primitive non-conservative form are now presented in the CPP coordinate system:

$$\frac{\partial \zeta}{\partial t} + \frac{\cos \phi_0}{\cos \phi} \frac{\partial(UH)}{\partial x'} + \frac{1}{\cos \phi} \frac{\partial(VH \cos \phi)}{\partial y'} = 0 \dots\dots\dots (3.6)$$

$$\begin{aligned} & \frac{\partial U}{\partial t} + \frac{\cos \phi_0}{\cos \phi} U \frac{\partial U}{\partial x'} + V \frac{\partial U}{\partial y'} - \left(\frac{\tan \phi}{R} U + f \right) V \\ & = - \frac{\cos \phi_0}{\cos \phi} \frac{\partial}{\partial x'} \left[\frac{p_s}{\rho_0} + g(\zeta - \eta) \right] + \frac{\tau_{s\lambda}}{\rho_0 H} - \tau_* U \dots\dots\dots (3.7) \end{aligned}$$

$$\begin{aligned} & \frac{\partial V}{\partial t} + \frac{\cos \phi_0}{\cos \phi} U \frac{\partial V}{\partial x'} + V \frac{\partial V}{\partial y'} + \left(\frac{\tan \phi}{R} U + f \right) U \\ & = - \frac{\partial}{\partial y'} \left[\frac{p_s}{\rho_0} + g(\zeta - \eta) \right] + \frac{\tau_{s\phi}}{\rho_0 H} - \tau_* V \dots\dots\dots (3.8) \end{aligned}$$

The corresponding GWCE in the CPP system is:

$$\begin{aligned}
& \frac{\partial^2 \zeta}{\partial t^2} + \tau_0 \frac{\partial \zeta}{\partial t} + \frac{\cos \phi_0}{\cos \phi} \frac{\partial}{\partial x'} \left[U \frac{\partial \zeta}{\partial t} - \frac{\cos \phi_0}{\cos \phi} UH \frac{\partial U}{\partial x'} - VH \frac{\partial U}{\partial y'} + \right. \\
& \quad \left. \left(\frac{\tan \phi}{R} U + f \right) VH - H \frac{\cos \phi_0}{\cos \phi} \frac{\partial}{\partial x'} \left(\frac{p_s}{\rho_0} + g(\zeta - \eta) \right) - (\tau_* - \tau_0)UH + \frac{\tau_{s\lambda}}{\rho_0} \right] \\
& + \frac{\partial}{\partial y'} \left[V \frac{\partial \zeta}{\partial t} - \frac{\cos \phi_0}{\cos \phi} UH \frac{\partial V}{\partial x'} - VH \frac{\partial V}{\partial y'} - \right. \\
& \quad \left. \left(\frac{\tan \phi}{R} U + f \right) UH - H \frac{\partial}{\partial y'} \left(\frac{p_s}{\rho_0} + g(\zeta - \eta) \right) - (\tau_* - \tau_0)VH + \frac{\tau_{s\phi}}{\rho_0} \right] \\
& - \frac{\partial}{\partial t} \left(\frac{\tan \phi}{R} VH \right) - \tau_0 \left(\frac{\tan \phi}{R} VH \right) = 0 \dots\dots\dots (3.9)
\end{aligned}$$

3.3 Bottom Friction in ADCIRC

In the ADCIRC-2DDI model, the bottom stress can be computed by three laws: linear bottom friction law, quadratic bottom friction law and hybrid nonlinear bottom friction law. The linear function is recommended when ADCIRC model is running in a linear mode. The quadratic bottom stress calculations both use the quadratic bottom friction function; however, the hybrid nonlinear bottom friction function considers of the bathymetry change. For example, the bottom friction coefficient is relatively constant in deep water, following the quadratic bottom friction law. In shallow water, the friction coefficient increases as the depth decreases (e.g. as in a Manning-type friction law) (Luettich and Westerink, 2000). As a result, this presenting research uses the hybrid nonlinear bottom friction formulation for the bottom friction calculation and calibration. The

hybrid bottom stress formulation generates more accurate solutions in shallow water modeling when wetting and drying algorithm is allowed.

The following quadratic bottom stress equations are applied:

$$\tau_* = C_f \frac{(U^2 + V^2)^{1/2}}{H} \dots\dots\dots (3.10)$$

where:

C_f = the bottom friction coefficient,

U, V = depth averaged horizontal velocities,

H = the total water column depth.

The bottom friction coefficient, C_f , is determined as:

$$C_f = C_{fmin} \left[1 + \left(\frac{H_{break}}{H} \right)^\theta \right]^{\frac{\lambda}{\theta}} \dots\dots\dots (3.11)$$

where:

C_{fmin} = the minimum bottom friction factor,

H_{break} = break depth,

θ = parameter that determines how rapidly the hybrid function approaches its upper and lower limits,

λ = parameter that describes how quickly the friction factor increases as water depth decreases.

The recommended value of θ and λ are 10 and 1/3 respectively. A value of 0.0025 is suggested for C_{fmin} in several ADCIRC studies (Cobb and Blain, 2001; Veeramony and Blain, 2001; Luettich, Carr et al., 2002). Figure 3.1 shows the performance of hybrid bottom friction formulation if C_{fmin} , θ and λ are fixed at the recommended values mentioned above. The bottom friction C_f is high in shallow water (when water column depth is small), and gradually decreases to a low value when it approaches deep water. By using the presented hybrid bottom stress formulation, spatially constant or spatially varying friction coefficients can be assigned over the entire grid, which offers ADCIRC-2DDI the flexibility of simulating bottom friction change from the deep ocean to shallow river inlets.

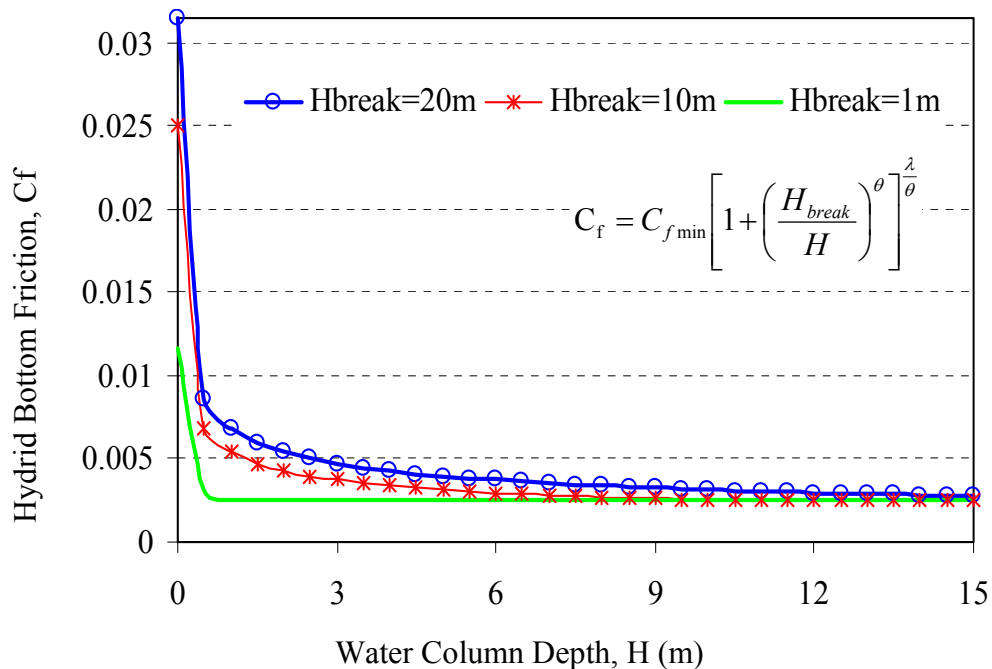


Figure 3.1 Variation in C_f with bathymetric depth for various values of H-Break, $C_{fmin} = 0.0025$, $\theta = 10$ and $\lambda = 1/3$. (Murray, 2003)

3.4 Possible Error Sources

Numerical simulation uses numerical methods to quantitatively represent the evolution of a physical system. From the numerical results of the Pascagoula River simulation presented herein, knowledge of estuarine tides and a physical understanding of the Pascagoula River basin can be obtained. Ideally, if numerical simulation uses the values that best describe the real environment and the system strictly obeys the laws that govern the real physical processes, the results of the numerical simulation would be a close representation of the real world. Accordingly, possible errors in this numerical research can be attributed to two main sources: the real values used for simulation (bathymetric data, boundary data, historical verification data, etc.) and the simulation tool itself (e.g. ADCIRC-2DDI).

Specifically, ADCIRC-2DDI is insufficient to describe the short waves (wind-induced waves) because the governing equations applied in this model are only capable of describing long wave activities, e.g. astronomic tides and storm surge. Funakoshi (2006) coupled hydrodynamic and wave models for the simulation of storm tides, showing the possibility of minimizing this major error source. Furthermore, the continuous domain as well as the boundary conditions is simplified into discrete elements in finite element method. The inaccuracy of model input data may also cause errors. For example, the river bathymetric data and historical water elevation data at gage stations may be inaccurate. In fact, the importance of obtaining accurate bathymetric data for the model is proven in this thesis (See Chapter 6). Clearly identifying possible error sources is required in order to minimize the model error and allow researchers to draw defensible

conclusions from the results, as well as to develop a better understanding of the complex mechanisms associated with astronomic tides.

CHAPTER 4. PRELIMINARY ASTRONOMIC TIDE MODEL DEVELOPMENT FOR THE PASCAGOULA RIVER

Developing an astronomic tidal model for the lower Pascagoula River is a major objective of this research, and forms the initial part of this study. Once the preliminary model is created, it can be used as a basis model to incorporate the effects of fresh water inflows, inundation areas and storm surge events. This chapter begins with the generation of a comprehensive inbank mesh for the lower Pascagoula River and its four principal tributaries: Black Creek, Red Creek, Escatawpa River and Big Creek. This model can be used as a digital elevation model for the Pascagoula River basin. After the preliminary comprehensive mesh is complete, it is abbreviated in order to be able to run the Pascagoula River model in an affordable time span. Preliminary testing is then initiated in order to determine the applicability of the model and assess its components (e.g., mesh resolution, bathymetry and forcings). Discussions about the model parameterizations and open boundary assignment are presented. Next, some preliminary results and conclusions are drawn with respect to model improvement. Finally, the model is inserted within the Western North Atlantic Tidal model domain and tested in order to further assess boundary forcings.

4.1 Preliminary Mesh Generation

In order to simulate the astronomic tides, a preliminary two-dimensional depth-integrated inbank model was first developed. It is comprised of five streams: the lower Pascagoula River, Black Creek, Red Creek, Escatawpa River and Big Creek. Among them, the lower Pascagoula

River, as the main channel, is the widest and longest. Table 4.1 summarizes the streams included in the preliminary mesh, as well as their lengths in river miles.

Table 4.1 Summary of the streams in the comprehensive Pascagoula River mesh

| <i>Stream Name</i> | <i>Location ID</i> | <i>Upstream Boundary Station</i> | <i>River Mile</i> |
|--------------------|--------------------|--|-------------------|
| Pascagoula River | MRRM6 | Pascagoula R. at Merrill, MS | 80.80 |
| Red Creek | VESM6 | Red Creek at Vestry Gauge, MS | 12.68 |
| Black Creek | WGAM6 | Black Creek near Wiggins, MS | 33.46 |
| Escatawpa River | AGRM6 | Escatawpa River at Highway 612 near Agricola, MS | 49.81 |
| Big Creek | BCDA1 | Big Creek Lake Dam Tailwater. AL | 19.80 |

* The location ID is referred to Figure 4.4.

The Surface-water Modeling System (SMS) was utilized as a mesh generation tool to create the two-dimensional mesh for ADCIRC-2DDI model. The mesh was developed in three steps: boundary digitization, mesh paving and bathymetry assignment.

The first step was to digitize the channel boundary according to aerial photographs in the study area. The aerial photographs using here were downloaded from TerraServer – USA (<http://www.terraserver-usa.com/>), a free online source of maps and aerial photographs of the United States. The high resolution maps and images are supplied to TerraSever – USA by the United States Geological Survey (USGS). Figure 4.1 & 4.2 shows the digitized boundaries in SMS at several locations. At times, the boundaries were not easily defined due to heavy forestion or erosion and deposition near the river bends (See Figure 4.1). Also, many small creeks exist

along the Pascagoula River, such as the marsh area near the inlet. For the above reasons, the boundary was digitized on only the main stream and four major tributaries at this stage of the model development.

The second step was to mesh over the domain with unstructured triangle elements. SMS is a powerful tool to produce high quality meshes with limited human effort. Since we know that most of the model area is composed of meandering streams (up to 196 miles, see Table 4.1) rather than broad surface water, e.g. lakes, bays, and oceans, it is important to control the element size in case that there are not enough elements to describe the cross section of the channel properly. Based on such concerns, the basic meshing rule for the Pascagoula River mesh generation was: at least three elements are required to describe the cross section. The feature in SMS called ‘scalar paving method’ provided us with an efficient way to generate the mesh while still satisfying the basic rule. Scalar paving allowed us to control the element size by setting appropriate values on the control points. After the initial mesh is automatically generated, minor mesh adjustments are manually applied to avoid unnecessary high resolution or undesirable coarseness. Over the entire mesh, the nodal spacing varies from 100 meters down to only several meters. The Pascagoula River main channel has the nodal spacing between 80m to 20m. The tributaries except Lower Escatawpa River have relatively smaller elements sizing less than 20 meters. The minimum element size, located in the Big Creek, is 1.4 meters (See Figure 4.2 (d)). The Lower Escatawpa River has similar spacing as the Pascagoula main channel. The elements grow as big as 100 meters at Beardslee Lake and Robertson Lake, and then decrease their size to 40 meters in the dredging channel.

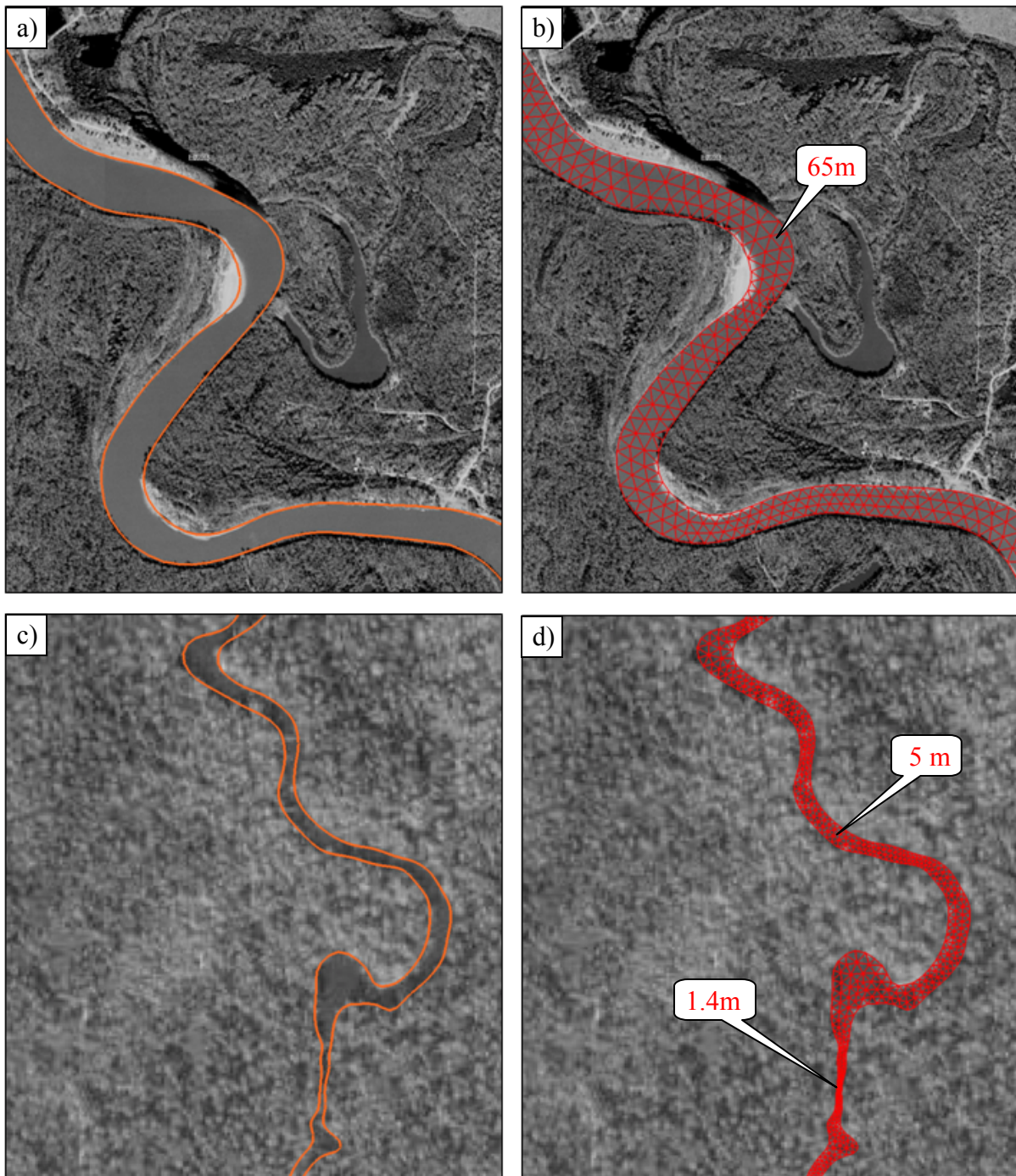


Figure 4.1 Mesh Generation Step 1 & 2 - digitized boundary and 2D mesh: (a) (b) Pascagoula River with erosion and deposition areas; (c) (d) Heavily forested reach in Big Creek, showing the minimum element size.

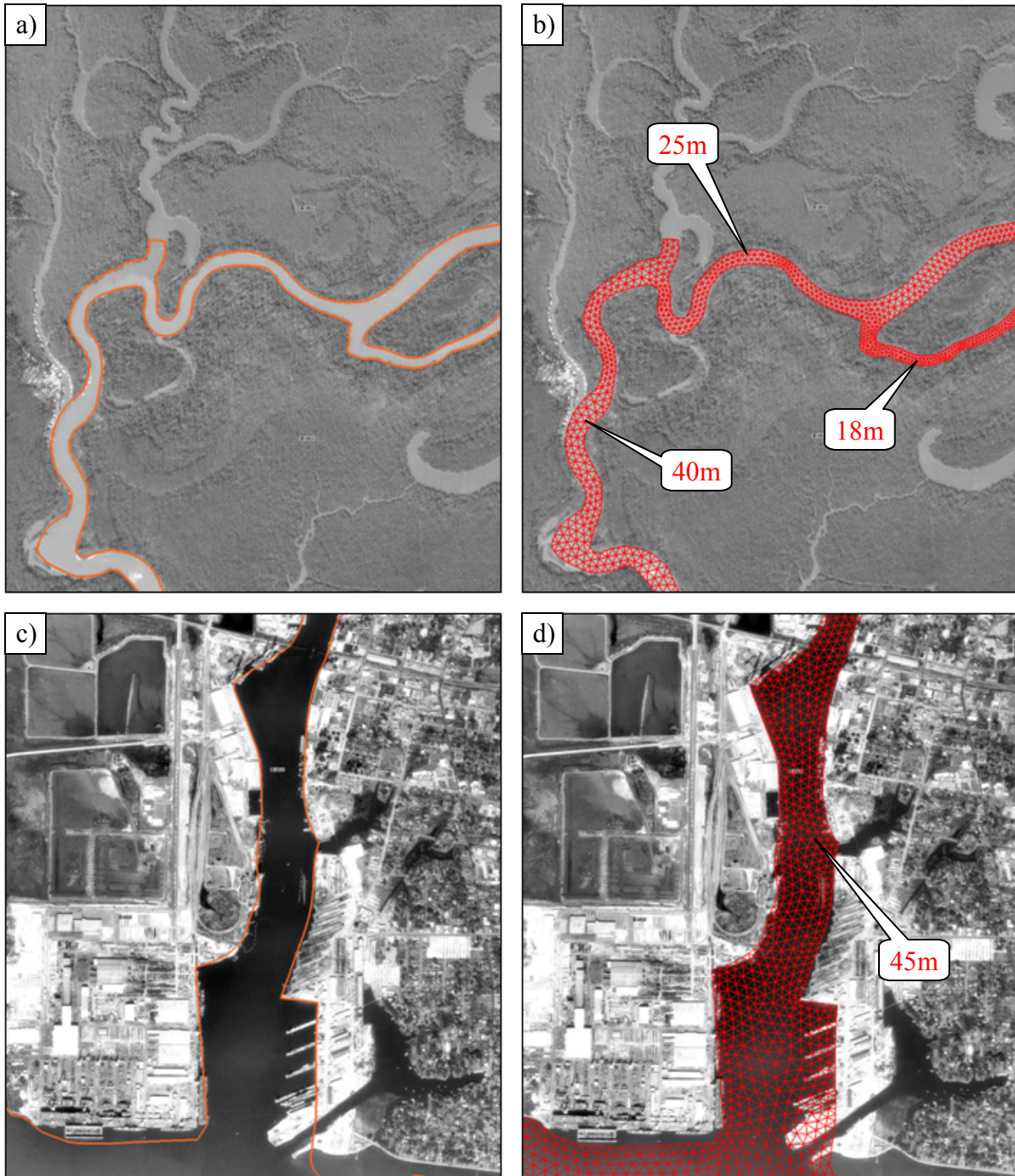


Figure 4.2 Mesh Generation Step 1 & 2 - digitized boundary and 2D mesh: (a) (b) Pascagoula River near Poticaw Landing, splitting into East Pascagoula River and West Pascagoula River; (c) (d) East Pascagoula River Inlet (The Port of Pascagoula).

The last step was to interpolate the bathymetry onto the finished 2D mesh. This step is easily done in SMS, once the topographic data for the model region is ready. The initial data source for this data was an existing storm surge model of Southeastern Louisiana known as the SL15 model, developed by Dr. Joannes Westerink and his team for the Federal Emergency Management Agency (FEMA) study of the Hurricane Katrina failures and hurricane protection risk for the New Orleans area. Various LIDAR mapping projects covering the southern Louisianan region were used as the SL15 model input. Some of the topography and bathymetric data were calibrated with modern GPS technology and measurements for quality control purposes (IPET Force - U.S. Army Corps of Engineers, 2007). The preliminary comprehensive Pascagoula mesh bathymetry is obtained directly from the SL15 model, given the fact that there is no better data source at that time.

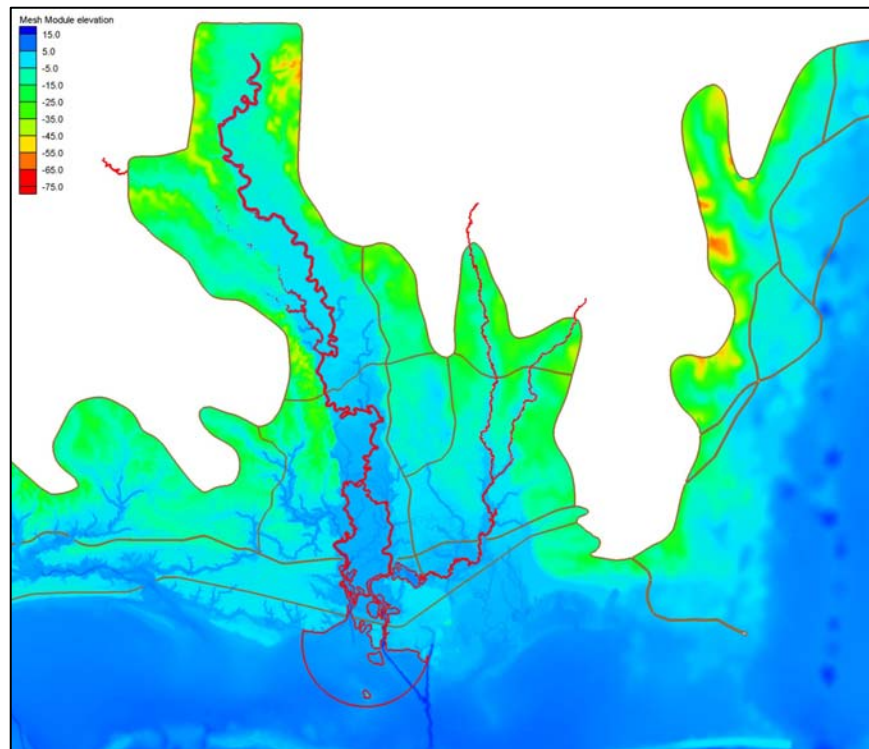


Figure 4.3 SL15 mesh (FEMA Southern Louisiana Gulf Coast Mesh) zoom into the Pascagoula River region (boundary showed in red).

As we know, accurate high-resolution topography and bathymetry are required to match the high resolution of the model. In order to examine whether the bathymetry resolution provided by the SL15 is enough to present the channel cross sections, it is necessary to compare the mesh resolution on both models. With respect to the mesh resolution, the comparison between the comprehensive Pascagoula River mesh and the SL15 mesh was made. Figure 4.4 presents the two meshes at two selected locations: the East Pascagoula River inlet and Middle Pascagoula River at Cumbest Bluff. Given the fact that the minimum element size in the SL15 mesh is 80 meters, it turns out that the SL15 has coarser elements than the preliminary Pascagoula River, which uses at least three elements to describe the channel. Since the mesh resolution in the SL15 model is lower than the preliminary Pascagoula River mesh, the SL15 might not provide enough bathymetric data to describe the channel cross sections in the preliminary Pascagoula River model. As a result, updating the model bathymetry becomes the first task to improve the Pascagoula River model. The efforts of updating the bathymetry will be discussed in Chapter 5.

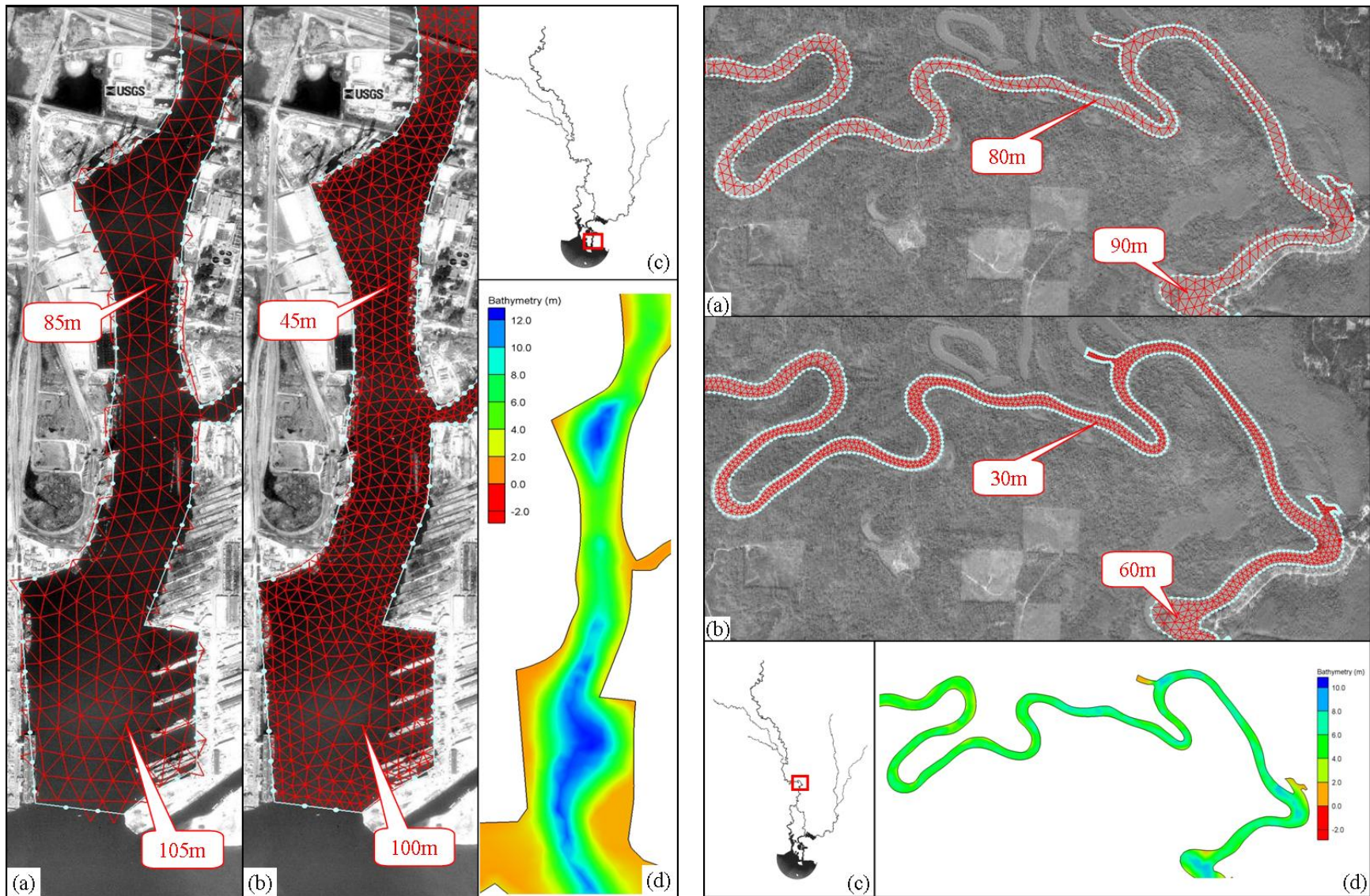


Figure 4.4 Mesh Comparison at the East Pascagoula River inlet (Left) and Cumbest Bluff, MS (Right): (a) SL15 mesh; (b) the preliminary comprehensive Pascagoula River mesh; (c) the location within the Pascagoula River model; (d) mesh bathymetry interpolated from the SL15.

Figure 4.5 & 4.6 present the preliminary comprehensive Pascagoula River mesh. It incorporates 136,676 computational points and 211,312 triangular elements. The basic meshing rule requires that there is at least three elements across each river section, which leads to high resolution in the tributaries. As shown in Figure 4.6, 71% elements are located on these tributaries (within the elliptical areas), although the total length of these tributaries is only 58% of the total channel length. All of the necessary features and flows are described in the mesh, such as barrier islands near the coastline, the marsh area between the East Pascagoula River and the West Pascagoula River.

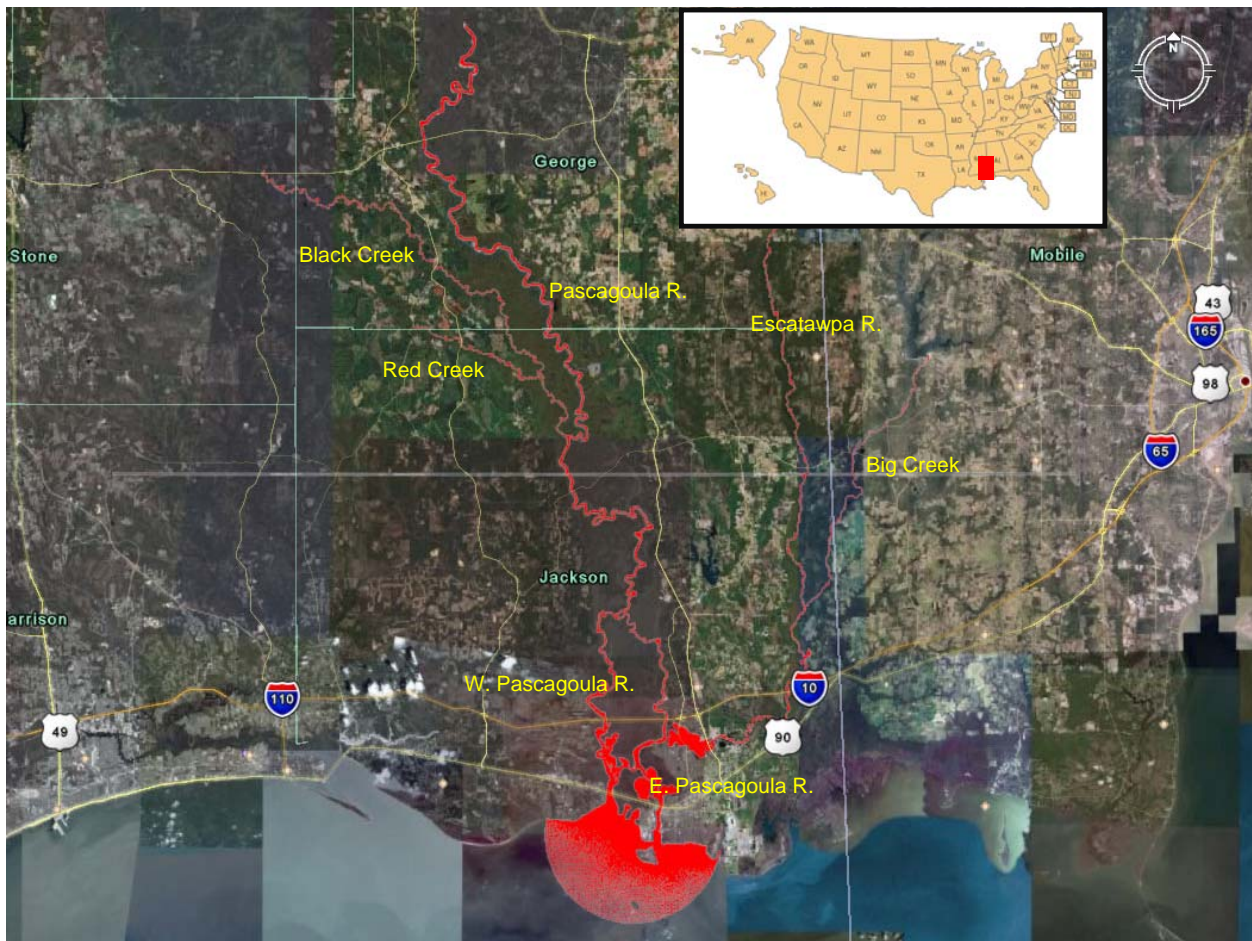


Figure 4.5 The comprehensive Pascagoula River mesh displayed on Google Earth (Version 4.3)

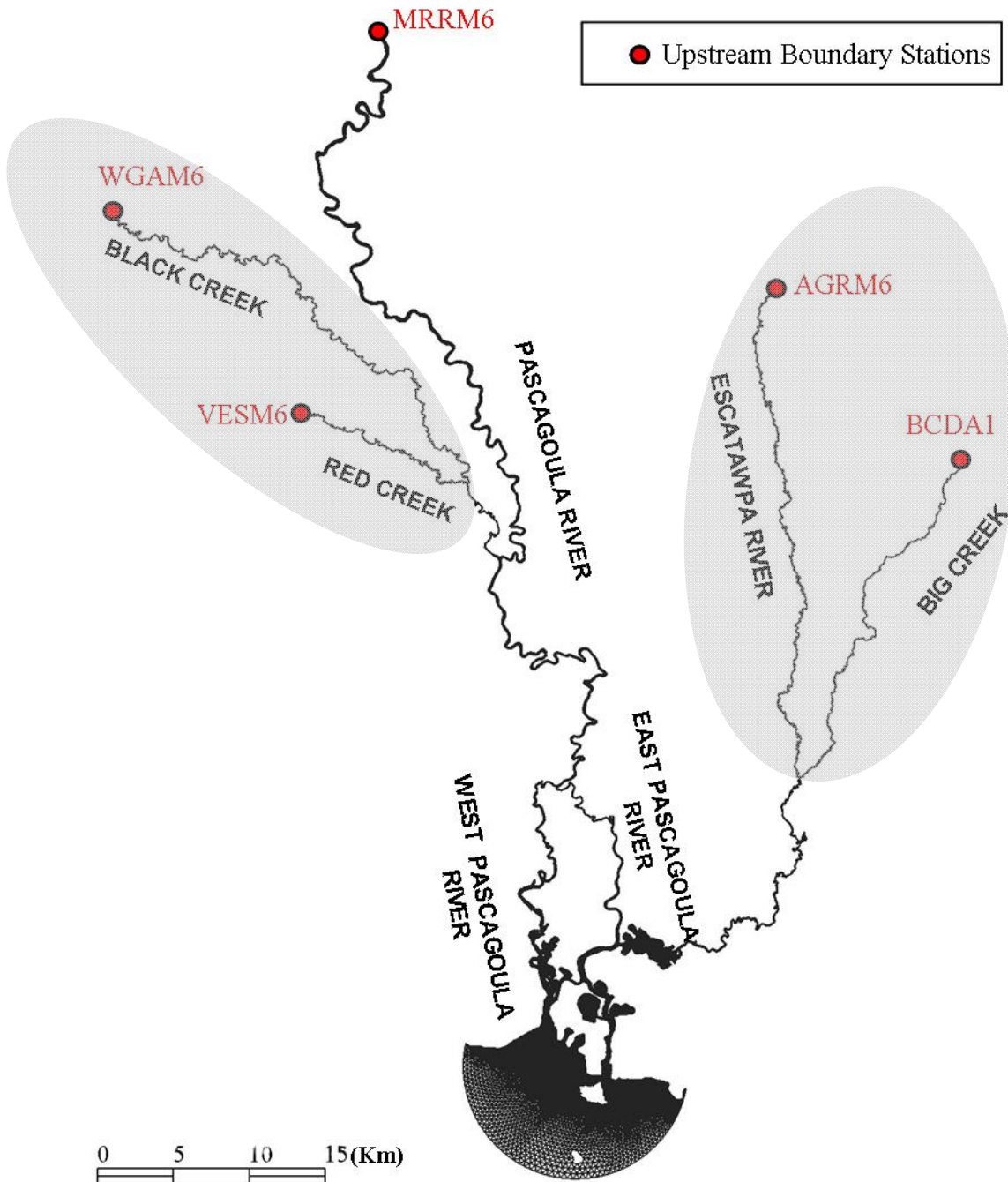


Figure 4.6 The preliminary comprehensive Pascagoula River mesh with 136,676 computational points and 211,312 triangular elements.

4.2 Mesh Adaptation and Variation

4.2.1 Mesh Adaptation

The preliminary comprehensive Pascagoula River mesh is composed of 136,676 computational points and 211,312 triangular elements. The amount of the computational nodes is considerably large considering its localized domain size. However, given the stream characteristics of the Pascagoula River basin, such mesh resolution is necessary in order to describe the bathymetry change in the meandering tributaries. Therefore, improving the computational efficiency of the mesh presents a challenge. To overcome such a challenge, the comprehensive Pascagoula River mesh was adapted, targeting the following two goals: First, reducing computational nodes; second, increasing the computational time step.

Obviously, reducing the number of nodes would directly save computation time. Furthermore, avoiding excessively small elements will allow the model to use a larger time step, according to the Courant number criterion. In computational fluid dynamics, the Courant-Freidrichs-Lewy condition (or shortened form: the Courant number) is a control criterion for model stability and convergence while solving partial differential equations numerically (e.g. GWCE). The suggested range of Courant number in ADCIRC model is (Westerink, Blain et al., 1994):

$$C_{\#} = \sqrt{gh}(\Delta t / \Delta x) \leq 1.0 \dots\dots\dots (4.1)$$

where h is the bathymetry depth, g is the gravitational acceleration; Δt and Δx are the computational time step and nodal spacing respectively.

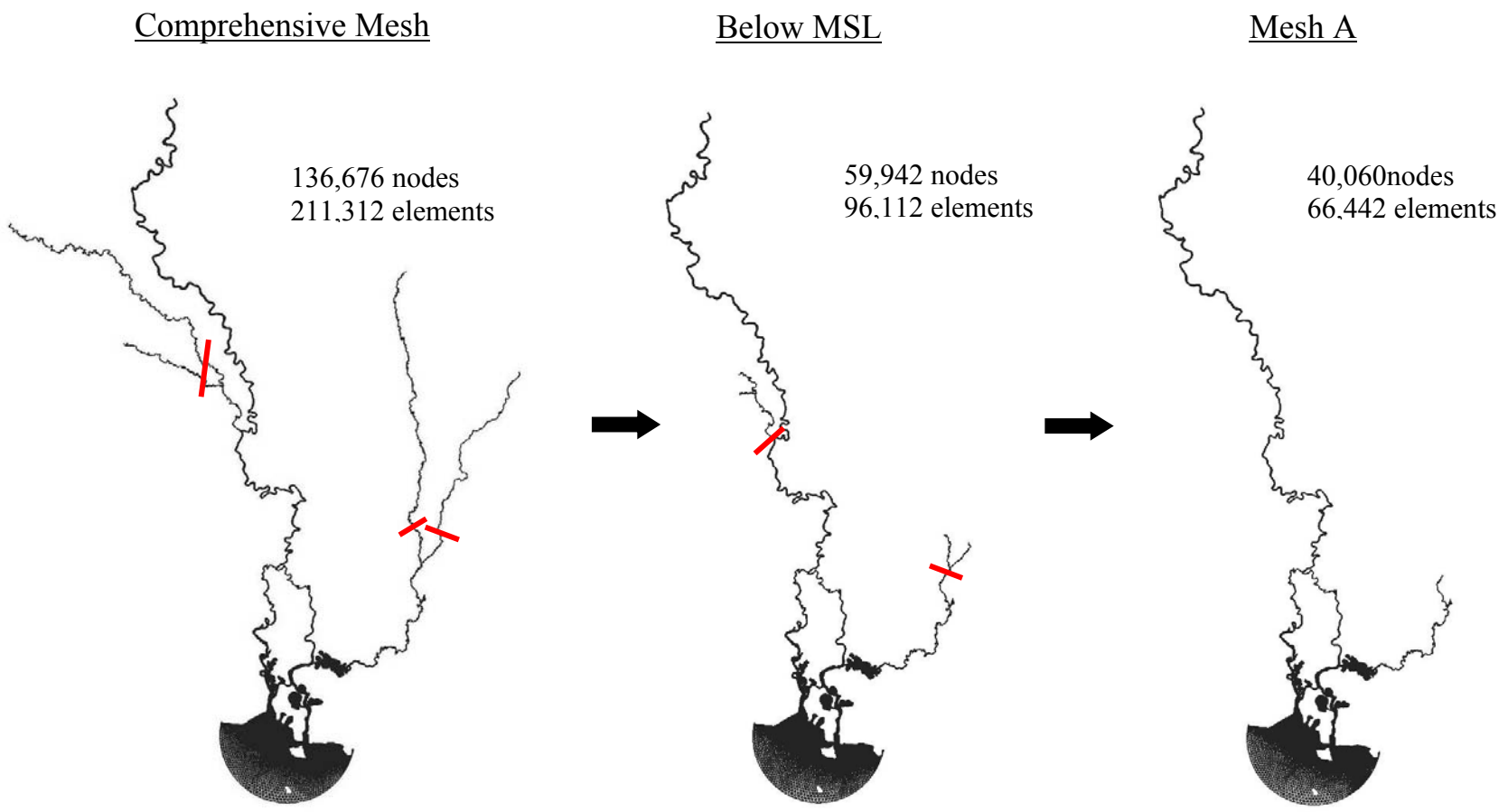


Figure 4.7 Mesh adaptation of the comprehensive Pascagoula River inlet-based mesh

According to the two goals, mesh adaptation was completed by taking the following steps. First, remove the tributaries above Mean Sea Level; second, remove high-resolution tributaries. By doing such adaptations, the computational expense of the Pascagoula River model was dramatically improved, while the key features of the study region were conserved. Figure 4.7 presents the two-step procedure of mesh adaptation. The final product – Mesh A includes 40,060 computational nodes and 66,442 triangular elements, both of which are less than one third of the original comprehensive mesh.

4.2.2 Mesh Variation

During the development of the preliminary Pascagoula River model, the marsh area between the two inlets attracted our attention. As a complex economical and hydrodynamic system, the marsh area and the two inlets are important to the tidal propagation and tidal currents, as well as the understanding of how the tides interact with the fresh water (See Figure 4.8).

In order to better understand the physics of the Pascagoula River inlet system, additional two meshes were developed based on Mesh A. The objective of building three different Pascagoula meshes was to investigate the importance of the two inlets (East Pascagoula River and West Pascagoula River), which could benefit the future model development. As displayed in Figure 4.9, the three meshes are identified as Mesh A, Mesh B and Mesh C. Mesh A provides a good description of both inlets, using 40,060 computational nodes and 66,442 triangular elements. Mesh B only includes the East Pascagoula inlet and part of its tributary named Escatawpa River.

Mesh C only includes the West Pascagoula inlet and has the smallest computational nodes and elements. All three inlet-based Pascagoula River meshes were completely developed, and become the first set of preliminary models which could be simulated by ADCIRC-2DDI.

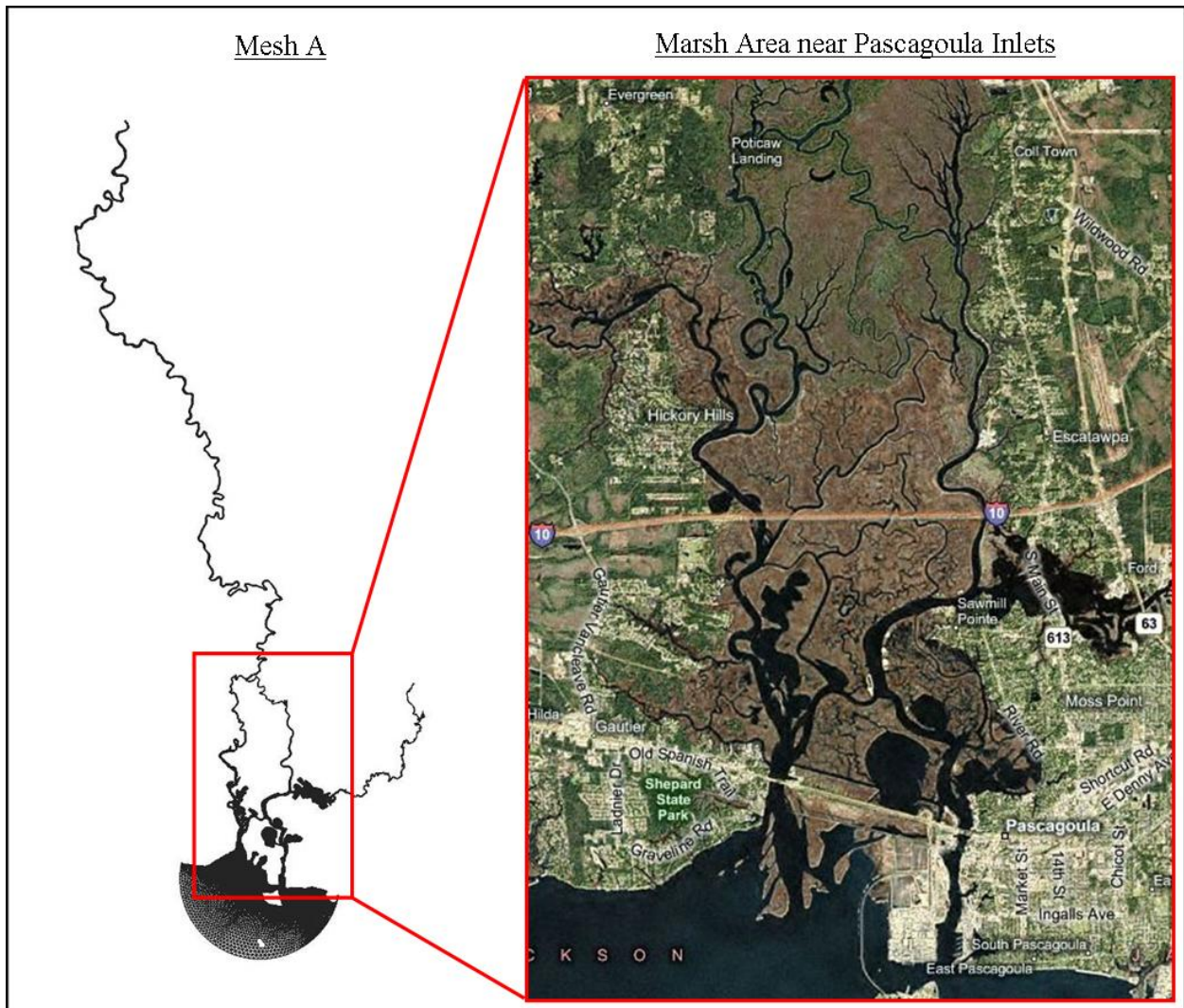


Figure 4.8 Zoom into the marsh area located near the Pascagoula inlets

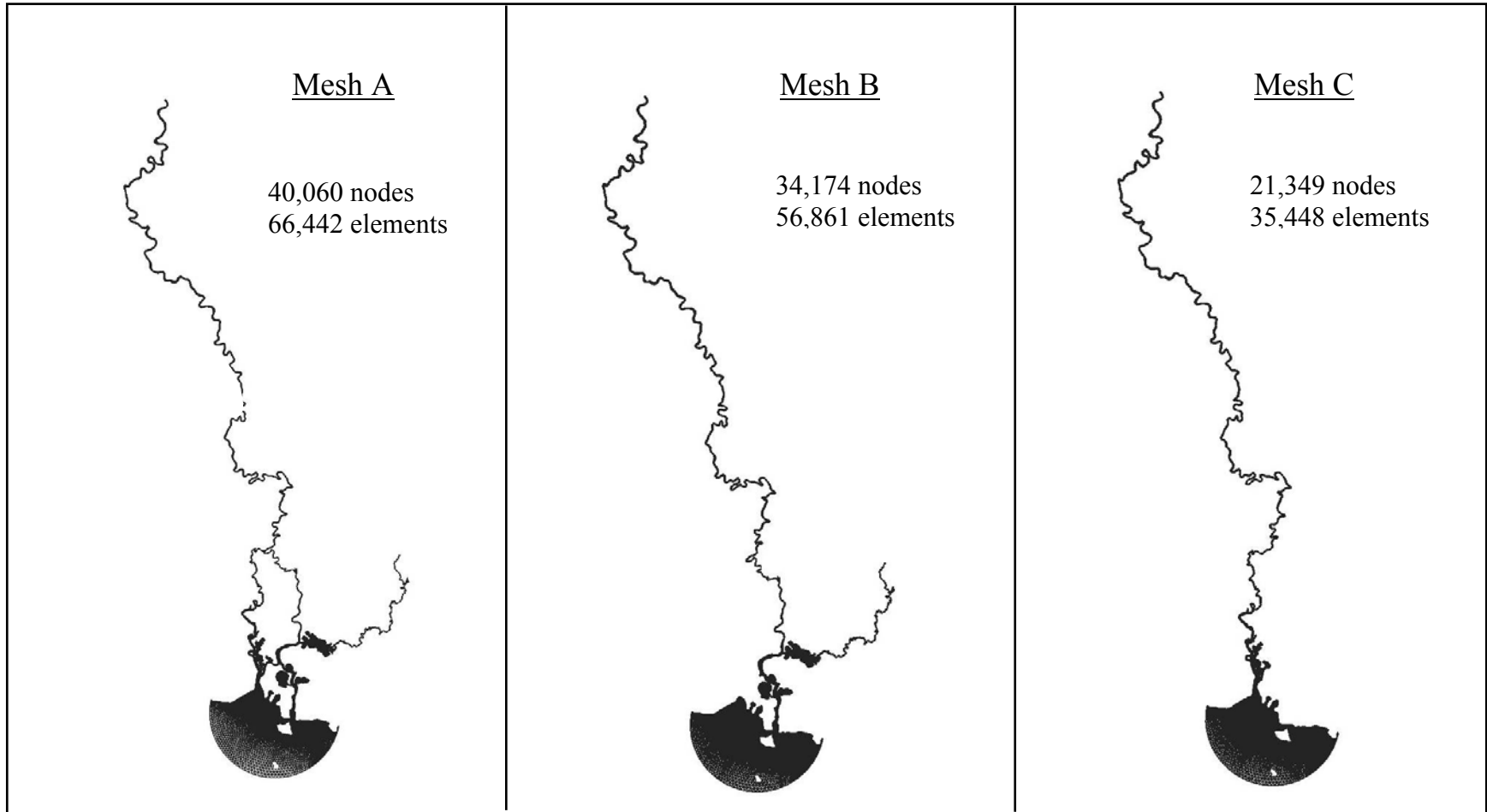


Figure 4.9 Variations of the Pascagoula River inlet-based meshes
(Mesh A: both inlets; Mesh B: only the East Pascagoula inlet; Mesh C: only the West Pascagoula inlet.)

4.3 Model Setup

The model setup of the inlet-based meshes (Mesh A, B & C) is discussed in this section. Identical astronomic tides are simulated in all the three inlet-based models for equal comparison. Hence, the model parameters and open boundary forcings remain the same in the three models. In ADCIRC simulations, the model parameters and open boundary forcings must be assigned in the input file called the Model Parameter and Periodic Boundary Condition file (fort.15). Model output settings, such as water elevation and velocity output locations, are also specified in the same input file.

4.3.1 Open Boundary Assignment

In order to run the inlet-based tidal models, the open boundary forcings at the inlet boundary need to be specified in the ADCIRC Model Parameter and Periodic Boundary Condition file. The method to obtain a good description of the tidal boundary conditions is to utilize the unstructured, 53K finite element WNAT mesh (See Figure 2.3). First, the WNAT model domain is forced with seven tidal potential forcings at 60° west meridian, and then the tidal harmonic constituents at the Pascagoula mesh boundary are extracted. These will then be applied as the open water boundary condition for the inlet-based models (See Figure 4.10).

Seven tidal constituents, K1, O1, M2, S2, N2, K2, and Q1, are used to force the WNAT model (Table 4.2). They are ramped over 10-day period. The whole simulation lasts 45 days with a time step of 1.25 seconds in order to ensure the model stability and accuracy.

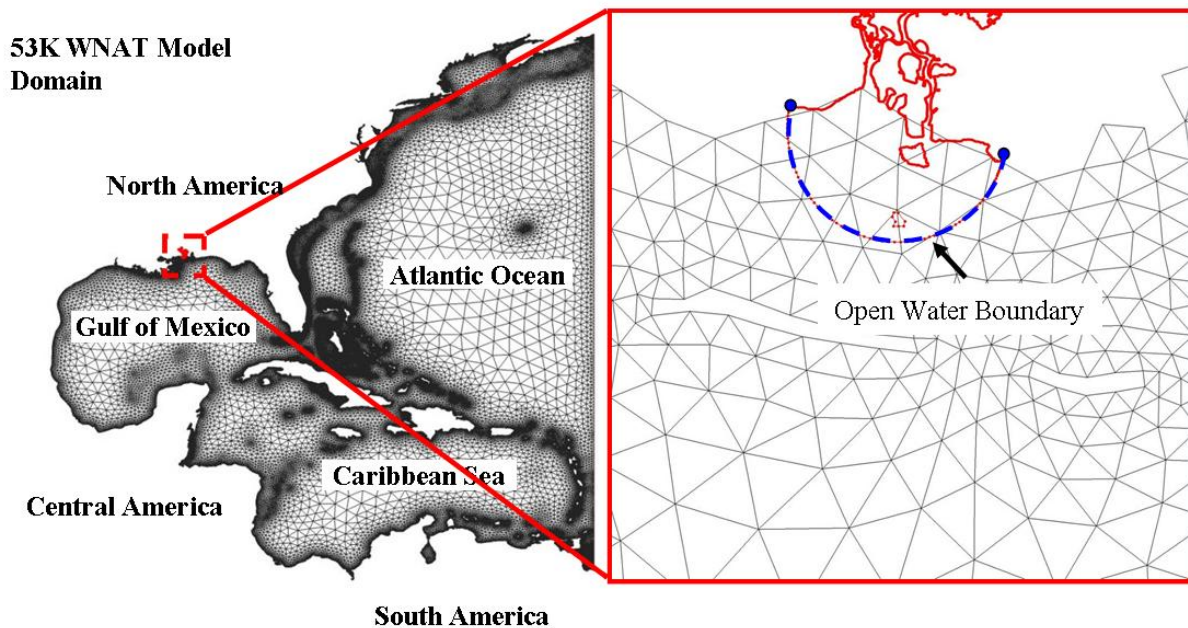


Figure 4.10 Open boundary assignment (Left: 53K WNAT model; Right: Open water boundary of the inlet-based Pascagoula River models)

Table 4.2 Tidal Constituents used to force the ADCIRC model

| <i>Constituent</i> | <i>Name</i> | <i>Period (hr)</i> | <i>Frequency (rad/s)</i> |
|--------------------|-------------------------------|--------------------|--------------------------|
| K1 | Luni-solar diurnal | 23.93 | 0.000072921158358 |
| O1 | Principal Lunar Diurnal | 25.82 | 0.000067597744151 |
| M2 | Principal Lunar Semidiurnal | 12.42 | 0.000140518902509 |
| S2 | Principal Solar Semidiurnal | 12.00 | 0.000145444104333 |
| N2 | Larger Lunar Elliptic | 12.66 | 0.000137879699487 |
| K2 | Luni-solar Semidiurnal | 11.97 | 0.000145842317201 |
| Q1 | Larger Lunar Elliptic Diurnal | 26.87 | 0.000064958541129 |

Meteorological forcings are not considered in this report. However, the meteorological forcing file is one of the input files for the ADCIRC storm surge model, which contains the wind stress and pressure data at specified time intervals. Takahashi (2008) presents the second report of the Pascagoula River project, which provides more detail on storm surge simulation.

4.3.2 Model Parameterizations

The astronomical tides model was built up within the Cartesian coordinate system, and the wetting and drying algorithm was applied. In the circumstances where the water depth is less than the minimum bathymetric depth, the computational nodes and their corresponding elements are considered to be dry. Spatially variable Coriolis force was considered. The advection terms in the governing equations were turned on or off to examine the model sensitivity. Bottom friction was computed by using the hybrid bottom friction formulation (Equation 3.10). The bottom friction coefficient C_f is defined as: $C_f = C_{fmin} [1+(H_{break} / H)^\theta]^\lambda$, where $C_{fmin}=0.0025$, break depth $H = 10\text{m}$, and dimensionless parameters $\theta=10$ and $\lambda=1/3$ (Murray, 2003). The horizontal eddy viscosity coefficient is set at 5m/s.

The astronomic tidal simulation was set to begin from the beginning of a tidal epoch, simulating a period of 60 days. The tidal boundary forcings were ramped over 20 days, according to a smooth hyperbolic tangent ramp function. By calculating the Courant number, the time step for the model was set at 0.5 seconds. Harmonic analysis was performed on last 30 days of the simulation results, considering 23 tidal constituents assigned in ADCIRC harmonic analysis utility. Meanwhile, global elevation and velocity in time-series were specified as model output.

4.4 Preliminary Model Results

Tidal resynthesis analysis was applied to qualitatively and quantitatively evaluate the tidal model performance. The analysis is presented into two major steps: First, historical tidal constituents were extracted from the available historical water elevation records. Second, tidal resynthesis was performed on both historical and model tidal signals, which allowed the comparison of water surface elevation between historical data and model results. The tidal signals are resynthesized through the superposition of multiple waves (See Equation (2.2)). A time period of a complete spring-neap tidal cycle (14 days) is considered.

Seven monitoring gauge stations are identified within the Pascagoula River model domain. Two of them are National Ocean Service (NOS) stations and the other five stations are USGS water level stations. Their locations within the model domain are presented in Figure 4.11. As shown, the four gauge stations near the coast cover the Pascagoula River inlet region well. The remaining three gauge stations are located further upstream on the Escatawpa River and the Pascagoula River. At the NOS stations, 37 tidal constituents were obtained from the historical data resynthesis. At the USGS stations, USGS water level data with a total length of 31-day were utilized to perform the harmonic analysis. 35 tidal constituents were considered in a least-squares fitting procedure called T_TIDE (Pawlowicz, Beardsley et al., 2002). Frequency range of the resulting harmonics was from fortnightly to eight-diurnal (See Appendix A). After harmonic analysis was performed, the historical water elevation was then adjusted by including the vertical

datum and Time Zone differences; therefore, the historical records can be compared with the ADCIRC model results under the similar circumstances.

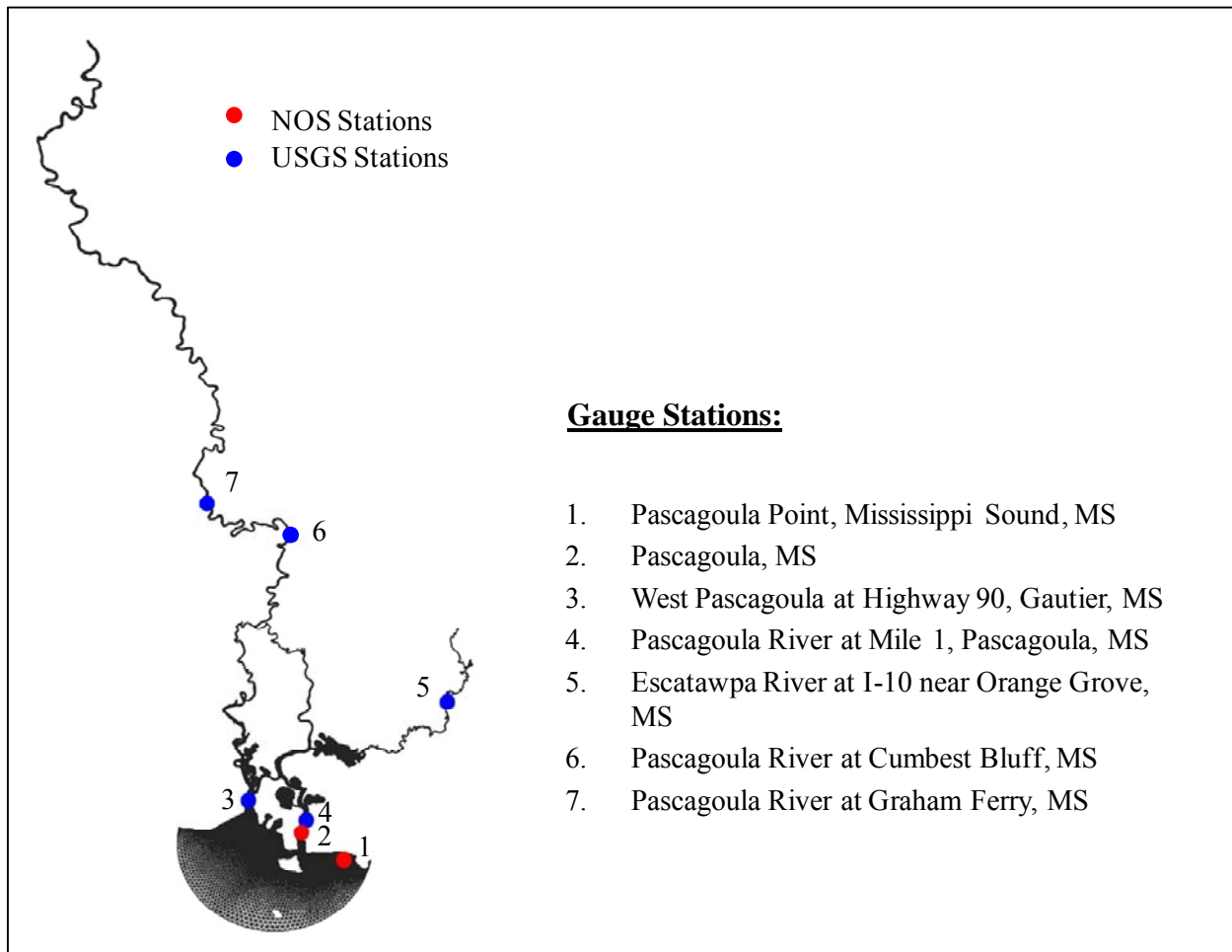


Figure 4.11 The historical gauge stations within the Pascagoula River model domain

The tidal results in ADCIRC employ 23 tidal constituents listed in Appendix C. The results of the 14-day resynthesis analysis on Model A, B and C are shown in Figures 4.12 - 4.15. The x-axis is the 14-day time frame, starting from the beginning of a tidal epoch. The y-axis is the

water elevation in meters. The vertical datum used herein is North American Vertical Datum of 1988 (NAVD 88).

Overall, the preliminary simulations demonstrate a good working model that produces reasonable results (Figures 4.12 – 4.15). The model tidal signals fit well with the historical records at the coastal stations, such as the station located at Pascagoula and the one at Pascagoula Point. However, there are several discrepancies observed at other stations. The model over-predicts the tidal amplitudes at the station on the West Pascagoula during the last 7 days of the spring-neap cycle. Also, at the three upstream stations (Pascagoula River at Graham Ferry, Pascagoula River at Cumbest Bluff, and Escatawpa River near Orange Grove), the model under-predicts both the peaks and troughs. Overall, the phases of the modeled tidal signals at these stations match quite well with the historical resynthesis results. Such discrepancies reveal the existence of different errors in the model. One the obvious reason for the inaccuracies is the incompleteness of the bathymetric data and the lack of fresh water flows from upstream. The next two chapters will primarily deal with the bathymetry improvements on these preliminary models, as well as the consideration of bottom friction calibration.

By comparing the tidal signals among Model A, B and C, the following conclusions are drawn out. First, Model A and Model C perform similarly when simulating the main channel of the Pascagoula River. However, it is important to include both inlets as Model A does. Second, by comparing Model B to Model C at the upstream stations, it is evident that the west inlet of the Pascagoula River is more dominant than the east inlet.

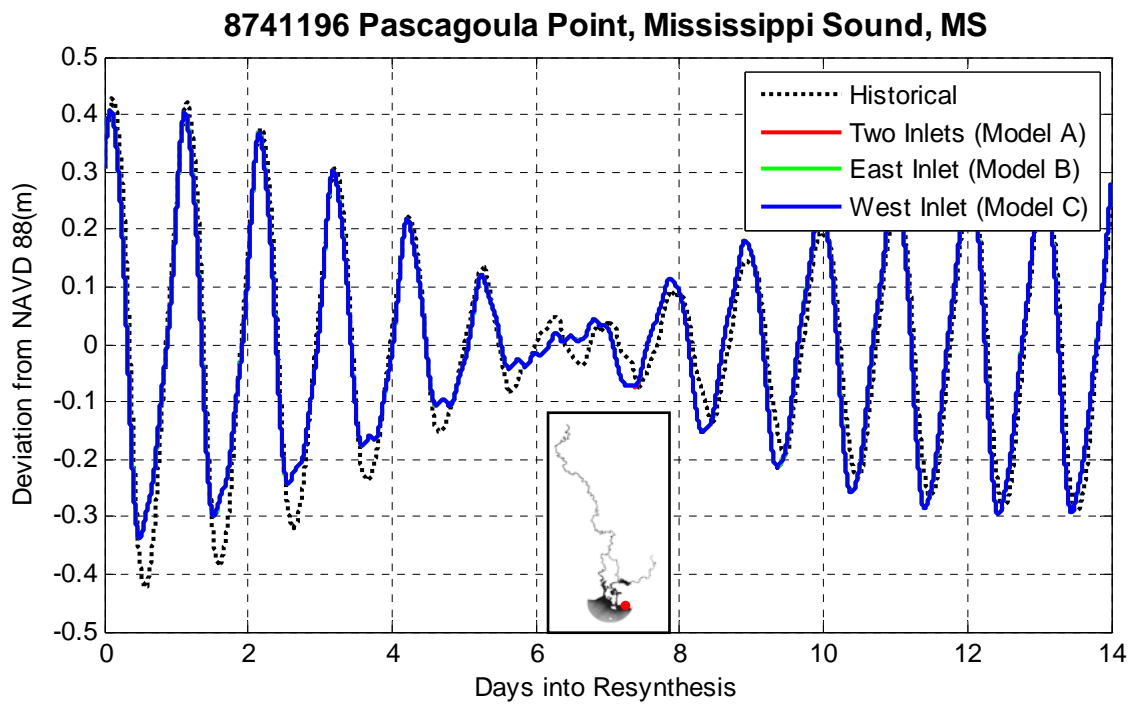
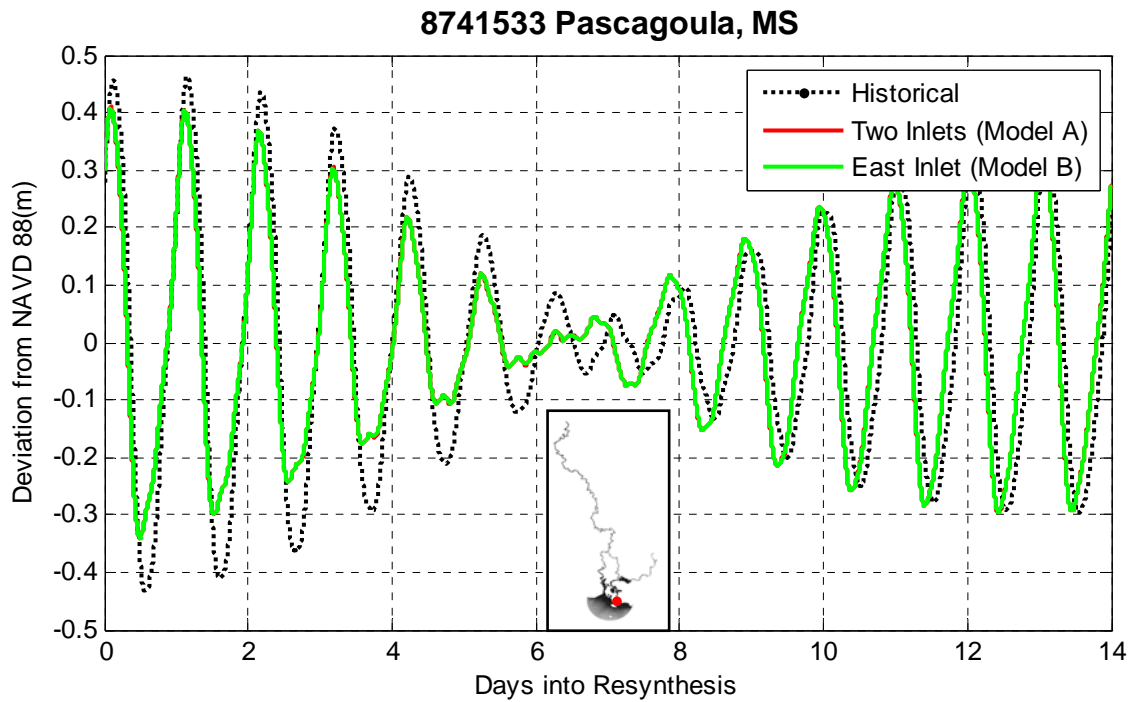


Figure 4.12 Resyntheses of historical and model tidal constituents, corresponding to the stations located at Pascagoula, MS and Pascagoula Point, Mississippi Sound, MS.

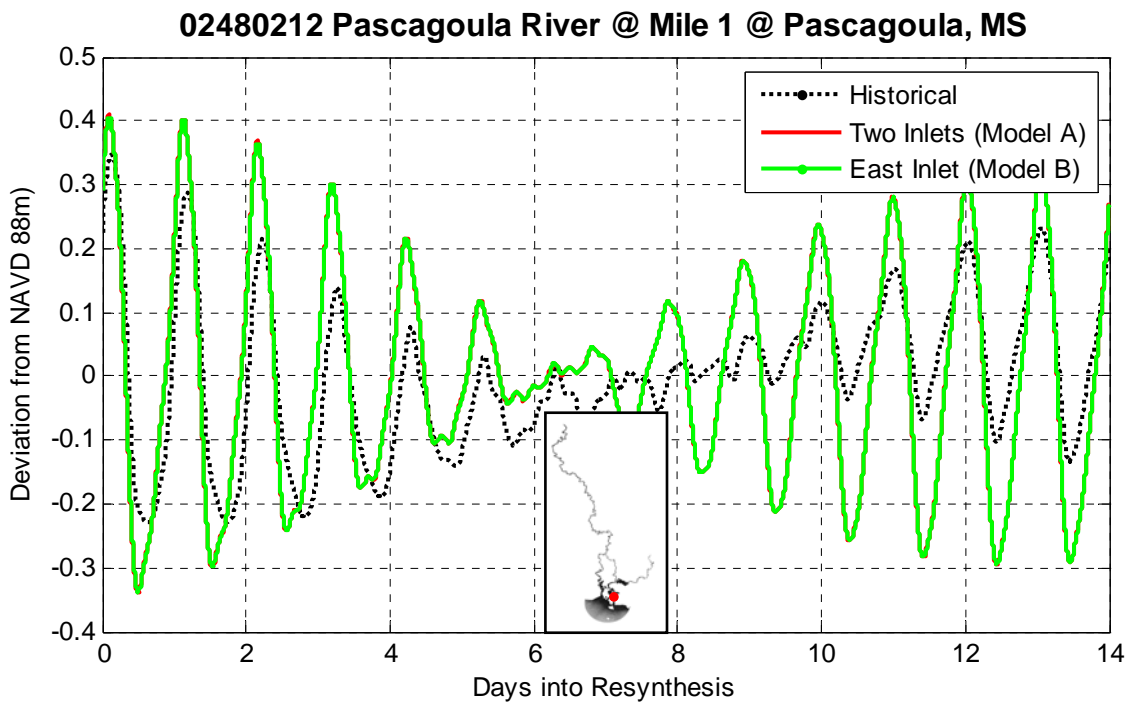
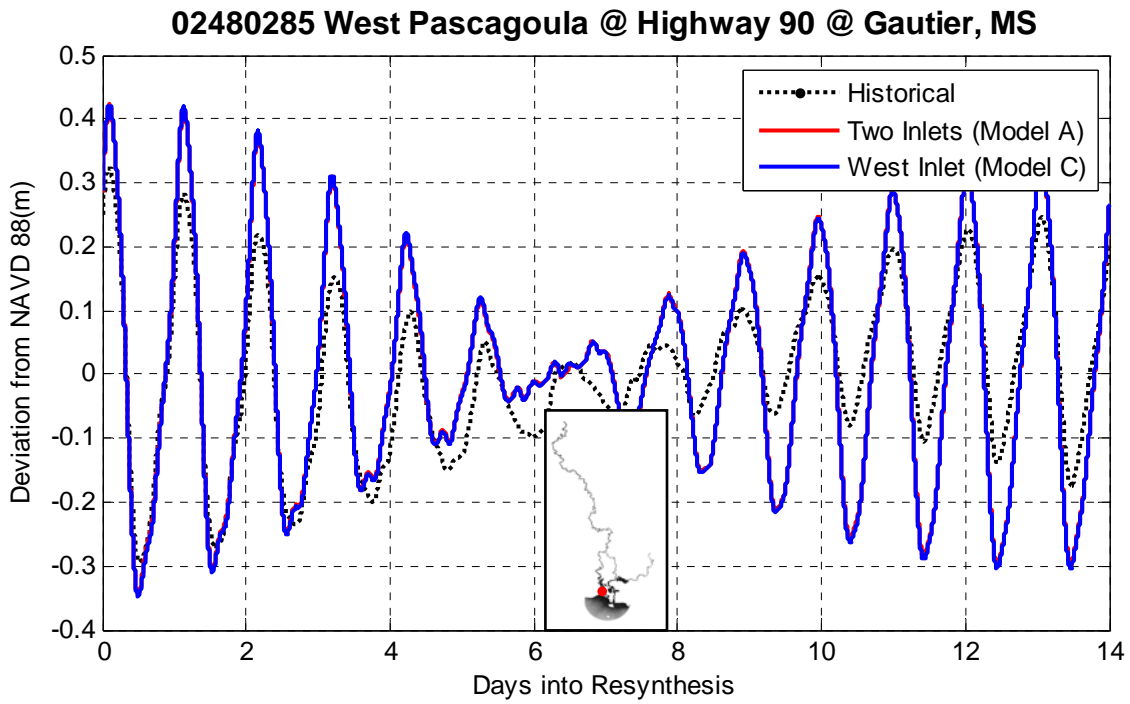


Figure 4.13 Resyntheses of historical and model tidal constituents, corresponding to the stations located at West Pascagoula at Gautier, MS and Pascagoula River Mile 1, MS.

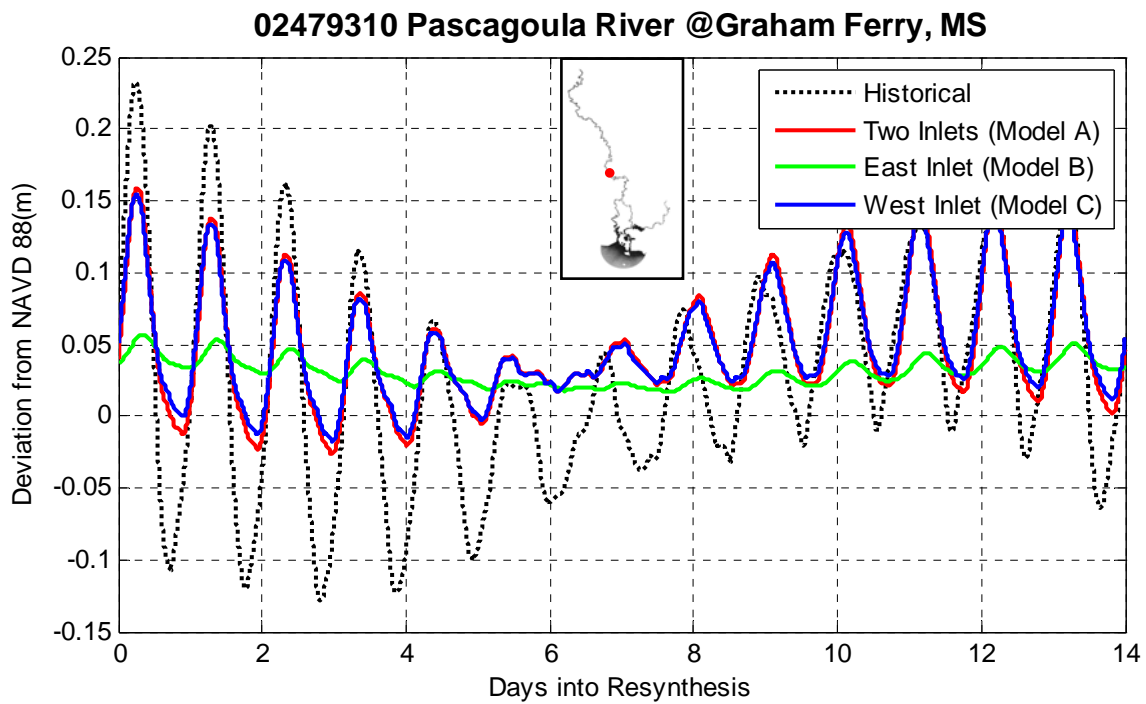
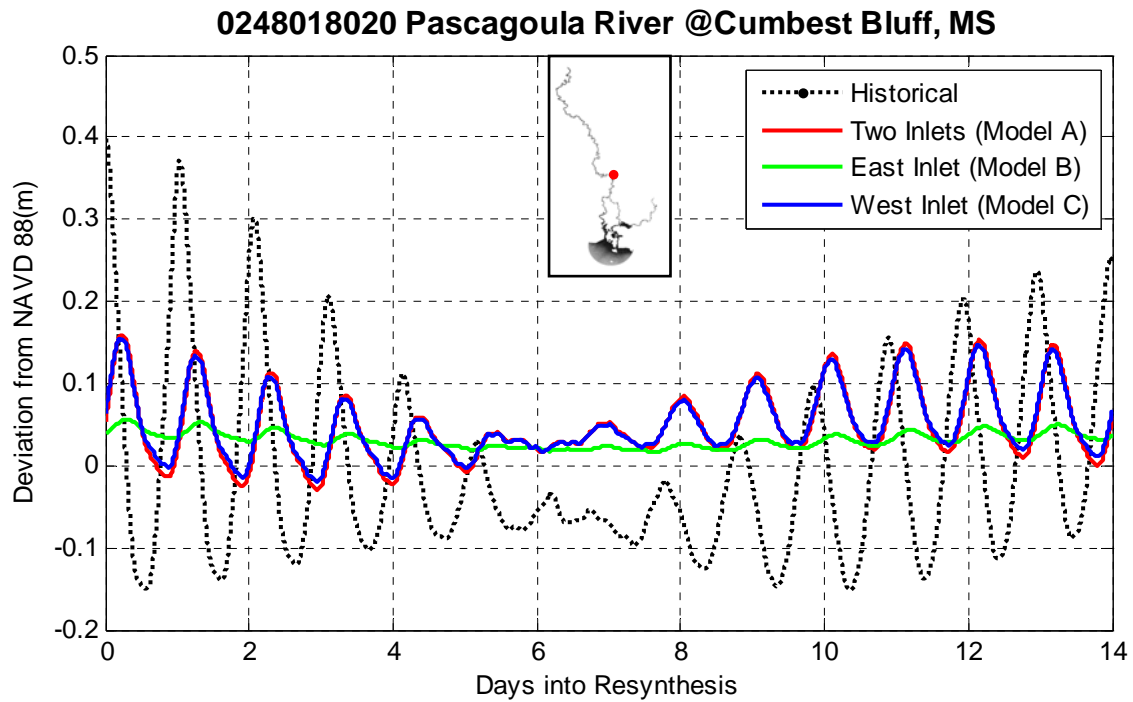


Figure 4.14 Resyntheses of historical and model tidal constituents, corresponding to the stations at Pascagoula River at Cumbest Bluff and Graham Ferry, MS.

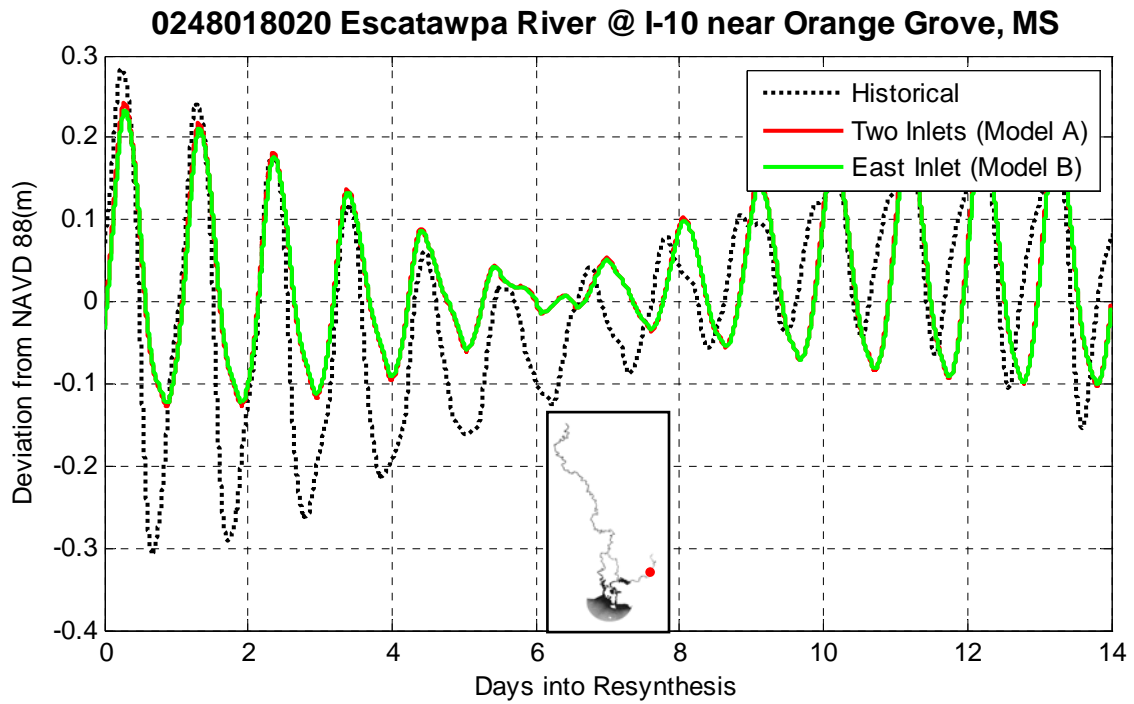


Figure 4.15 Resyntheses of historical and model tidal constituents, corresponding to the station located at Escatawpa River at I-10 near Orange Grove, MS.

4.5 Model Domain Verification

The previously presented preliminary model results were from an inlet-based Pascagoula River domain bounded by a semi-circular arc with a 500 meter radius. Although the open boundary assignment was generated through the WNAT tidal domain, the WNAT tidal domain did not include the local Pascagoula domain. It is suspected that interactions between the local domain and the ocean domain may exist. As a result, the inlet-based model domain was further examined by incorporating the local Pascagoula River model into the WNAT model domain. Figure 4.16 displays a WNAT + Pascagoula model domain, where WNAT model was modified to incorporate the local Pascagoula River model (Model A). To compensate for the nodal spacing discrepancy between the WNAT model and the local model, the nodal spacing was smoothly transitioned from three kilometers down to 400 meters. Furthermore, the barrier islands located in the Mississippi Sound are better described due to the higher resolution in the transition area.

The WNAT + Pascagoula model has been similarly set up as described in Section 4.3. The model results are presented in the same format as the preceding section. Figures 4.17 and 4.18 display the tidal resynthesis comparison between the WNAT + Pascagoula model and Model A at three gauge stations. Overall, the water elevation changes at the gauge stations are almost identical to the results generated by Model A. This indicates that at the semi-circular boundary, the tidal signals are very close to those generated by the WNAT tidal domain. It also means that the open boundary assignment of Model A is very reasonable. Therefore, we suggest that researchers continue to use the inlet-based boundary instead of the WNAT + Pascagoula domain, from a computational efficiency point of view.

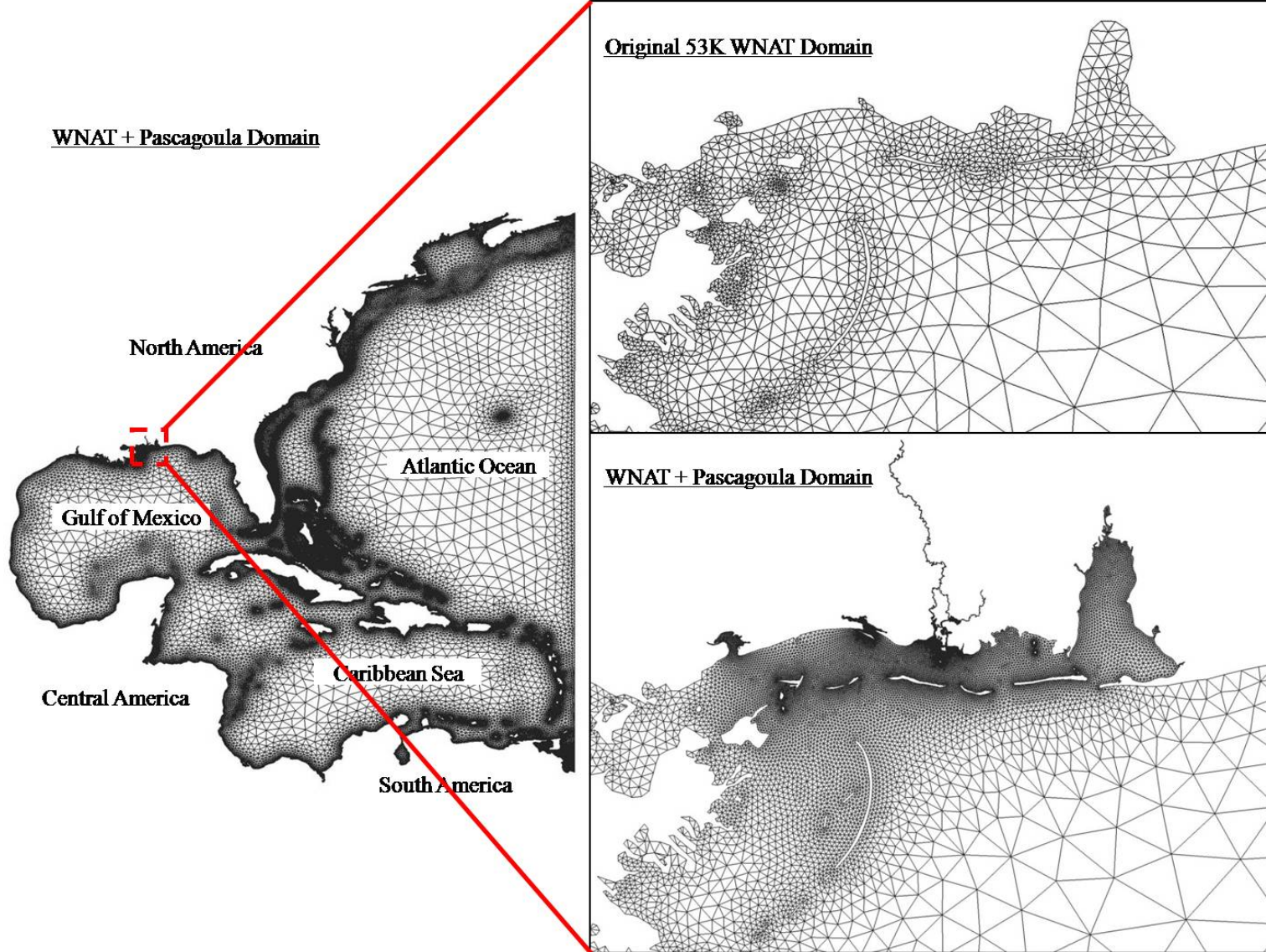


Figure 4.16 Finite element mesh of the WNAT + Pascagoula model, compared to the Original 53K WNAT model domain

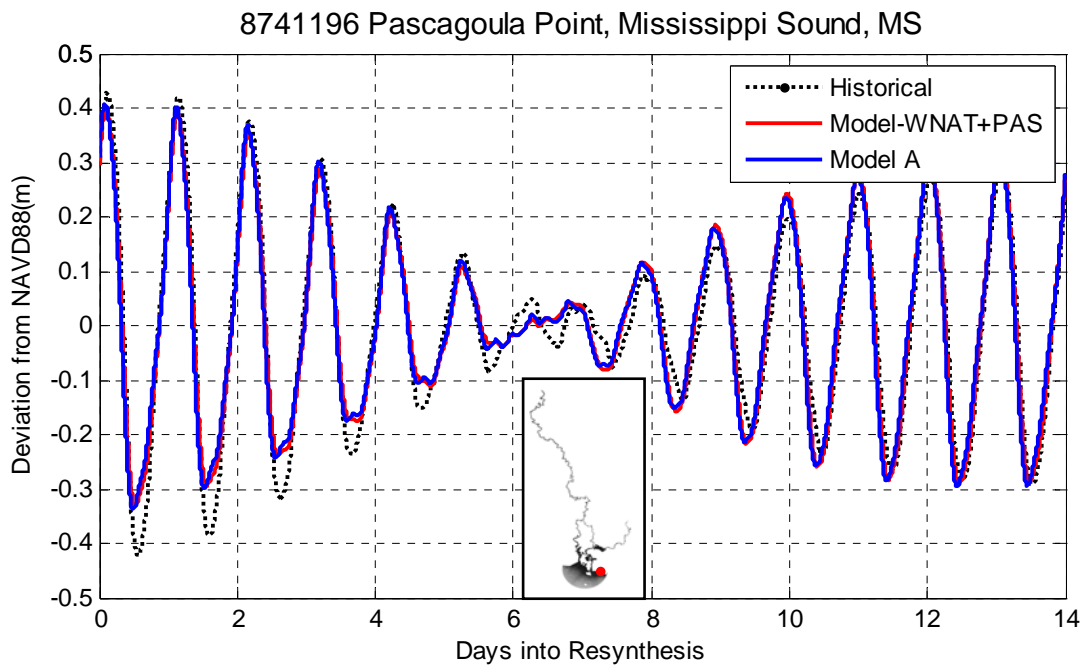
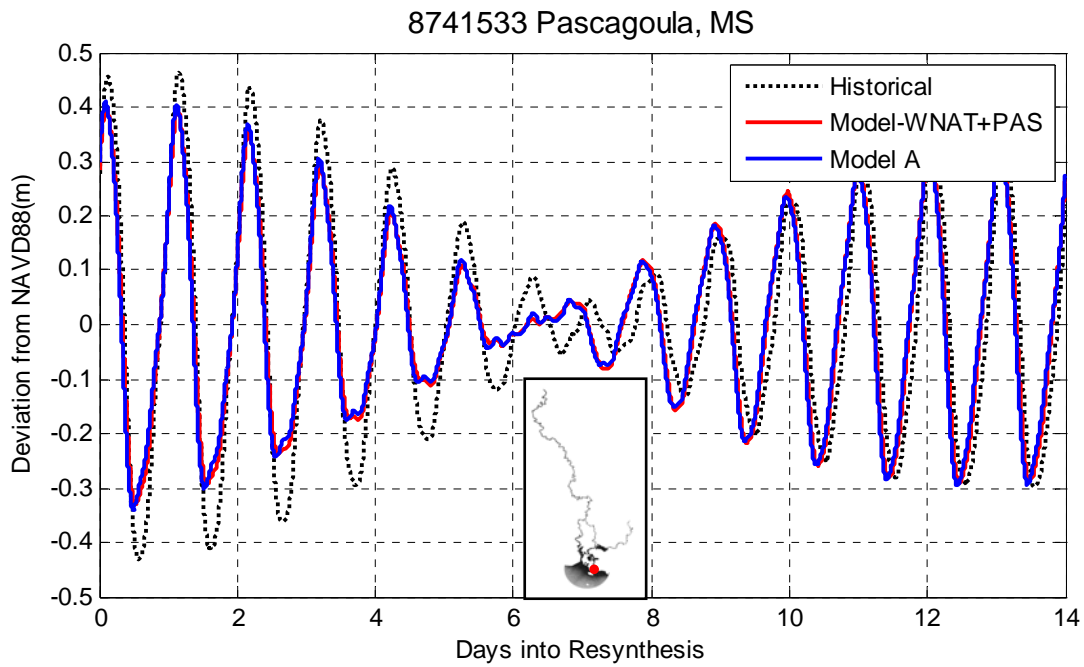


Figure 4.17 Tidal resynthesis analysis plots at two Pascagoula stations, comparing the WNAT + Pascagoula model and the Model A.

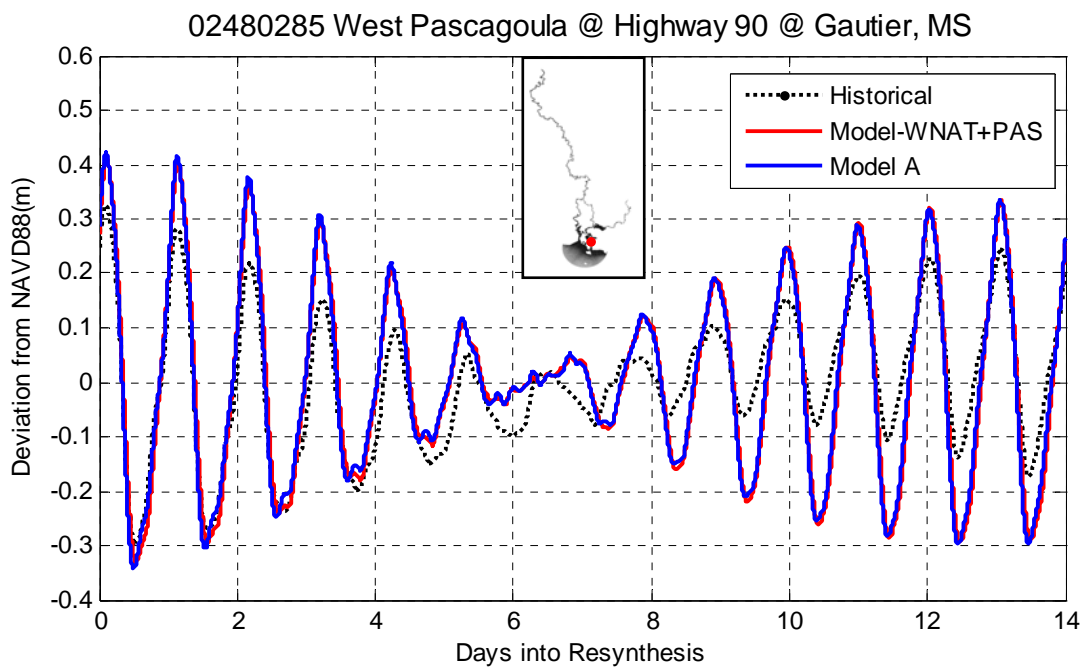
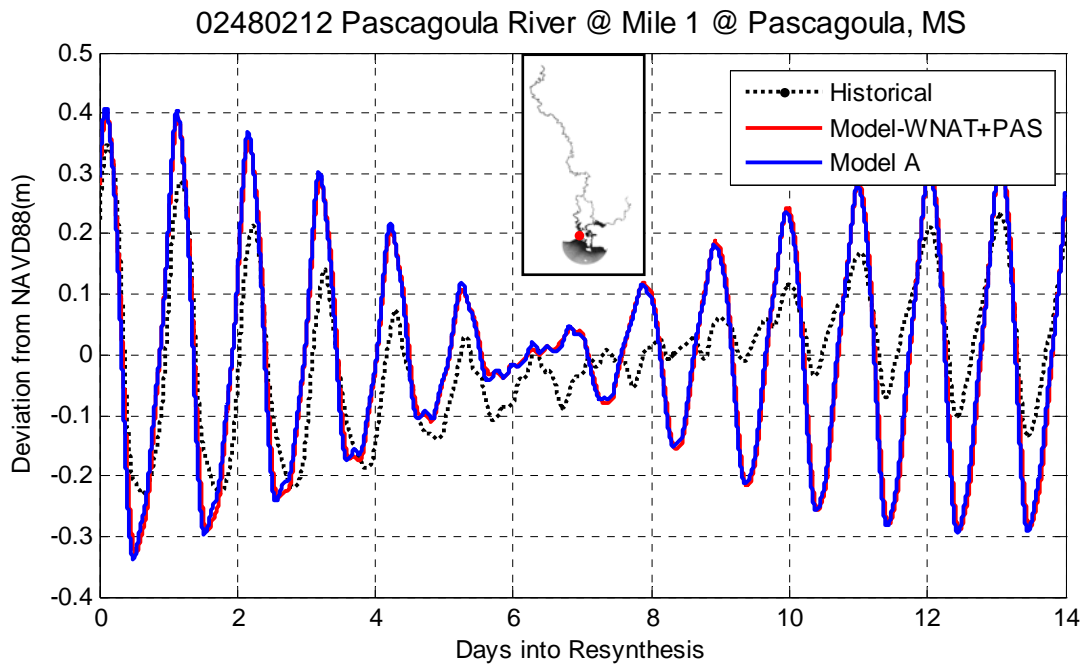


Figure 4.18 Tidal resynthesis analysis plots at two Pascagoula stations, comparing the WNAT + Pascagoula model and the Model A.

CHAPTER 5. BATHYMETRY IMPROVEMENTS TO THE ASTRONOMIC TIDE MODEL FOR THE PASCAGOULA RIVER

It is recognized that bathymetry variation has an effect on tidal currents and tide propagation. Accurate high-resolution topography and bathymetry are required to meet the high resolution of the finite element model in near-shore regions (Jones and Davies, 2007). As stated in Chapter 4, the preliminary Pascagoula River model used bathymetry from the SL15 mesh; however, the SL15 mesh had lower resolution than the Pascagoula River mesh in most mesh locations. In an attempt to improve the preliminary model, more comprehensive bathymetric data were incorporated into the Pascagoula River model so that the natural bathymetry could be matched by the mesh resolution.

This chapter starts with a comprehensive presentation of the available bathymetric data sets from different sources. The variety of data format and datum gives us a challenge to update the 2D model properly. To overcome the difficulty in using the cross section data, the Cross Section Interpolation Toolbox is developed for interpolating 1D cross section data into a 2D model. The toolbox is introduced in a separate section, followed by the two examples of bathymetry interpolation. Finally, the preliminary model is updated by using the demonstrated Cross Section Interpolation Toolbox. The simulation of the bathymetry updated Pascagoula River model shows some significant improvements in the results.

5.1 Description of Bathymetry Data

The new bathymetric data imported to update the preliminary Pascagoula River model were obtained from the LMRFC (Lower Mississippi River Forecast Center). The data were collected by several sources over a long time span. It is necessary to document these different bathymetric data sets, such as the data type, data coverage, data history and horizontal/vertical datum; a good investigation and summarization of the available data sets can aid in the implementation of the data into the model. Hence, the bathymetric data are briefly summarized in Table 5.1. Following that, the different data sets are compared in more detail.

Table 5.1 Summary of the Pascagoula River bathymetric data sets

| Data Source | #1 USGS Survey | #2 Mobile Hydrographic Survey | #3 NOS Hydrographic Survey |
|------------------|---|---|---|
| Area Coverage | Pascagoula River Escatawpa River Black Creek Red Creek | Lower East Pascagoula River extending to the gulf Lower Escatawpa River | Lower Pascagoula River Lower Escatawpa River Mississippi Sound Biloxi Bay, Grand Bay |
| Data Format | 51 cross sections in “Distance from river bank vs. Elevation” | High density scatter points in (x,y,z) | High density scatter points in (x,y,z) |
| Horizontal Datum | No Geo-reference River miles provided | State Plane NAD83, Mississippi East Zone | Geographic NAD 83 |
| Vertical Datum | NGVD29 | NGVD29 / NAVD88 | NAVD88 |
| Survey Date | 1980 - 2005 | April - June, 2007 | 1917 - 1989 |

The first source of the bathymetry data obtained from the LMRFC consisted of 51 cross sections located at various points in the river basin (called #1 USGS survey in Table 5.1). In order to better understand the complex estuarine and tide-affected riverine system in the Pascagoula River, USGS surveyed the lower 35 miles of the Pascagoula River to collect channel geometry data including channel-bed cross sections (up to Graham Ferry). These channel-bed cross sections were surveyed by boat with a graphical fathometer and geo-referenced by using the grade Global Positioning System (GPS). These data were then digitized into a Geographic Information System (GIS). Most of the cross sections presented here were obtained from that USGS study during 1993 to 1995 (Turnipseed and Storm, 1995). Figure 5.1 presents the cross sections in the lower Pascagoula River basin. In the main channel including the East Pascagoula River and West Pascagoula River, 36 cross sections are densely spread along the lower 35 miles of the Pascagoula River; the remaining two cross sections are located upstream between Graham Ferry and Merrill (a distance of 44 miles). Meanwhile, 13 cross sections are identified in the four tributaries: nine cross sections in Escatawpa River, two cross sections in Black Creek and two cross sections in Red Creek.

USGS survey data well covered the lower Pascagoula River. However, its horizontal datum was in river miles with no geo-reference. But the locations of the cross sections were built in the GIS, so we were still able to identify the locations within the ADCIRC model. The second bathymetric data source (called #2 Mobile Hydrographic Survey in Table 5.1) was obtained from U.S. Army Corps in Mobile District (accessed from <http://navigation.sam.usace.army.mil/surveys/index.asp> on January 8, 2008). The up-to-date data

was surveyed in 2007. The bathymetric data were downloaded in the format of scatter points with (x,y,z) values, which can be easily read in SMS. However, limited coverage is the disadvantage of this data set, as it only describes the geometry near the coast and part of the Escatawpa River dredging channel. The third data source (called #3 NOS Hydrographic Survey in Table 5.1) is from the NOS online survey database (accessed from http://map.ngdc.noaa.gov/website/mgg/nos_hydro/viewer.htm on April 11, 2008). It includes dozens of surveys over the Lower Pascagoula River, Lower Escatawpa River, Mississippi Sound and its adjacent bays. The data were surveyed during the 1910s to the 1980s without any substantial quality control. The data format is similar to the Mobile hydrographic survey data.

Since the data sets overlap with each other at East Pascagoula River and Lower Escatawpa River, several locations were selected to verify the accuracy of the bathymetric data by comparing different data sets at the same location. The plots of the cross sections (Figure 5.1) show that USGS survey and Mobile hydrographic survey match well at the locations, which indicates that it is reasonable to apply these two sets of bathymetric data to the Pascagoula River model.

Based on the above comparison, the USGS survey became the major bathymetric data set used in improving the preliminary Pascagoula River model, due to its coverage of the river basin. The Mobile hydrographic survey was used to update the bathymetry of the dredging channels at the East Pascagoula River and Lower Escatawpa River. Figure 5.2 displays the coverage of the bathymetric data used for updating the preliminary Pascagoula River model. NOS hydrographic

survey was not considered due to the lack of quality control and superior nature of the other two surveys.

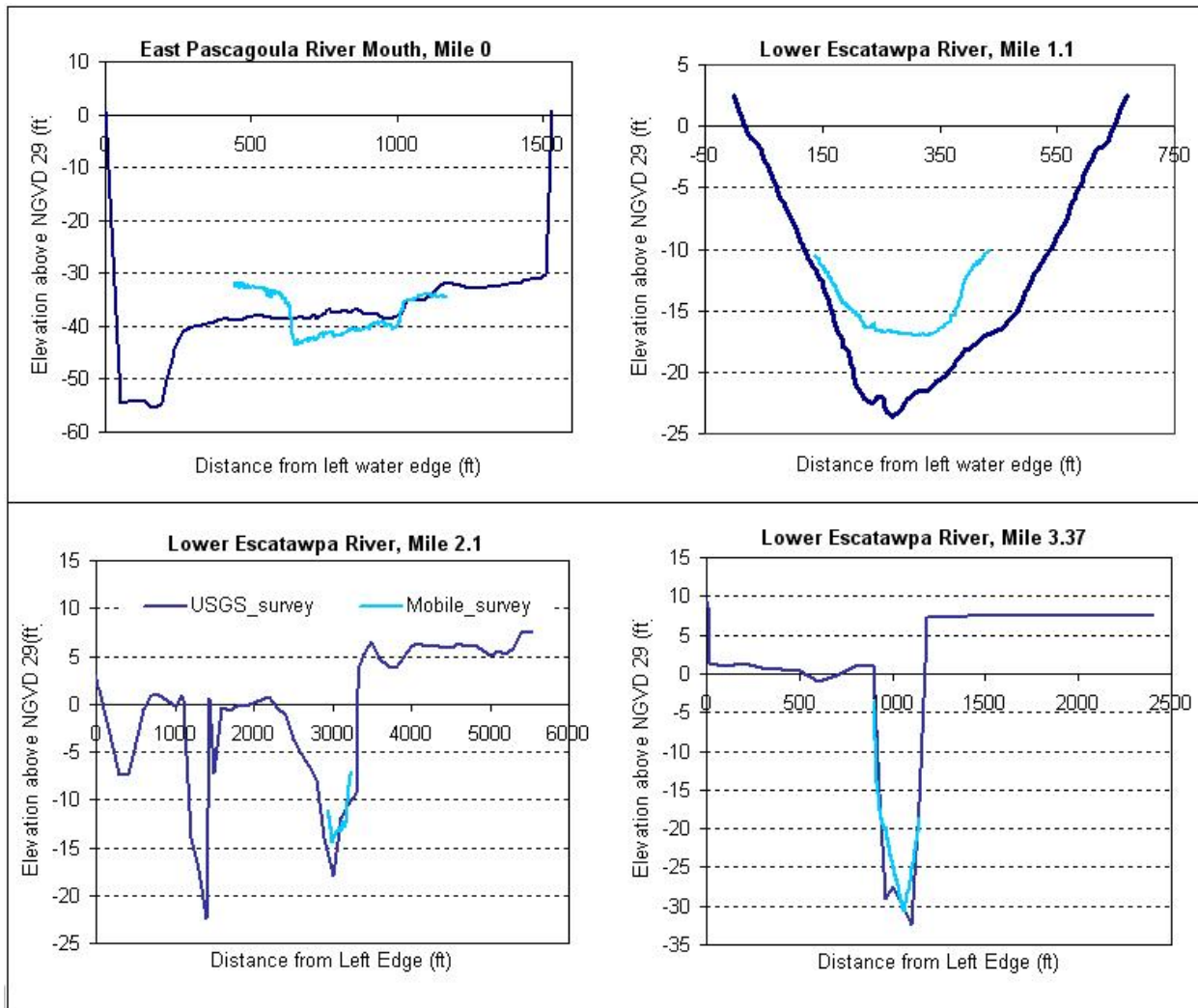


Figure 5.1 Cross section comparison between USGS survey data and Mobile hydrographic survey at East Pascagoula River and Lower Escatawpa River

Pascagoula Bathymetric Data

#1 USGS Survey

- West Pascagoula River: **01 - 14**
- East Pascagoula River: **15 - 28**
- Middle Pascagoula River: **29 - 36**
- Upper Pascagoula River: **37 - 38**
- Red Creek: **39 - 40**
- Black Creek: **41 - 42**
- Lower Escatawpa River: **43 - 49**
- Upper Escatawpa River: **50 - 51**

#2 Mobile Hydrographic Survey

- Pascagoula Bar: **M1**
- Pascagoula Lower Sound: **M2**
- Pascagoula Upper Sound: **M3**
- East Pascagoula River Mouth: **M4**
- Lower Escatawpa River: **M5**

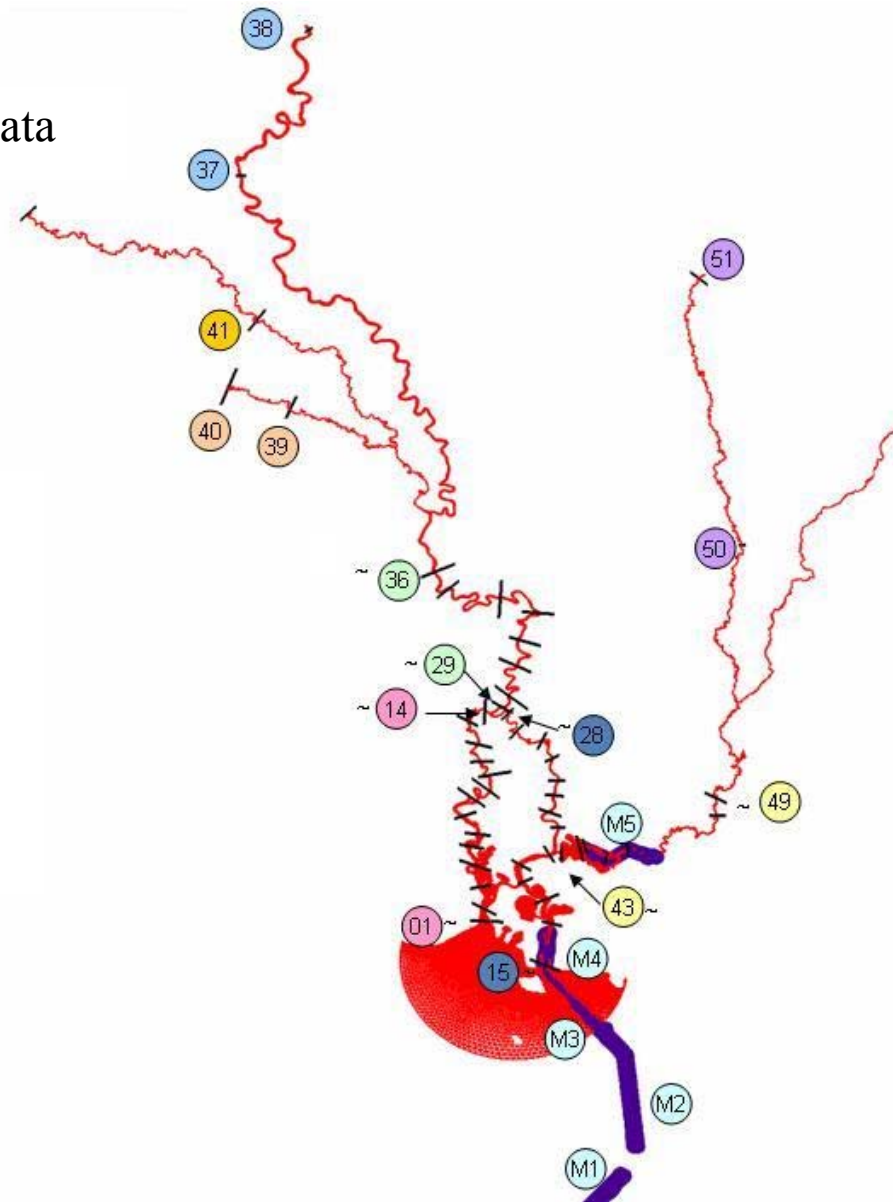


Figure 5.2 Bathymetric data coverage of USGS Survey and Mobile Hydrographic Survey

5.2 Cross Section Interpolation Toolbox

In SMS (Surface-water Modeling System), the mesh bathymetry can be easily interpolated from a two-dimensional scatter set. For example, the bathymetry of the preliminary tide model in Pascagoula River was obtained from the existing two-dimensional SL15 model. However, the limitations of using one-dimensional cross sections into the two dimension model were discovered in the SMS during the bathymetry improvement of the Pascagoula River tide model, which motivates the development of a cross section interpolation toolbox to support the current SMS. This section will introduce the methodology of this toolbox. Two examples of the toolbox application will be presented, followed by some discussion. Its application to the Pascagoula River tide model will be presented in Section 5.3.

The idea for the Cross Section Interpolation Toolbox was necessitated by the fact that hydrologic survey provided discontinuous cross section profiles over surveyed river reaches. Such incomplete bathymetric data made it difficult to interpolate the bathymetry along 2D river channel topography in the SMS. Figure 5.3 illustrates the ineffective interpolation of the bathymetry on a river reach, if the interpolation is done using the standard features of SMS. The cross sections at upstream point A and downstream point B are provided by hydrologic survey and the channel bank is shown in black. Also shown in Figure 5.3, the interpolation processed by SMS is limited to the triangles (in red) formed by connecting the points on the cross sections A and B. As a result, these triangles fall out of the actual channel, and the channel is assigned unreasonable bathymetry values.

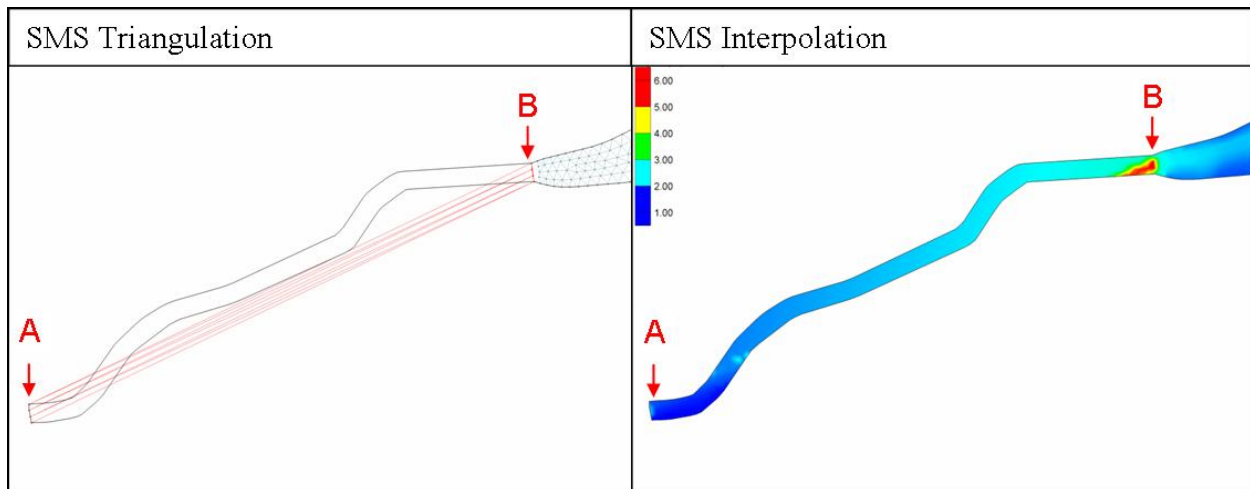


Figure 5.3 Triangulation and the ineffective interpolation in SMS

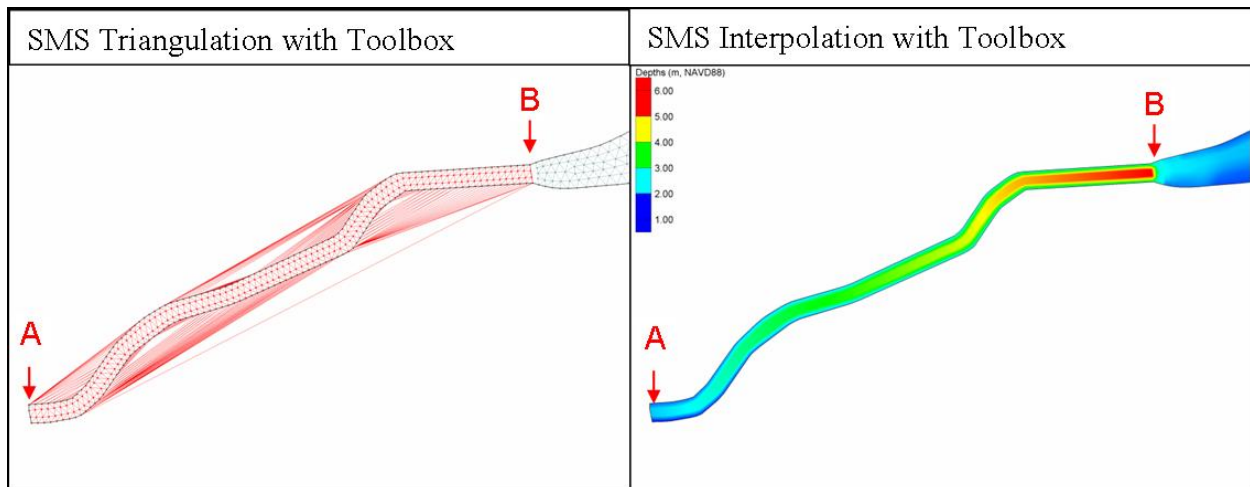


Figure 5.4 Triangulation and correct interpolation in SMS using the Cross Section Interpolation Toolbox

Figure 5.4 presents the targeted triangulation and interpolation between the cross sections A and B. The Cross Section Interpolation Toolbox aims to align scatter set triangulation nicely along the channel. By the use of toolbox, a linear bathymetry interpolation along the channel can be achieved.

The development of such a toolbox is meaningful since it can supplement the SMS meshing tool. Furthermore, the toolbox application is not limited to 2D bathymetry interpolation, it can be used to interpolate any quantitative one dimensional variable into a two-dimensional river reach, such as water level, nodal spacing, and so on. In all, this toolbox helps the mesh generation process and has the potential to be included into SMS as a functional module.

5.2.1 Methodology

Problem Statement and Assumptions

A typical problem for the Cross Section Interpolation Toolbox is as follows: A river reach has an upstream cross section and downstream cross section. Each cross section is described by several bathymetric points with initial values; however, these points need to be updated with new bathymetric values. Also, the topography of the river reach is given in the pre-existing mesh. The task for the tool box is to create a corresponding scatter set which generates a smooth linear transition of the channel bed between cross sections A and B.

The toolbox was developed based on the following assumptions: (1) Channel bed is uniform and has linear transition; (2) Same number of bathymetric points describing upstream and downstream cross sections; (3) The two boundaries describing the channel topography have the same number of evenly distributed identification points (or called bathymetric points); (4) 1-D geometry assumes the positive axis from downstream to upstream.

The linear interpolating function applied here is derived from Maclaurin series expansion:

$$f(x) = \sum_{n=0}^{\infty} \frac{f^{(n)}(0)}{n!} x^n = f(0) + xf'(0) + \frac{x^2}{2!} f''(0) + \frac{x^3}{3!} f'''(0) + \dots$$

$$\approx f(0) + xf'(0) \dots \dots \dots (5.1)$$

First order term is defined by the boundary conditions: $f(0) = a$; $f(L) = b$

$$f'(0) = \frac{f(L) - f(0)}{L} = \frac{b - a}{L} \quad \Rightarrow$$

$$f(x) \approx a + x \frac{b - a}{L} \dots \dots \dots (5.2)$$

Methodology

As explained in Figure 5.5, the input data is composed of two files: One file contains the updated cross section information at the upstream and downstream locations. The other stores the channel topography boundary (i.e. bank) information in the form of (x, y). A FORTRAN code (Cross Section Interpolation Toolbox, see Appendix B) was developed to generate topographic points evenly spread through the reach and assign new bathymetric values to all topographic points. The new bathymetric data were calculated using the updated cross section information by applying the simplified Maclaurin series formulation (Equation 5.2). The output from the toolbox is simply an updated scatter set, which can be read directly by SMS and used for updating the mesh bathymetry.

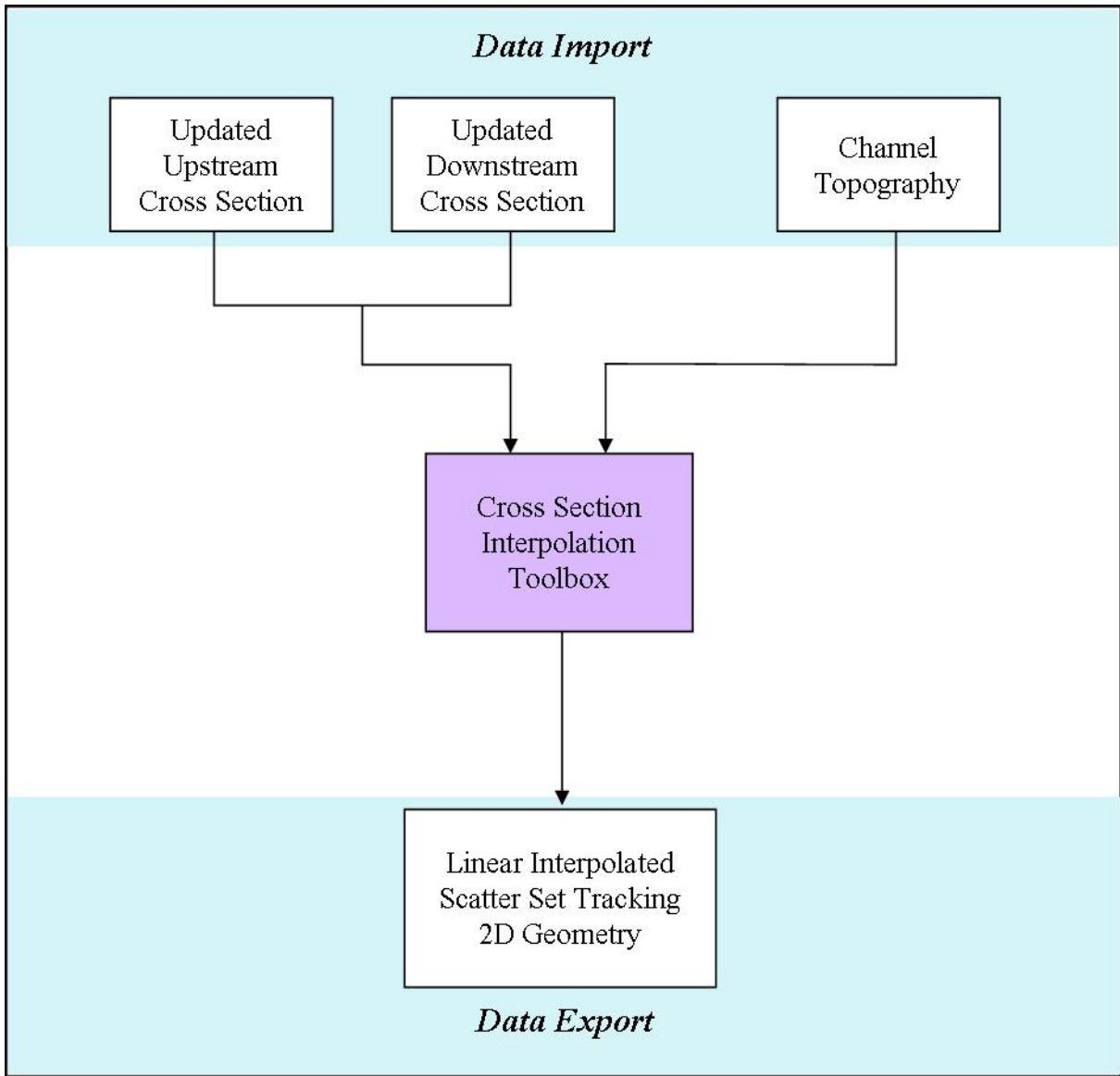


Figure 5.5 Cross Section Interpolation Toolbox Workflow

The five main steps of the Cross Section Interpolation Toolbox are summarized as follows:

Step 1: Define the channel topographic boundaries;

Step 2: Redistribute one boundary to match the other with respect to the number of vertices and convert to scatter points. Save the scatter set as one input file;

Step 3: Build the other input file with the updated cross section information;

Step 4: Run the Cross Section Interpolation Toolbox code;

Step 5: Apply the output file as a new scatter set in SMS and update the 2D mesh bathymetry.

5.2.2 Toolbox Examples

Example 1:

This example is utilized to demonstrate the methodology of the toolbox. A fictitious river reach with two cross sections is created as the initial test of the toolbox code. A is the downstream cross section with 1m depth, while B is the upstream cross section with 9m depth. The algorithm of the toolbox code is shown in six steps (see Figure 5.6).

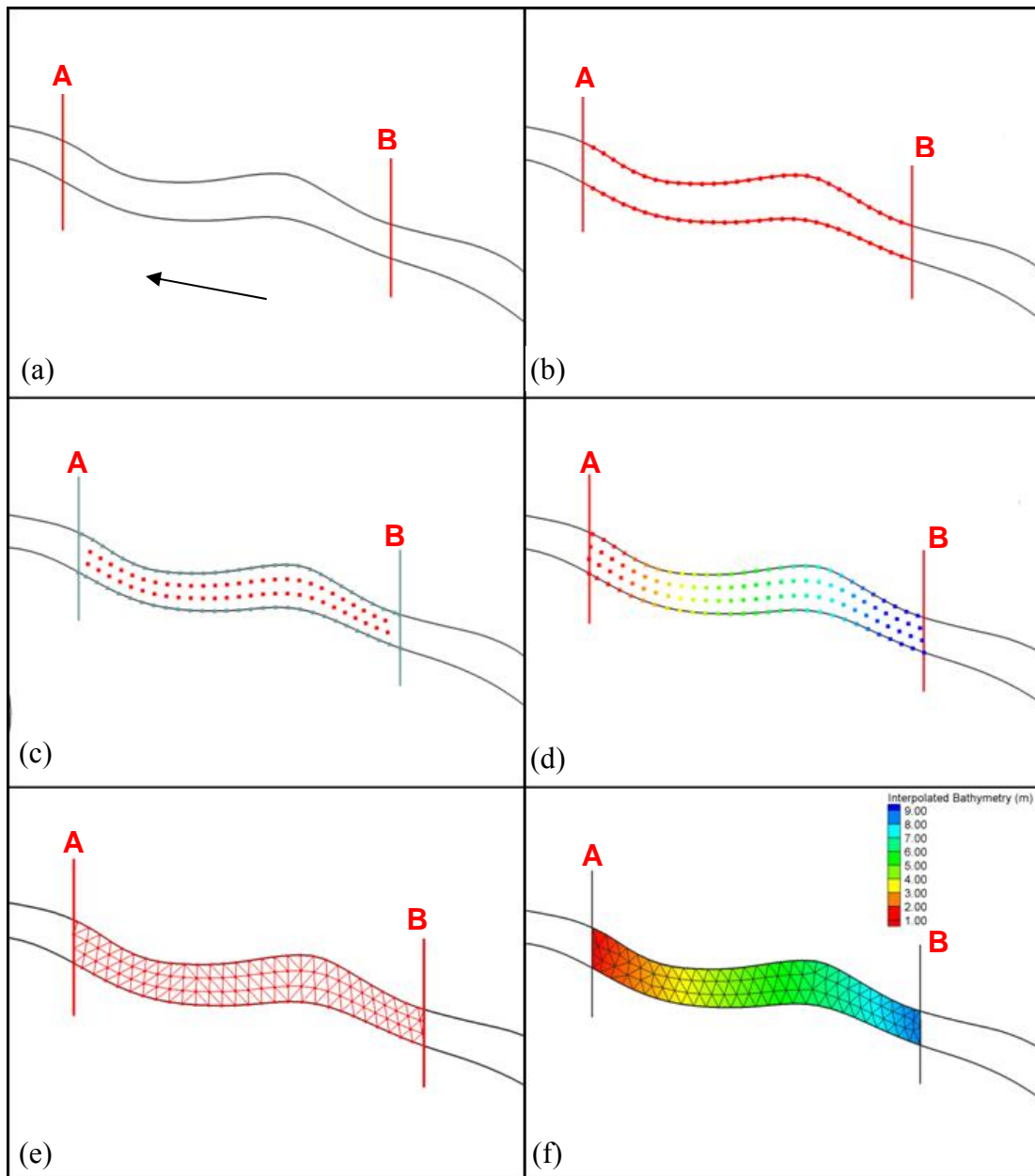


Figure 5.6 The steps executed by the Toolbox code - An example of simple river reach bathymetry interpolation

- (a) Input two given cross section profiles: A-downstream, B-upstream;
- (b) Track the channel topography by two boundary arcs (same number of evenly spaced vertices);
- (c) Compute the horizontal coordinates (x, y) of the inner scatter points;
- (d) Interpolate the cross section depth (z) to each scatter point, and generate the corresponding scatter set (x, y, z) ;
- (e) Triangulation in the SMS follows the correct channel topography;
- (f) The mesh contour plot with updated bathymetry interpolated from the scatter set.

Example 2:

The Loxahatchee River in the Southeastern Florida is the second example to demonstrate the application of the toolbox in a real situation. The selected river reach is located on C-18 Canal (Bacopoulos, 2006). This reach is a typical uniform channel with little lateral/vertical variation. The task of the Cross Section Interpolation Toolbox is to update the bathymetry between cross section A and B.

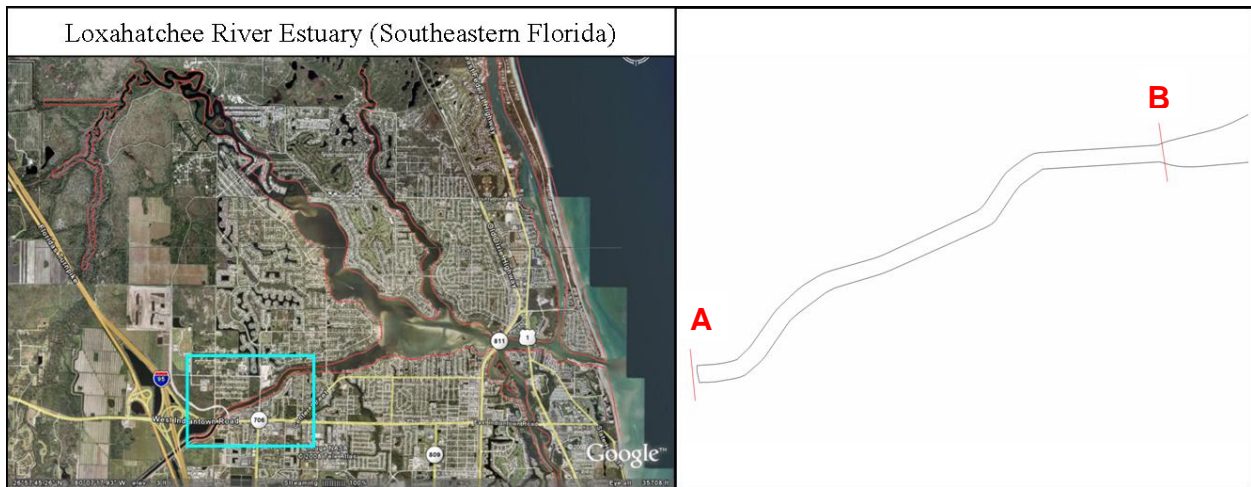


Figure 5.7 A river reach in the Loxahatchee River

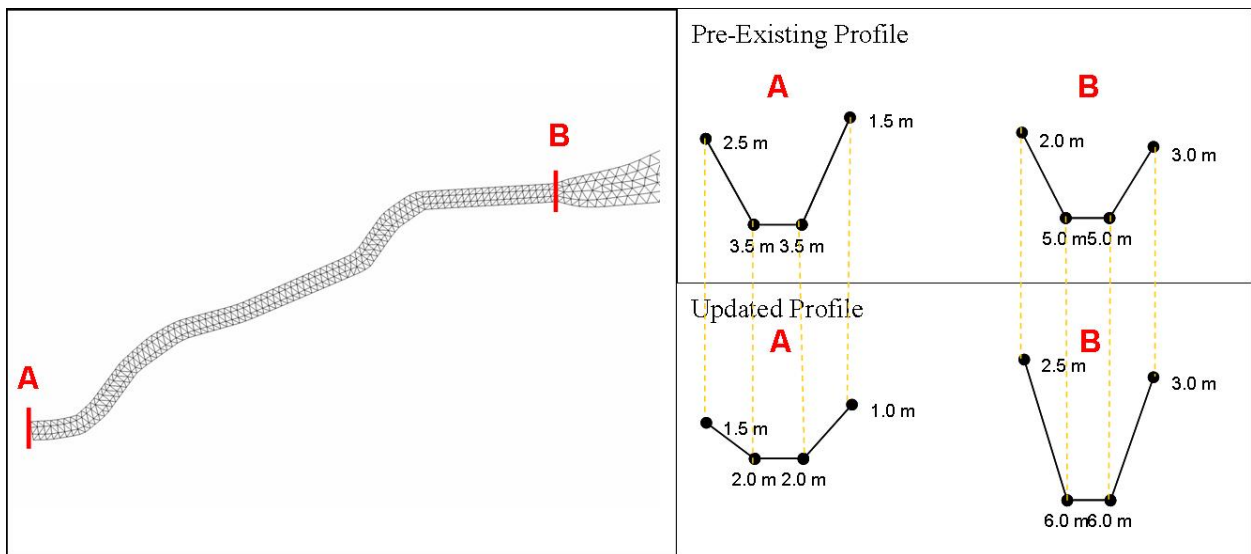


Figure 5.8 Two cross sections for one river reach (A: upstream, B: downstream)

First, prepare the cross section input file. The pre-existing mesh is given, as well as the two cross sections. Figure 5.8 presents the two cross section profiles in both the pre-existing mesh and the updating mesh. Cross section A needs to adjust from deep to shallow, while cross section B will become deeper. Accordingly, the input file “Cross_Section_Profile.dat” is built as shown in Table 5.2. While the number of the bathymetric points within any one cross section is random, the number of bathymetric points at both cross sections needs to be the same. (In this example, the number of bathymetric points is four.)

Second, the channel topography is tracked by building two boundary arcs. If the two generated arcs have different vertices, the one with fewer vertices needs to be redistributed to match the other. The vertices are converted to scatter points, which are then saved as the second input file “Boundary_Topo.xy” (Table 5.2). This SMS scatter file stores the topography information along the channel.

Table 5.2 The format of Cross Section Interpolation Toolbox input files

| <i>Cross_Section_Profile.dat</i> | <i>Boundary_Topo.xy</i> |
|---|---|
| <p style="text-align: center;">Downstream Upstream</p> <p style="text-align: center;">Left → 1.5 2.5 2.0 6.0 2.0 6.0 Right → 1.0 3.0</p> | <pre> SCAT2D BEGSET NAME "EXAMPLE 2" ID 22329 DELEV 0.000000000000000e+000 IXY 88 1 3.496681198671823e+005 3.361364113416656e+006 2 3.496523025505784e+005 3.361406612482951e+006 3 3.496280265538621e+005 3.361444660261883e+006 4 3.495991983630448e+005 3.361479760030349e+006 5 3.495776522120915e+005 3.361519585967065e+006 6 3.495558497917674e+005 3.361559272453617e+006 7 3.495272781876246e+005 3.361594523078666e+006 8 3.494943742938367e+005 3.361625724521410e+006 9 3.494573969337698e+005 3.361652003045116e+006 ... </pre> <p style="text-align: center;">Topography Information in (x, y)</p> |

After the execution of the FORTRAN code, an output file named “Interpolated_Scatter_Set.dat” is created. This file is read into SMS and interpolated to the mesh. Now, a new bathymetry has been assigned to the existing mesh based on a linear interpolation between the two cross sections (Figure 5.9).

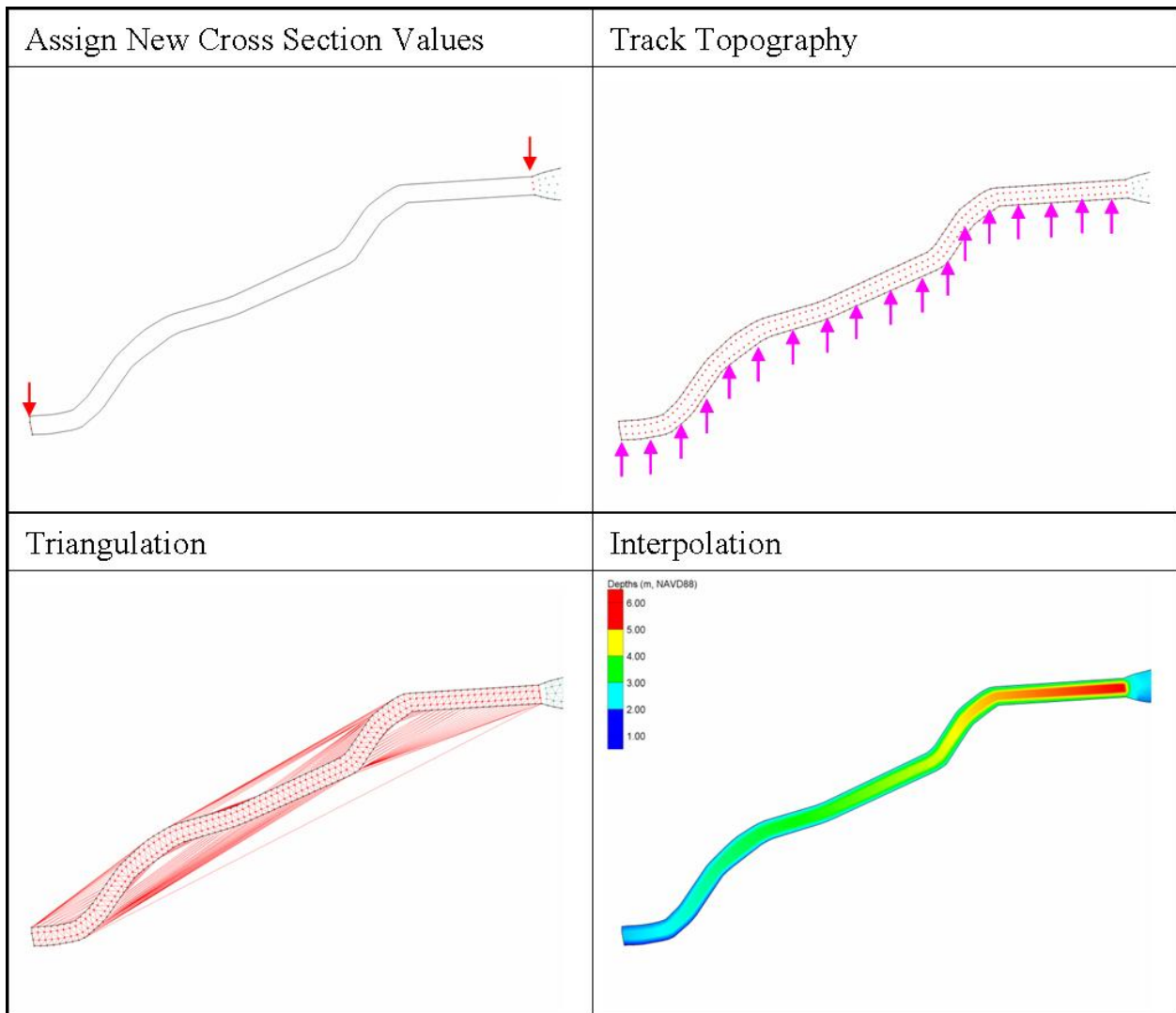


Figure 5.9 The methodology of the Cross Section Interpolation Toolbox applied to an example channel in the Loxahatchee River, FL.

5.2.3 Discussions

The Cross Section Interpolation Toolbox was required during the mesh generation for the Pascagoula River system, given that the current SMS interpolation could not provide the needed results. The advantages of the toolbox are obvious: (1) Limited input information is required to use the toolbox: cross section profiles and channel topography boundaries; (2) The number of bathymetric points used on the cross section is user-defined, according bathymetry complexity; (3) The toolbox is not only limited to interpolating the channel bathymetry, it can be utilized to interpolate any physical variable along the 2D channel such as initial water level.

The toolbox has some limitations and can be improved in certain respects. For example, the toolbox requires the same number of bathymetric points at upstream and downstream locations. If two cross sections have a different number of points, then extra bathymetric points need to be manually added on one cross section in order to satisfy that requirement. As shown in Figure 5.10, four points are presented on cross section A, while cross section B has six bathymetric points. To use the toolbox properly, the bathymetric points on cross section A need to be modified (increased from four to seven points). Such an improvement could enable the toolbox to handle reaches with dramatic topography changes. Another limitation of using the toolbox is that whether the geometry variation of the stream is fully described depends on the available number of the cross sections. This limitation can be overcome by attaining a good data set with enough cross sections. Overall, the toolbox performed very well in the typical river reaches such as the Pascagoula River, and it could be included into SMS as a mesh generation tool.

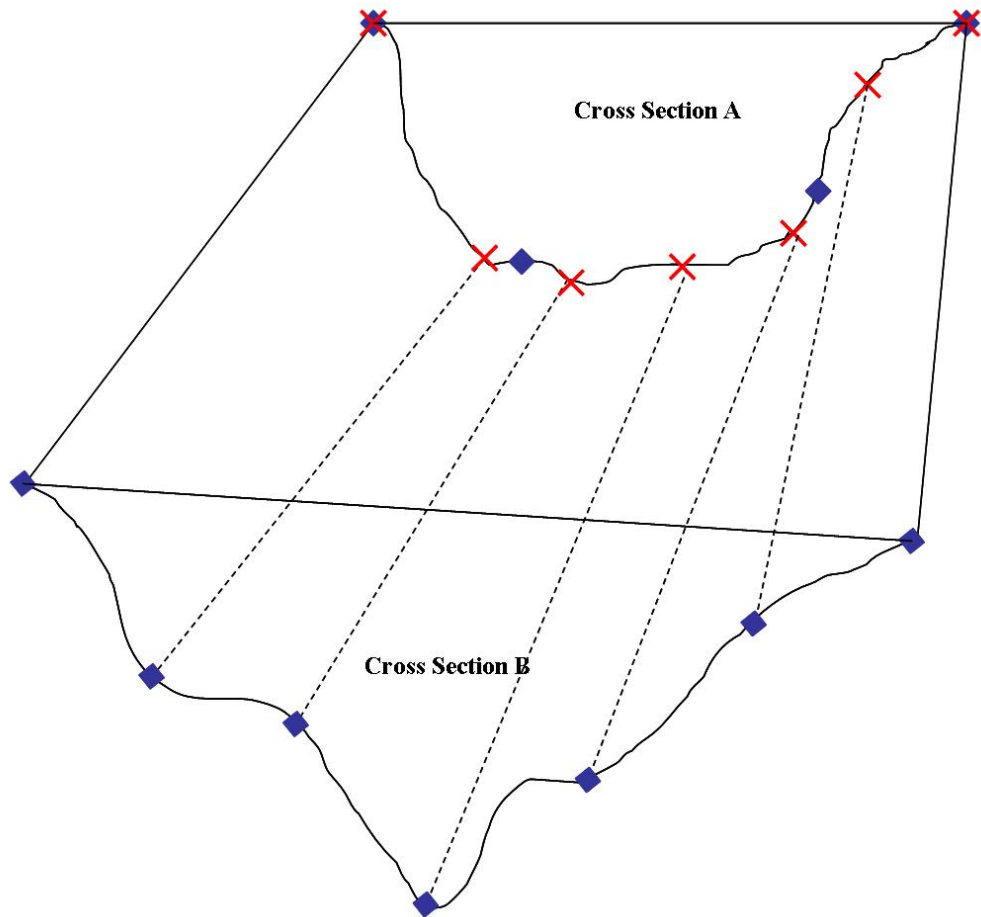


Figure 5.10 Demonstration of bathymetric point adjustment when two cross sections have different numbers of bathymetric points (Original points in diamond shape; modified points in cross shape)

5.3 Cross Section Interpolation Toolbox Applications on the Pascagoula River

Although the data format of the Mobile hydrographic survey allow it to be directly interpolated to the mesh, it was difficult to adapt the 1D cross sections given in the USGS survey into a 2D model. Hence, the Cross Section Interpolation Toolbox was developed for that purpose. The cross sections used to update the preliminary model are No. 01 – 38 and No. 43 – 49 in Figure 5.2. The bathymetry was linearly interpolated between every two cross sections. Since the methodology of the toolbox has been demonstrated, this section only presents the updated Pascagoula River bathymetry by applying the toolbox.

The Cross Section Interpolation Toolbox requires two inputs: cross section information and channel topography. USGS Survey provided the cross section information; while the channel boundary information was from the preliminary Pascagoula River mesh. Figure 5.11 shows a comparison of the model bathymetry between the preliminary model and the updated model in the lower Pascagoula River. It is clear that the preliminary model predicted shallower depths than actually occur. The updated mesh gives a better description of the Lower Pascagoula River dredging channel, as well as the Lower Escatawpa River dredging channel (Location A and B in Figure 5.11).

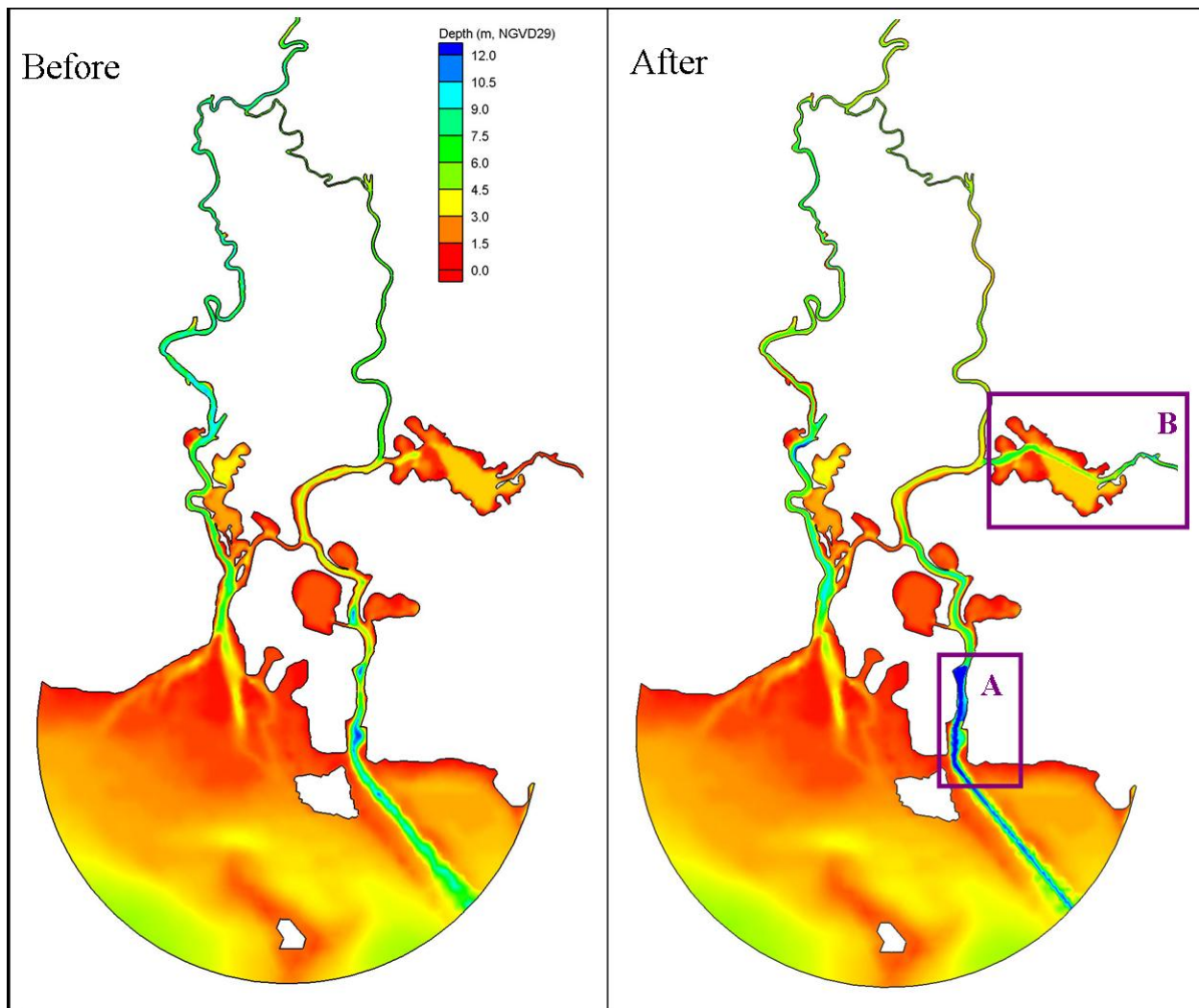


Figure 5.11 Plots of model bathymetry in lower Pascagoula River region (Left: bathymetry from the preliminary model; Right: Updated bathymetry)

The flexibility of using various bathymetric points is specially examined by the example of one reach in the West Pascagoula River. Instead of four bathymetric points, six were used on each cross section. Accordingly, six parallel arcs composed of scatter points were created. Figure 5.12 presents the bathymetry contour before and after using the toolbox. Both cross sections are plotted for comparison. As shown, the toolbox was effective in the region of complex topography.

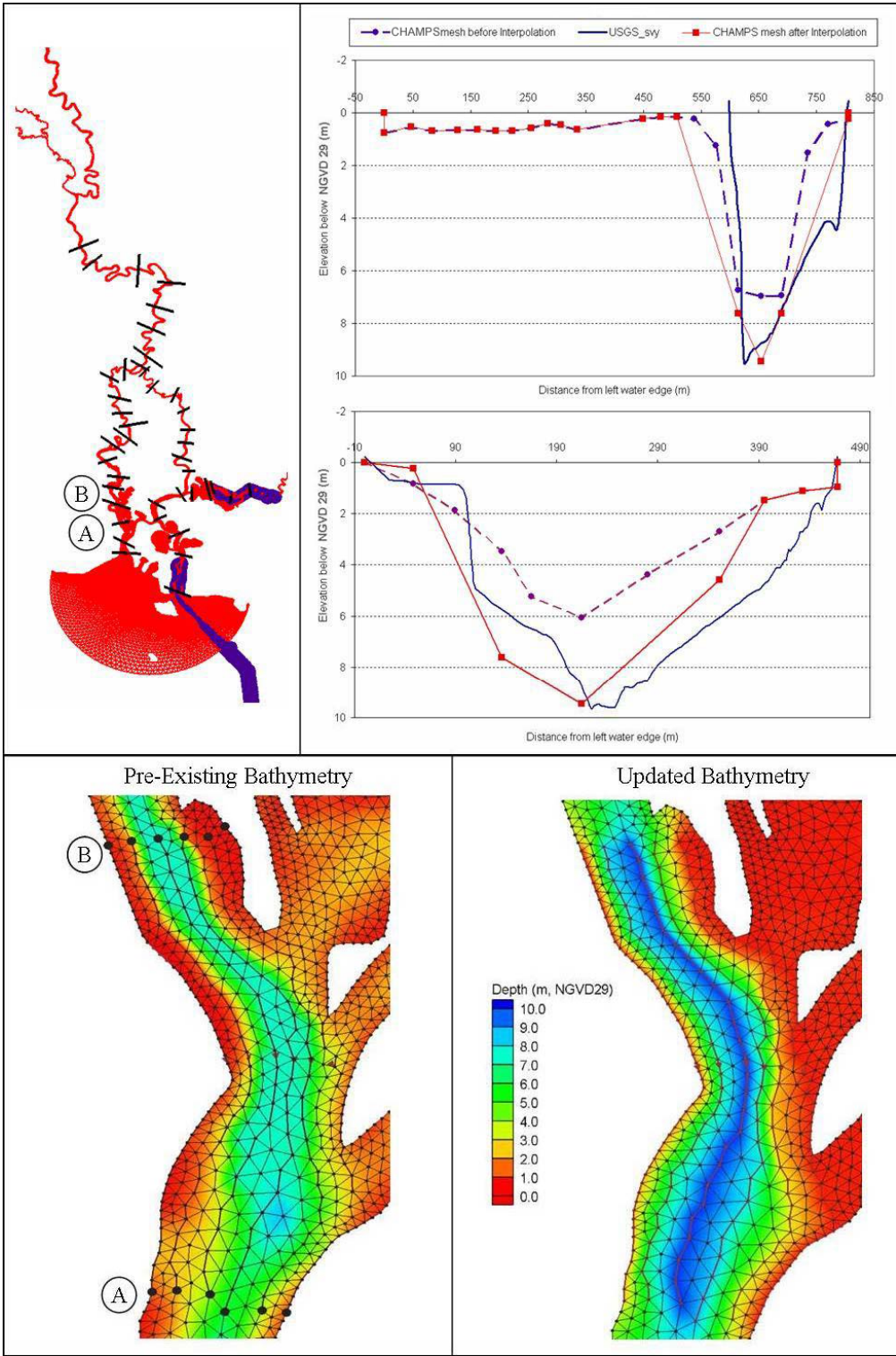


Figure 5.12 An example of the Toolbox application on West Pascagoula River: (a) Reach location; (b) Surveyed cross sections and cross sections applied to model; (c) Bathymetry before update; (d) Bathymetry after update.

5.4 Model Setup and Results

Maintaining the consistency in model initialization is vital to an accurate comparison between two versions of the model. Therefore, the bathymetry updated Pascagoula River model (called “the updated model” below) was set up following the preliminary mode. All of the control parameters were kept the same as presented in Section 4.3 except the mesh bathymetry so that the improvement of the model can be verified. 60-day astronomic tides were run over the entire domain with the same forcings ramped over 20 days.

Tidal resynthesis was applied on the resulting model harmonic constituents. The corresponding plots were generated, presenting the historical and modeled resynthesis results from the two models (Figure 5.13 – 5.16). As shown, the two models offer similar results at the stations near the coastline (NOS stations at Pascagoula Point and Pascagoula); however, when the station locations move into the inlets (such as Pascagoula River station at mile 1, West Pascagoula station at Gautier), the tidal resynthesis results start to show a slight difference in amplitude. When the monitoring stations move upstream, the effect of bathymetry change can be better investigated simply by comparing the results between the preliminary model and the updated model, based on the fact that the tidal signals propagated more miles to arrive at the upstream ones. Hence, the Pascagoula River station at Graham Ferry was chosen for comparison. At this location, a larger amplitude was shown in the updated model compared to the under-prediction in the preliminary model. Similarly, the modeled tides at Cumbest Bluff also matched the actual tide amplitude better than the preliminary model. Regarding the last upstream station on the

Escatawpa River near Orange Grove, the updated model produced higher peaks and lower troughs through most of the spring-neap tidal cycle, and unfortunately an over-prediction in amplitude was recognized.

Overall, the bathymetry updates improved the preliminary model performance on the Pascagoula River main channel, although there are still some discrepancies between the historical and modeled tidal resynthesis. There are various possible reasons for these discrepancies. As stated in the literature review, the Pascagoula River has not generated much attention over the years with respect to hydrologic study. The survey data over this region is limited, and possibly obsolete. Therefore, the model bathymetry update aims to use the available data wisely in an attempt to reflect the real bathymetry as closely as possible. The toolbox was tailored to utilize the available survey data most efficiently in the 2D model. Furthermore, results from the updated model indicate that the Pascagoula River inbank model was sensitive to the bathymetry, which revealed the importance of accurate bathymetry data for developing the astronomic tide model. In addition to a better bathymetry data source, several other components were also found to potentially cause the model discrepancies, such as spatially varied bottom friction. The following chapter will discuss these issues in order to further improve the Pascagoula River tidal model.

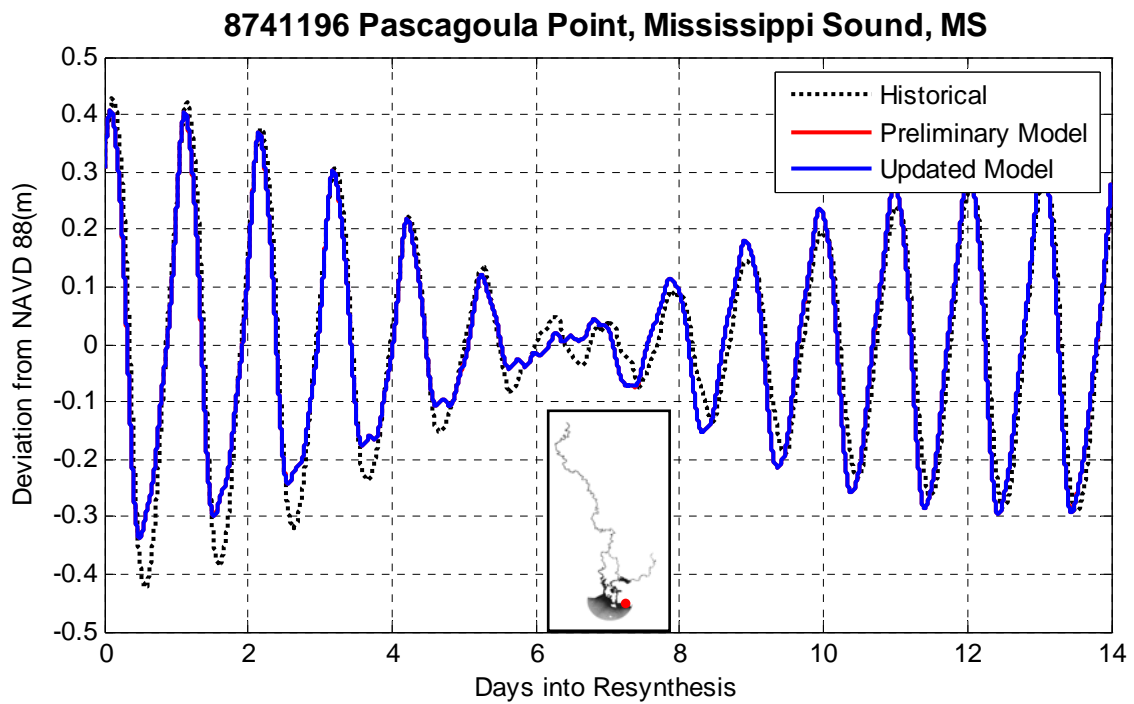
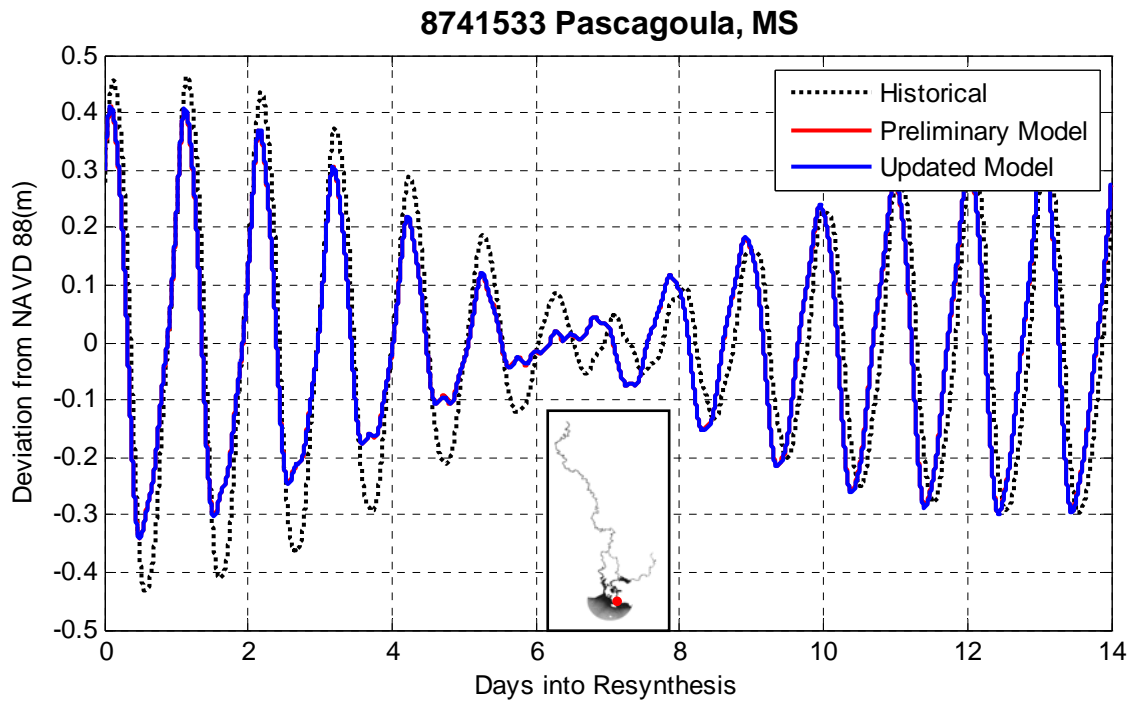


Figure 5.13 Resynthesis of historical and two models' tidal constituents, corresponding to the stations at Pascagoula, MS and Pascagoula Point, Mississippi Sound, MS

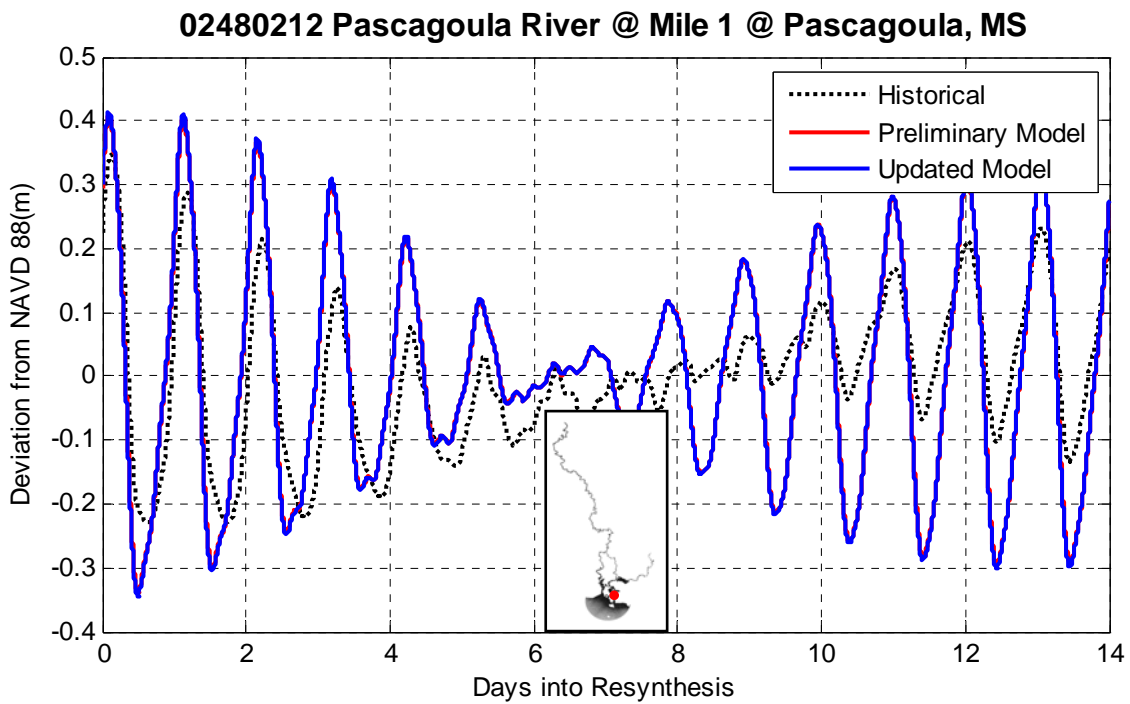
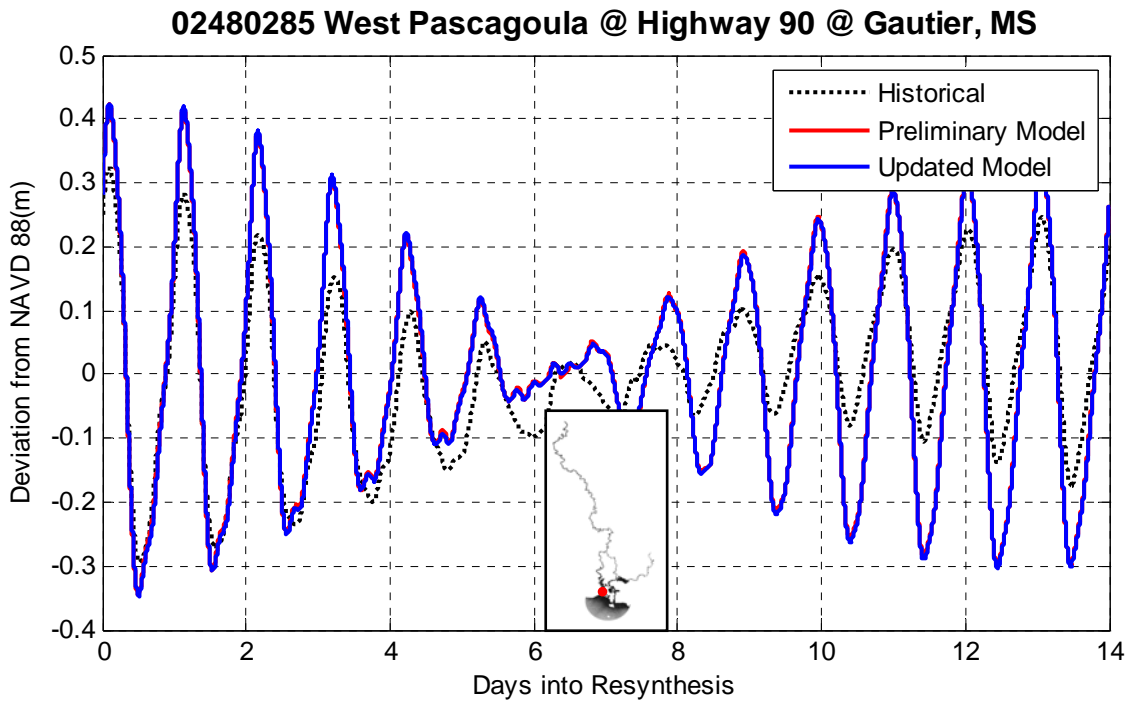


Figure 5.14 Resynthesis of historical and two models' tidal constituents, corresponding to the stations at West Pascagoula at Gautier, MS and Pascagoula River Mile 1, MS

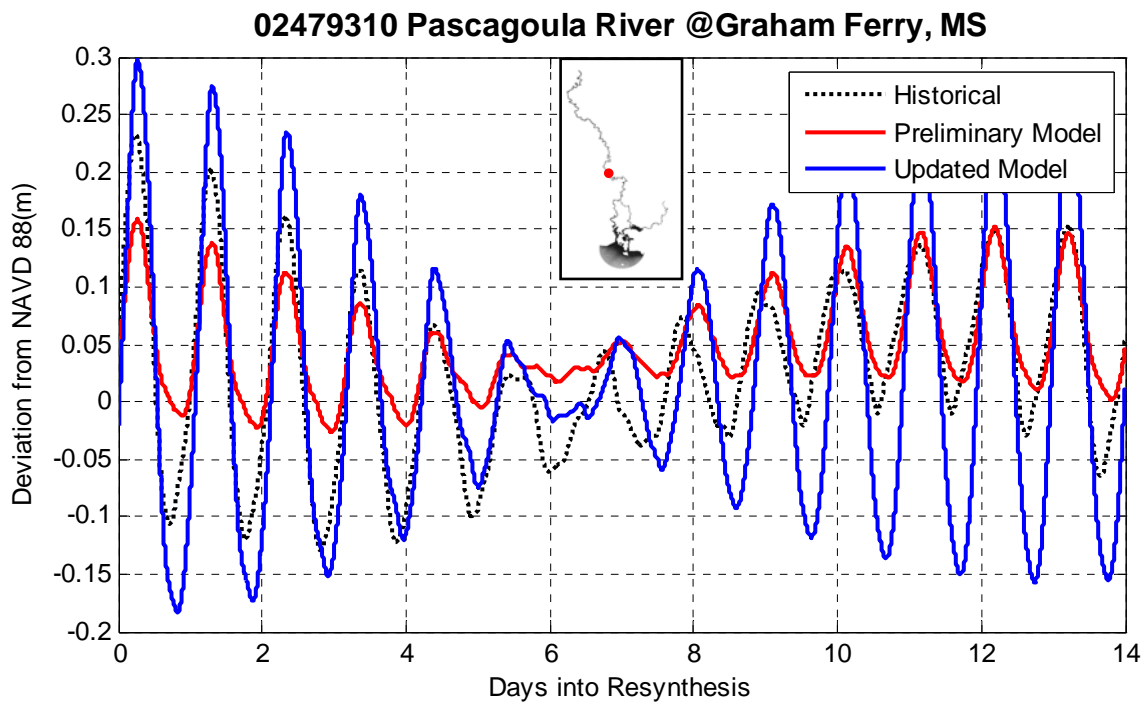
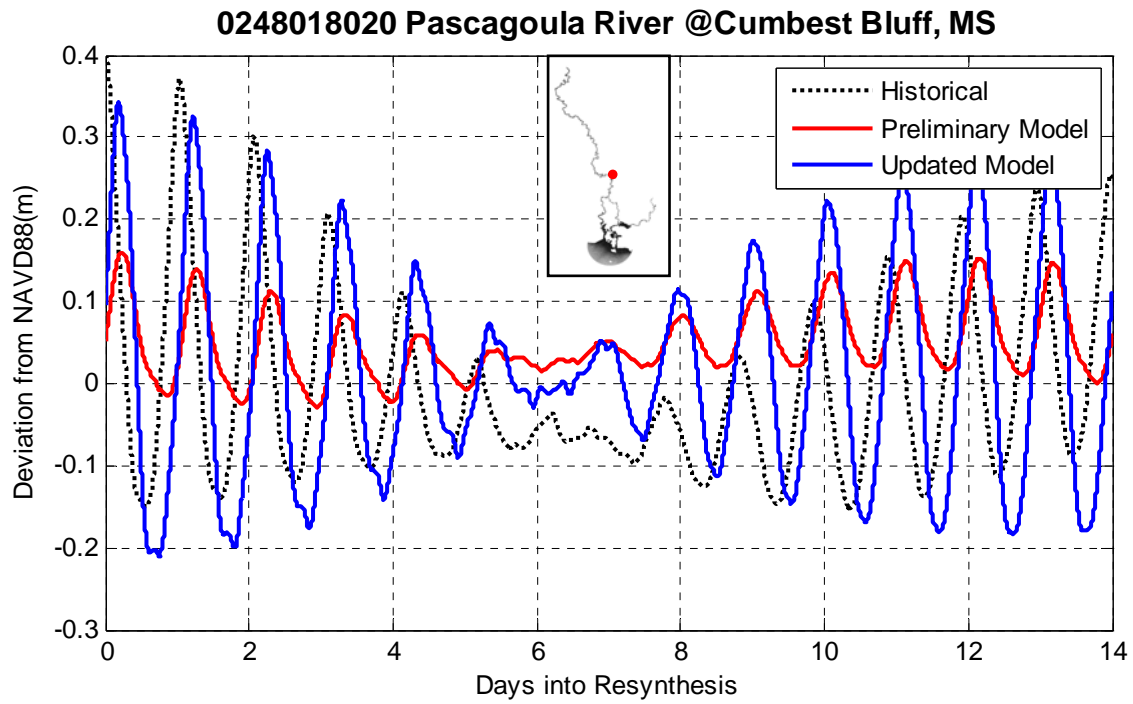


Figure 5.15 Resynthesis of historical and two models' tidal constituents, corresponding to the stations at Pascagoula River at Cumbest Bluff and Graham Ferry, MS

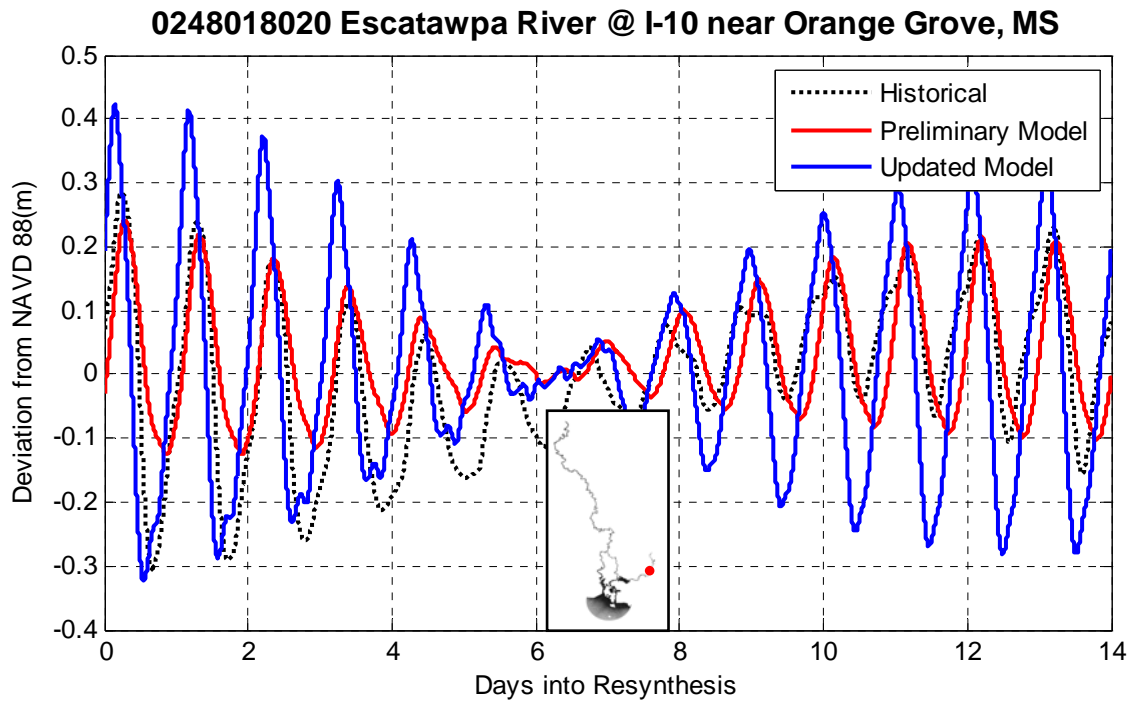


Figure 5.16 Resynthesis of historical and two models' tidal constituents, corresponding to the station at Escatawpa River at I-10 near Orange Grove, MS

CHAPTER 6. MODEL SENSITIVITY ANALYSES

In the previous chapter, the preliminary model was updated by a better representation of the real bathymetry in the numerical model. In an attempt to test the model and further improve the results, sensitivity analyses are performed with regard to 1) a preliminary assessment of the effect on accuracy of bottom friction in shallow water, and 2) the advective flow effect on tidal circulation and water elevation. The sensitivity analyses allow us to better understand the physics within the system and incorporate a more complete representation of the physics into the Pascagoula River model. In turn, this builds upon an objective of providing an accurate and intuitive tidal model for storm surge simulation. In this chapter, a set of bottom friction coefficients were tested on the tidal model, and the model errors are assessed. After the preliminary examination of the model's sensitivity to bottom friction, an exploration and discussion of the influence of advection on the tidal propagation and velocity residuals are presented based on the improved Pascagoula River tidal model.

6.1 A Preliminary Sensitivity Analysis on Bottom Friction

The role of friction in modeling the tidal dynamics in shallow water and coastal regions is well recognized and relatively well studied (Godin and Martinez, 1994; Grenier, Luetlich et al., 1995; Murray, 2003; Bacopoulos, 2006). In shallow water, the friction factor has a stronger influence on the circulation of flow than it does in deep water. The Pascagoula River has a meandering

shallow character and various topographic features are included, such as tributaries, lakes, and marsh areas. Therefore, the parameterization of frictional process remains an important modeling aspect in this study. A variety of sensitivity simulations modifying the bottom friction parameters were performed so that the model response on bottom friction can be examined. Furthermore, understanding the friction parameterization on the Pascagoula River is likely to benefit the next development of a storm surge model. However, it is recognized that a thorough calibration of bottom friction cannot be completed until the influence of marsh and inundation areas is examined, which is beyond the scope of this thesis.

The ADCIRC-2DDI model employed in this study enables the usage of a hybrid bottom friction function in shallow water (Equation 3.10). The hybrid bottom friction relationship allows the bottom friction coefficient, C_f , to vary with the bathymetric depth. The sensitivity analyses on bottom friction were performed by adjusting the minimum bottom friction factor, C_{fmin} . The updated Pascagoula River model was initialized in the same manner (See Section 4.3) except for the assignment of the minimum bottom friction factor. Two methods have been employed to assign the minimum bottom friction factor within the Pascagoula River model: 1) C_{fmin} has been taken as a universal value over the entire domain; 2) C_{fmin} was assumed to be spatially varied.

In the first method, four universal C_{fmin} values were assigned over the entire model domain separately: 0.0015, 0.0025, 0.0035, and 0.0040. It is noted that 0.0040 is the maximum value tested in the study because the model runs using 0.0045 and above generated numerical overflow.

In the spatially varied C_{fmin} tests, the model was divided into three sub-domains each using different bottom friction coefficients. Figure 6.1 shows two domain divisions tested on the Pascagoula River model. Domain Division 1 divided the entire domain into three sub-domains - downstream, middle stream and upstream - in order to better represent the channel bed characteristics within the model. Researchers believe that channel roughness is related to the particle size distribution of the sediment transported throughout the river. Upstream stations Graham Ferry and Orange Grove were used as the divide-points for upstream and middle stream, since no geology or soil reports were available for these locations. Similarly, the upper boundary of the marsh area (approximately 10 river miles from the mouth) was used to separate the middle stream and upstream domains.

Domain Division 2 is based more on the land features. The ocean domain was separated first, as the water depth was considerably deeper than in the river. The second domain includes the marsh area in Lower Pascagoula River and Lower Escatawpa River so that the unique features of the marsh area can be considered. The remaining channels were defined as the third domain.

Table 6.1 lists the five combinations of spatially varied C_{fmin} assigned in the sensitivity tests. Test 1 through Test 3 apply to Domain Division 1; and Test 4 & Test 5 apply to Domain Division 2. The selected C_{fmin} started from the suggested standard value 0.0025 (Cobb and Blain, 2001; Luetlich, Carr et al., 2002), and gradually increased to a maximum value 0.0055 (Bacopoulos, 2006). Higher values (0.0065, 0.0075) were used in marsh areas.

Table 6.1 Summary of the assigned spatially-varying C_{fmin}

| <i>Domain Division</i> | <i>No. of Test</i> | <i>Assigned Spatially Varied C_{fmin}</i> | | |
|------------------------|--------------------|--|---------------------|---------------------|
| | | <i>Sub-domain 1</i> | <i>Sub-domain 2</i> | <i>Sub-domain 3</i> |
| 1 | Test 1 | 0.0025 | 0.0025 | 0.0035 |
| | Test 2 | 0.0025 | 0.0035 | 0.0045 |
| | Test 3 | 0.0035 | 0.0045 | 0.0055 |
| 2 | Test 4 | 0.0025 | 0.0075 | 0.0035 |
| | Test 5 | 0.0025 | 0.0065 | 0.0035 |

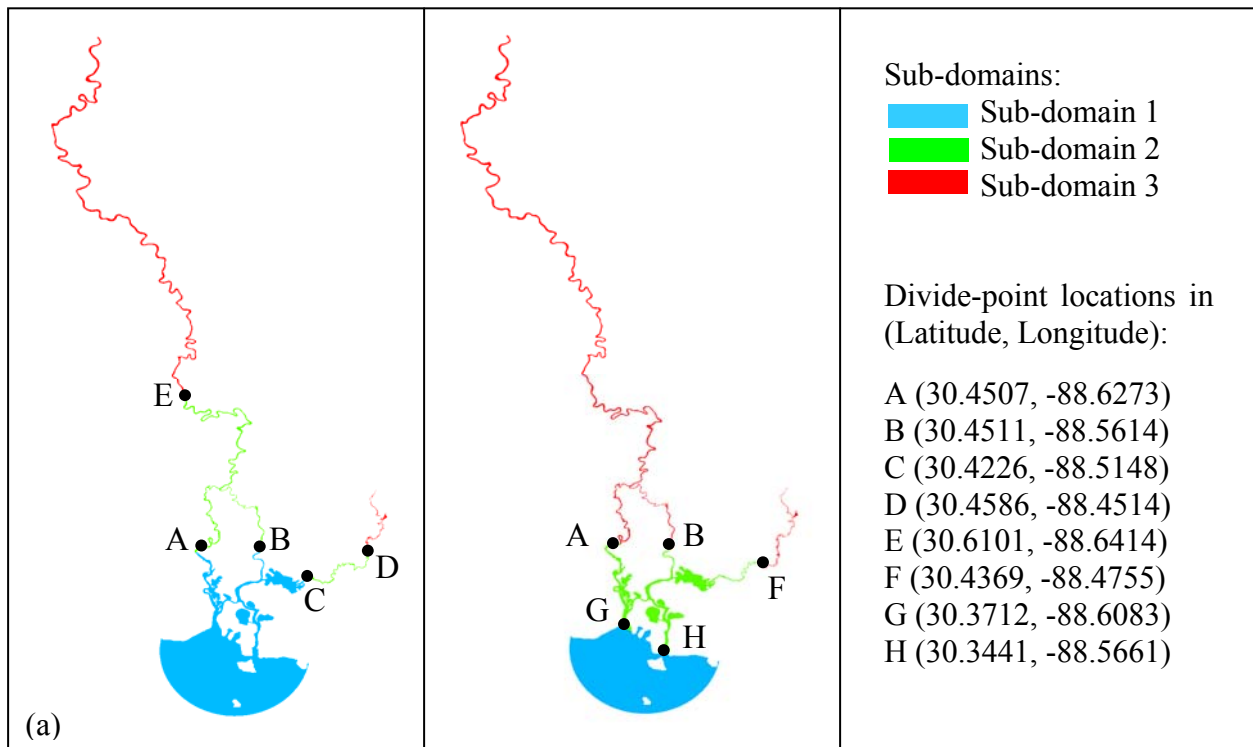


Figure 6.1 Division of sub-domains: applying spatially varied C_{fmin} on the Pascagoula River model. (a) Domain Division 1, (b) Domain Division 2.

The model results were assessed through a statistical analysis of the errors between the historical and model tidal signals. The error estimation uses the Root Mean Square (RMS) error as a measure of the disparity between the historical and model tidal records (Zwillinger, 2003):

$$RMS = \sqrt{\frac{\sum_{i=1}^N (Hist_i - Mod_i)^2}{N}} \dots\dots\dots(6.1)$$

where

N = the total number of discrete points used in the error estimation;

$Hist_i$ = the historical record at the i^{th} discrete point;

Mod_i = the modeled results at the i^{th} discrete point.

The model results attained from a series of sensitivity simulations are summarized in Tables 6.2 - 6.3. The model errors (RMS) at the seven stations (See Figure 4.11) were calculated after every simulation, and these values were compared to identify the optimal bottom friction parameter of the model.

The RMS errors presented in Tables 6.2 -6.3 are an assessment of tidal model performance in both phase and amplitude. Table 6.2 presents the RMS errors generated by applying the universal minimum bottom friction factor varying from 0.0015 to 0.0040. It appears that as the minimum bottom friction factor increases, the RMS errors decrease at all upstream stations. The model using constant $C_{fmin} = 0.0040$ yields the lowest RMS error among the seven stations. Figure 6.2 is a representative comparison plot of the tidal resynthesis at Pascagoula River near Graham Ferry when the C_{fmin} equals 0.0025 and 0.0040. An improvement of the tidal signals in phase and

amplitude is observed with the larger C_{fmin} ; however, no C_{fmin} value larger than 0.0040 has been successfully tested due to numerical overflow. It is found that the overflow occurred at 13 miles upstream from Graham Ferry, where the channel invert started to rise above the datum. The simulated water only passed through one third of the actual channel width, because the side elements above the datum kept as dry elements in ADCIRC v42.06. Hence, the initialization of water levels for the upstream portions of the model (where the channel invert is above the datum) is required in the future development.

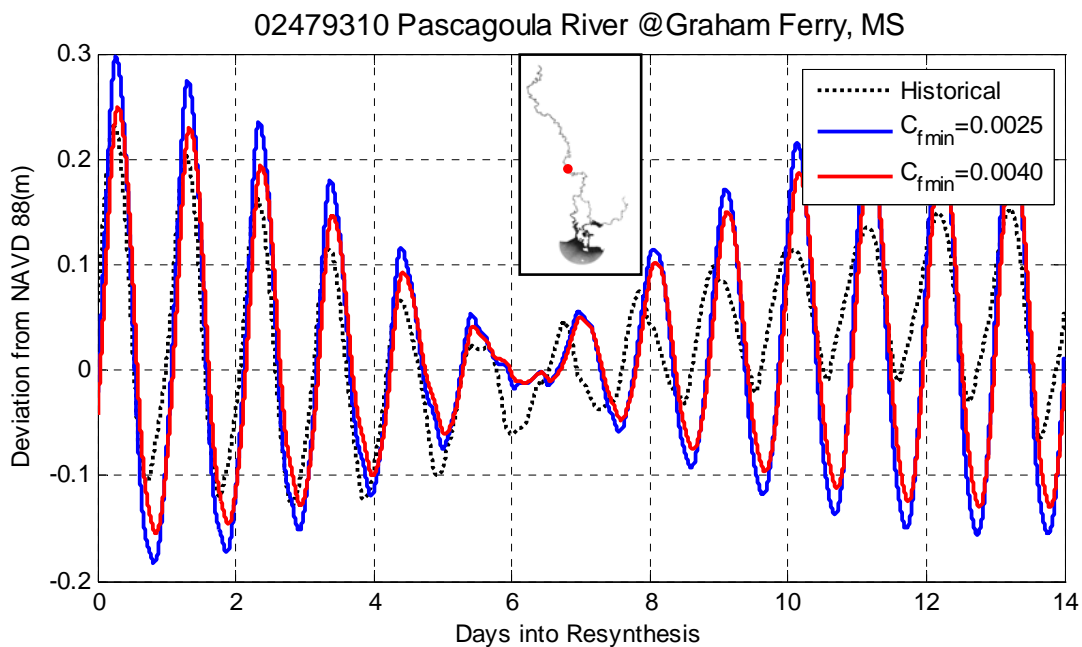


Figure 6.2 Tidal resynthesis analysis plots at upstream station-Graham Ferry, comparing C_{fmin} equals 0.0025 and 0.0040. Higher value 0.0040 fits better with historical record.

Table 6.3 displays the results of testing spatially-varying C_{fmin} on the Pascagoula River tidal model. As shown, the C_{fmin} combination of 0.0035-0.0045-0.0055 in Domain Division 1 provides

the smallest RMS error at Stations No.5&6; however, the best result at Orange Grove (Station No.7) was attained when the marsh area was separated and assigned with a $C_{fmin} = 0.0075$. All RMS errors at the coastal stations (No.1 to No.4) in Table 6.3 were similar to those using a universal $C_{fmin}=0.0040$. Comparing the application of universal C_{fmin} and spatially-varying C_{fmin} , the advantages of using spatially-varying bottom friction coefficient are evident. First, a larger regional C_{fmin} was allowed when it is spatially varied within the model domain. Second, a larger time step can be used with spatially-varying C_{fmin} , enabling the model to run more efficiently.

In all, the results of both sets of sensitivity simulations indicate that the Pascagoula River tide model response is sensitive to bottom friction. Adjusting the universal or spatially-varying C_{fmin} leads to improved results as shown by the minimization of RMS errors. However, a spatially varied bottom friction coefficient is more efficient and reasonable than a globally uniform bottom friction coefficient. This is due to the better description of bottom roughness related to the stream characteristics in the model and also its increases in model stability and computational efficiency. It is reasonable to assign the standard value 0.0025 in the ocean region, since bottom friction in deep water is not as important as it is in shallow water. However, the marsh area requires a high roughness coefficient (e.g. $C_{fmin} = 0.0075$). The upstream and middle stream Pascagoula is suggested to use a C_{fmin} between 0.0035 and 0.0055. Consequently, a spatially varied C_{fmin} 0.0025(ocean region)-0.0075(marsh area)-0.0055(middle stream & upstream) is suggested as a good starting point for the Pascagoula River tidal model.

Table 6.2 RMS errors associated with model sensitivity analyses on uniform minimum bottom friction factor, C_{fmin}

| No. | Water Level Gauging Station | Spring Tidal Range ^a (m) | Root Mean Square (RMS) | | | |
|-----|---|-------------------------------------|------------------------|--------|--------|---------------------------|
| | | | Universal C_{fmin} | | | |
| | | | 0.0015 | 0.0025 | 0.0035 | 0.0040 |
| 1 | Pascagoula, MS | 0.93 | 0.085 | 0.085 | 0.084 | 0.084 ^b |
| 2 | Pascagoula Point, Mississippi Sound, MS | 0.86 | 0.048 | 0.048 | 0.048 | 0.048 |
| 3 | West Pascagoula at Gautier, MS | 0.65 | 0.082 | 0.081 | 0.080 | 0.080 |
| 4 | Pascagoula River, Mile 1 at Pascagoula, MS | 0.69 | 0.109 | 0.109 | 0.108 | 0.108 |
| 5 | Pascagoula River at Cumbest Bluff, MS | 0.80 | 0.144 | 0.142 | 0.142 | 0.142 |
| 6 | Pascagoula River at Graham Ferry, MS | 0.47 | 0.081 | 0.068 | 0.064 | 0.063 |
| 7 | Escatawpa River at I-10 near Orange Grove, MS | 0.61 | 0.137 | 0.127 | 0.120 | 0.117 |

Table 6.3 RMS errors associated with model sensitivity analyses on spatially varied minimum bottom friction factor, C_{fmin}

| No. | Water Level Gauging Station | Spring Tidal Range ^a (m) | Root Mean Square (RMS) | | | | |
|-----|---|-------------------------------------|--------------------------------------|--------|---------------------------|--------|--------------|
| | | | Assigned Spatially Varied C_{fmin} | | | | |
| | | | Test 1 | Test 2 | Test 3 | Test 4 | Test 5 |
| 1 | Pascagoula, MS | 0.93 | 0.085 | 0.085 | 0.084 | 0.085 | 0.085 |
| 2 | Pascagoula Point, Mississippi Sound, MS | 0.86 | 0.048 | 0.048 | 0.048 | 0.048 | 0.048 |
| 3 | West Pascagoula at Gautier, MS | 0.65 | 0.081 | 0.081 | 0.080 | 0.080 | 0.080 |
| 4 | Pascagoula River, Mile 1 at Pascagoula, MS | 0.69 | 0.109 | 0.109 | 0.108 | 0.108 | 0.108 |
| 5 | Pascagoula River at Cumbest Bluff, MS | 0.80 | 0.142 | 0.140 | 0.140 ^b | 0.144 | 0.143 |
| 6 | Pascagoula River at Graham Ferry, MS | 0.47 | 0.068 | 0.063 | 0.062 | 0.065 | 0.065 |
| 7 | Escatawpa River at I-10 near Orange Grove, MS | 0.61 | 0.127 | 0.127 | 0.120 | 0.103 | 0.107 |

^a: Historical spring tidal range; ^b: best performing model results shown in bold.

6.2 Advection Effect on Velocity Residuals and Tidal Elevation

The advection term plays an important role in tidal propagation and tide-induced residual circulation. Previous studies have concluded that the spatial representation of the advection term has considerable influence on computed tidal propagation (Leendertse, 1988). Bacopoulos (2006) also mentioned in his study of the St. Johns River that highly advective flows exist throughout the St. Johns River and contribute to the astronomic tides. Similarly, the Pascagoula River model was tested with and without the inclusion of advection in order to explore the importance of the advection term on the astronomic tides and tidal circulation.

The ADCIRC numerical code includes the advection terms within the GWCE (Equation 3.5), and provides an option to enable/disable the advection terms in the shallow-water momentum equations. Velocity residuals and water elevations were examined with respect to the model performance on advection. The velocity residuals were calculated using the average tidal cycle (ATC) defined by Winant and Gutierrez de Velasco (2003). A 14-day length of global velocity model output was analyzed in order to include a complete spring-neap tidal cycle in the calculation of the residual circulation. The resulting residual circulation patterns would then be representative of the net tidal flows occurring within the estuary and provide information relating to the flood or ebb dominance of the overall tidal circulation (Bacopoulos, 2006).

Winant and Gutierrez de Velasco (2003) defined the ATC as the average of any property as a function of tidal phase, computed by dividing time-series data into sections of length equal to the

period of the M2 tidal constituent and averaging the sections. Therefore, a moving window approach for averaging the sections (of width equal to the period of the M2 tidal constituent) was applied through the 14-day global velocity model output. The longitudinal and latitudinal velocities were computed by the following averaging equations respectively:

$$\left(\bar{U}_{M_2}, \bar{V}_{M_2}\right) = \sum \frac{\left(U_{M_2}, V_{M_2}\right)}{N_{M_2}} \dots\dots\dots (6.1)$$

The averaged velocities (from Equation (6.1)) were then averaged through the 14-day length of global velocity model output to provide the residual circulation:

$$\left(\bar{U}_{14day}, \bar{V}_{14day}\right) = \sum \frac{\left(\bar{U}_{M_2}, \bar{V}_{M_2}\right)}{N_{14day}} \dots\dots\dots (6.2)$$

Figures 6.3 – 6.4 display velocity residuals at the Pascagoula River inlets and the Escatawpa River near the Beardslee Lake and Roberson Lake; the residuals were calculated from global velocity model output obtained from the updated model with advection enabled/disabled. It is recognized that the Pascagoula inlet area is dominated by a seaward tidal flow. Compared to the no advection runs, residual eddys near the east inlet are attained when advection is enabled. The inclusion of advection also induces more residual circulations within the river channel. As a result, much stronger outflow conditions arise at the coastal area near the west inlet. Figure 6.4 further confirms that the channel flow has a higher velocity scale with advection enabled than without. On the Escatawpa River lake area, the residual patterns are considerably different. Based on the above comparisons, the spatial gradient in the horizontal motion (flow advection)

can potentially affect the astronomic tides. The influence of advection was further examined by comparing the simulated water elevations.

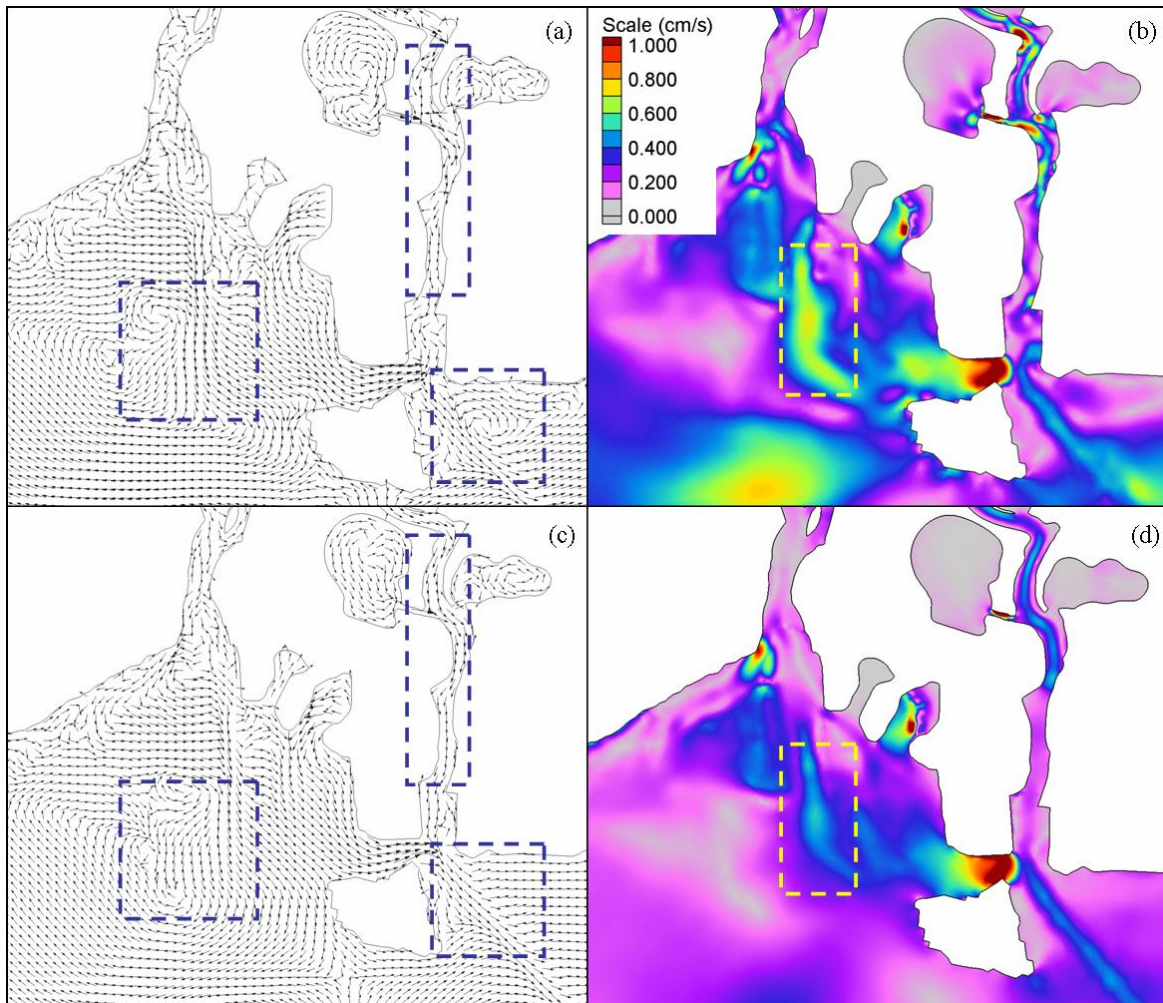


Figure 6.3 Computed velocity residuals at the Pascagoula River inlets: (a) (b) vector and magnitude plots (advection enabled), (c) (d) vector and magnitude plots (advection disabled)

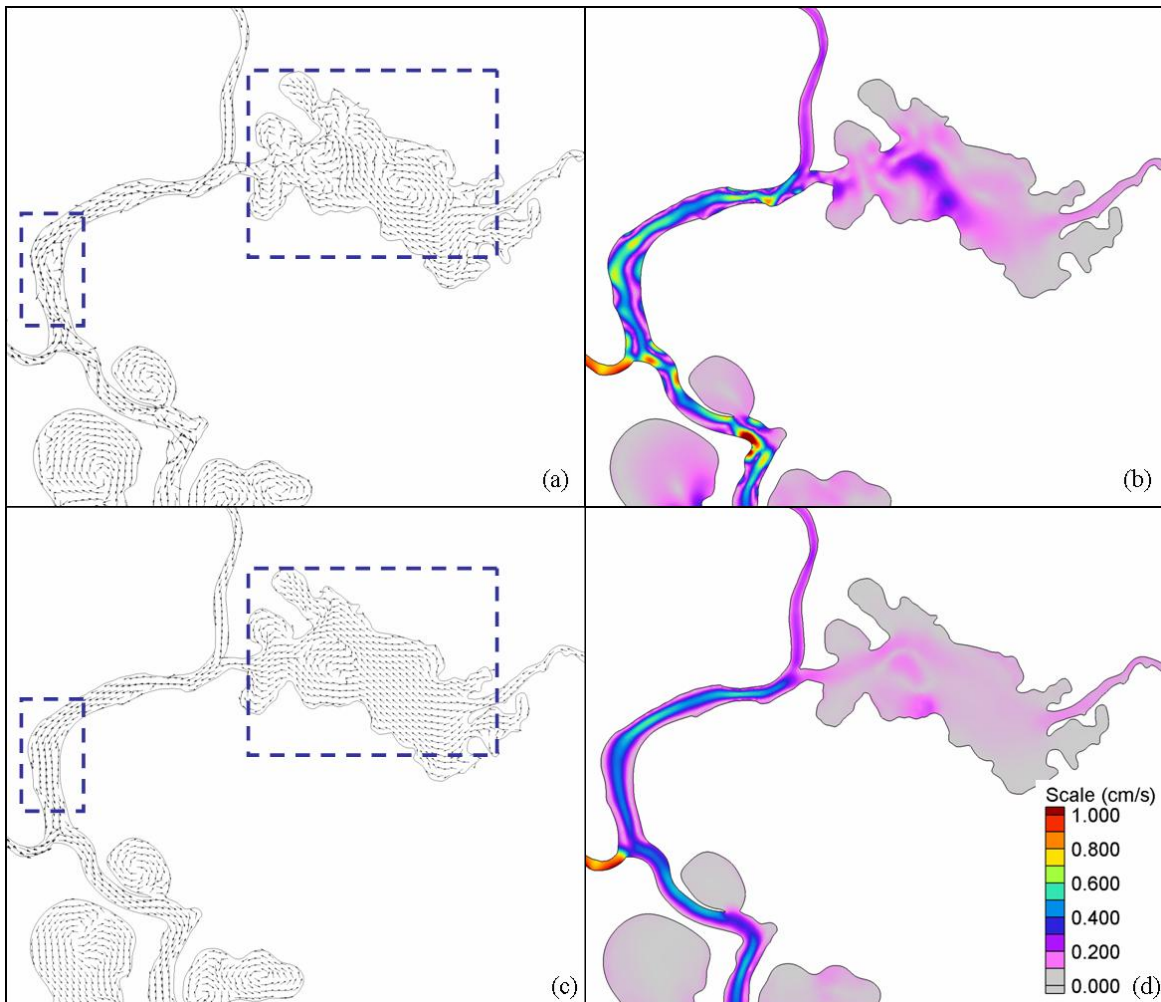


Figure 6.4 Computed velocity residuals at the Escatawpa River near the Beardslee Lake and Roberson Lake: (a) (b) vector and magnitude plots (advection enabled), (c) (d) vector and magnitude plots (advection disabled)

While simulating astronomic tides with advection enabled/disabled, model harmonic constituents were output for a 14-day tidal resynthesis. Three upstream gauge stations were selected to generate the water elevation plots under advection enabled/disabled conditions. In Figure 6.5, the water elevations overlap, indicating that the effect of advection is not significant in the simulated water elevations. To further confirm such observation, another four locations were randomly selected, and their tidal elevations are displayed in Figure 6.6. Similar to the two previous

stations, the discrepancy of water levels between advection enabled and advection disabled is minimal.

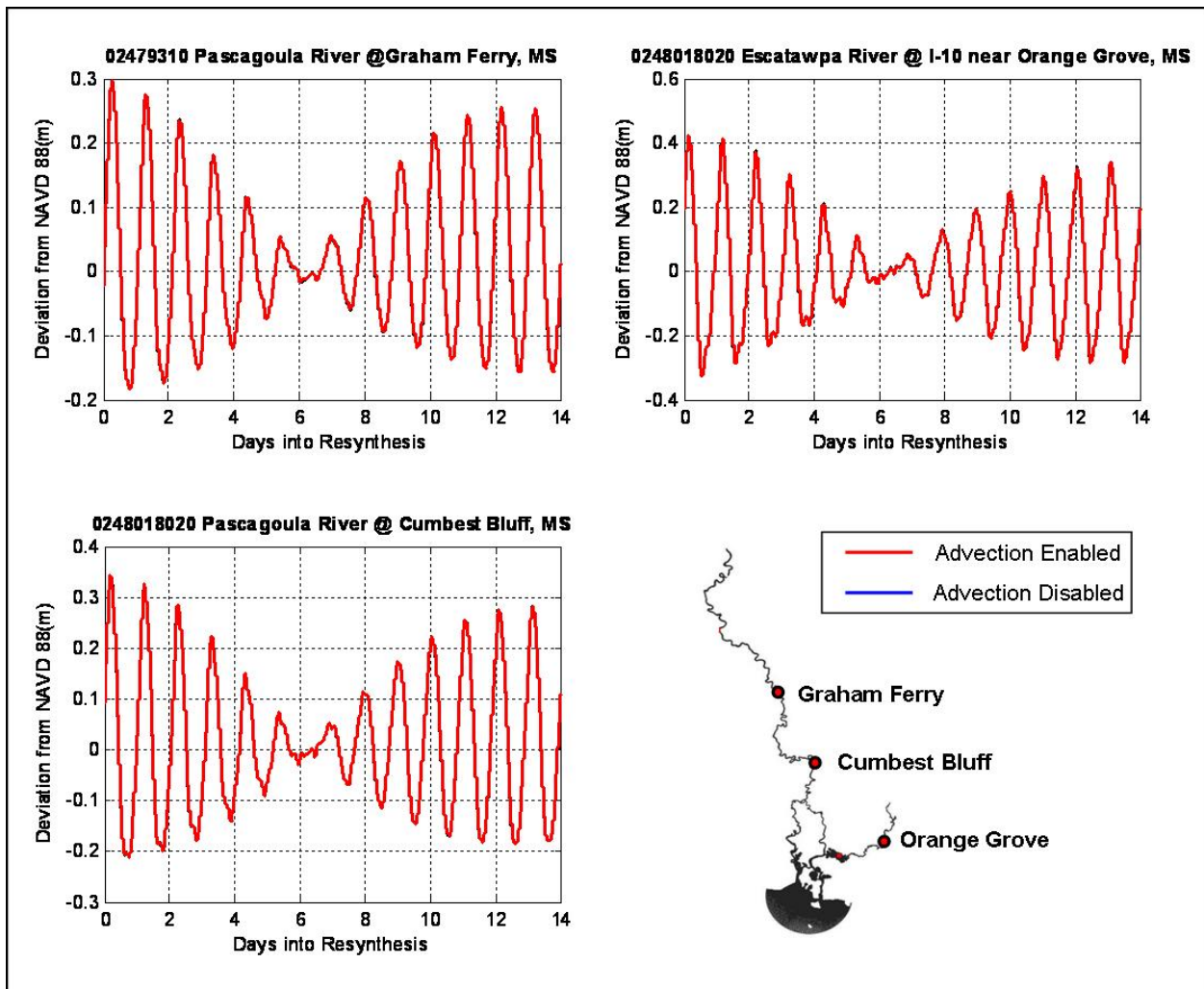


Figure 6.5 Tidal resynthesis plots at selected stations, comparing advection enabled and disabled

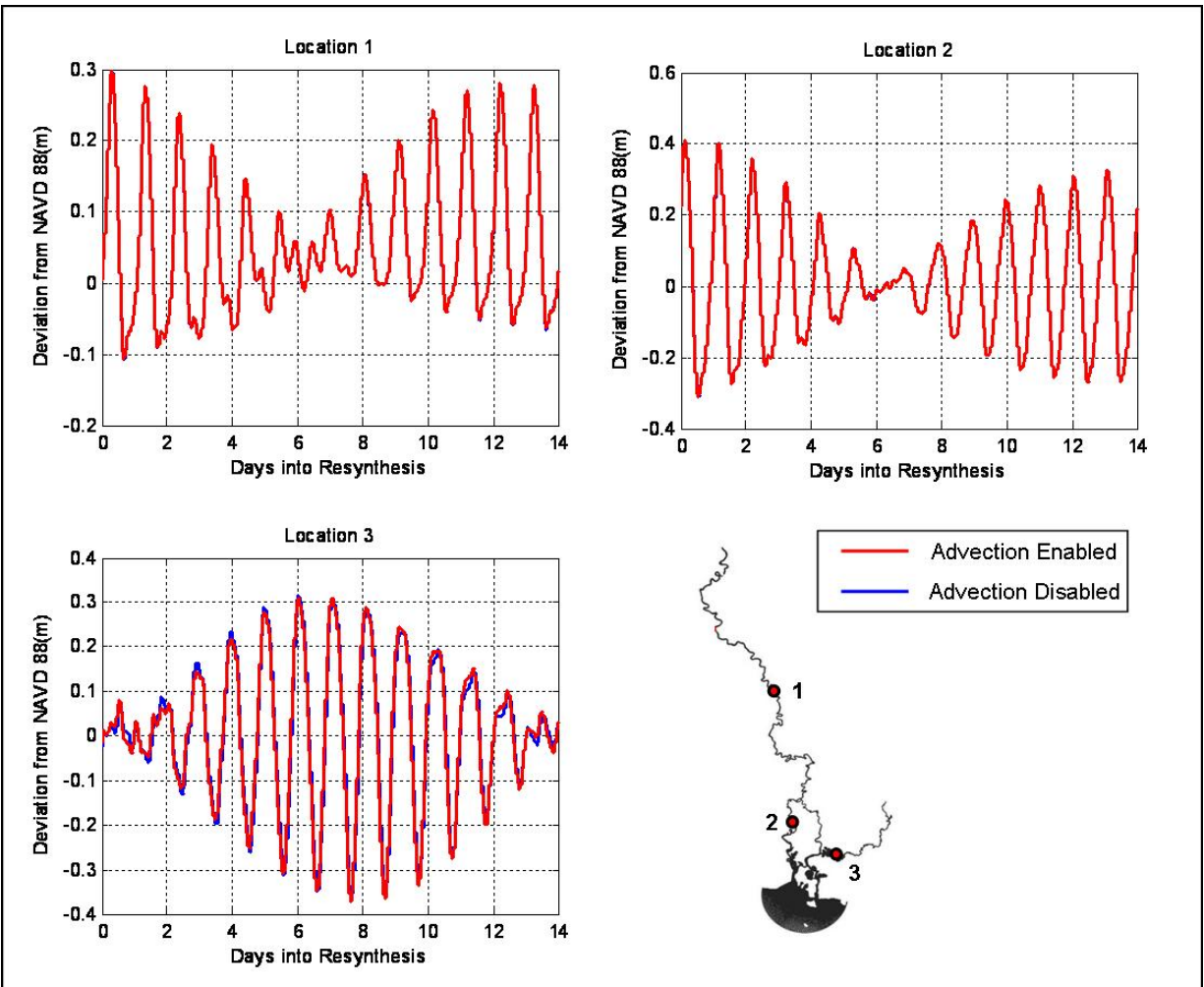


Figure 6.6 Tidal resynthesis plots at randomly selected locations, comparing advection enabled and disabled

After testing the updated Pascagoula River model with/without advection, the influence of advection on velocity residual patterns and tidal elevations can be summarized as follows: Advection provides a positive influence on the velocity simulation, and may significantly alter the simulated flow field. However, the simulated water elevations within the Pascagoula River are insensitive to advection.

CHAPTER 7. CONCLUSIONS AND FUTURE WORK

In this thesis, a finite element model simulating the astronomic tides on the Pascagoula River and its estuary has been developed for the purpose of 1) building an astronomical tidal model to serve as the basis for a storm surge model; 2) providing the nearshore tidal elevation boundary for other local riverine models. The model development began with a comprehensive digital elevation model (DEM) of the lower Pascagoula River including the main channel and four tributaries; later, the preliminary astronomic tide model was generated based on the DEM. Further, three different versions of the preliminary model were developed to investigate the importance of the two inlets within the system. Moreover, an improved Pascagoula River tide model was developed with high resolution bathymetry incorporated into the model. Finally, model sensitivity analyses were conducted with respect to bottom friction and advection. This chapter presents the conclusions of this study and recommendations for future work on this research topic.

7.1 Conclusions

Initial mesh generation efforts were applied to a DEM of the Pascagoula River; this mesh then became a prototype for the preliminary Pascagoula River tide model. During the development of the preliminary Pascagoula River tide model, it was evident that there is a minimum resolution requirement of three elements crossing a channel section in order to adequately describe the

meandering streams within the model region. However, the unprecedented high mesh resolution (with a minimum mesh spacing on the order of five meters) presents a challenge in assigning the model bathymetry. The SL15 model was initially utilized as a bathymetry source, interpolating its model bathymetry to the Pascagoula River tide model. However, the discrepancy in the nodal spacing between the two models reflected that the SL15 model did not provide enough bathymetric resolution for use in the Pascagoula River model. The inappropriate bathymetric data could potentially cause the malfunction of the wetting/drying conditions of the ADCIRC model and introduce a loss in accuracy when computing water levels and velocities.

Based on facts stated, the bathymetry of the preliminary model was updated using the cross section data from USGS and the Mobile hydrographic survey. A useful Cross Section Interpolation Toolbox was developed for the model bathymetry updates that enabled various cross sections to be easily applied into the 2D model with the required resolution. Moreover, the toolbox has the potential for interpolating physical variables other than the bathymetric depths into a 2D model. The improved Pascagoula River tide model performed well in terms of astronomic tides. Improvements on tidal signals were attained at upstream stations after the bathymetry updates were applied. Therefore, the necessity of having similar resolution on the mesh and its bathymetry has been confirmed. Overall, the model results show satisfactory agreement with the historical records at the monitoring gauge stations.

In order to study the complex inlet system of the Pascagoula River, the astronomic tide model has been varied in three ways: inclusion of both inlets, the eastern inlet only and the western inlet

only. Comparing the simulation results from the three models, it has been concluded that the western inlet of the Pascagoula River is more dominate than the eastern inlet. However, it is necessary to include both inlets in the model.

In the preliminary model sensitivity analyses, the model response to adjusting the bottom friction coefficient was examined first. Universal and spatially-varying minimum friction factors (C_{fmin}) were assessed separately. The results of both sets of sensitivity simulations indicate that the Pascagoula River tide model response is sensitive to bottom friction. Results are improved by adjusting the universal or spatially-varying C_{fmin} as shown through the minimization of the RMS errors. However, a spatially varied bottom friction coefficient is more reasonable and effective than a universal bottom friction coefficient. Not only because the bottom roughness related to the stream characteristics can be better described in the model, but also due to its advantages in model stability and computational efficiency. A spatially varied C_{fmin} 0.0025(ocean region)-0.0075(marsh area)-0.0055(middle stream & upstream) is suggested as a good starting point for the Pascagoula River tidal model. Second, the influence of the advection on the tide model has been investigated. After comparing the model results from advection enabled/disabled runs, it is recognized that while advection plays a significant role in velocity simulation, water elevations are insensitive to advection.

7.2 Future Work

The completion of the astronomic tide model provides a solid basis for the storm surge model development. The following suggestions are mainly geared towards the development of a storm

surge model for the Pascagoula riverine system, which will ultimately lead to an operational model for the Lower Mississippi River Forecast Center.

Future work 1: Freshwater inflows should be included on the upstream boundaries, together with the astronomic tidal forcings on the ocean boundary. A pragmatic approach will require initialization of water levels for the upstream portions of the model where the channel inverts are above the datum.

Future work 2: The marsh areas near the inlets should be incorporated into the current inbank model and an assessment performed with respect to astronomic tides.

Future work 3: Inundation areas relative to the surge levels caused by Hurricane Katrina should be added. The more fully developed flood plain model can then be tested for a storm surge simulation driven by Hurricane Katrina.

After employing the suggestions for the future work, the ultimate objective of this overall project – developing an operational storm surge model for the Pascagoula River - can be achieved.

APPENDIX A.
ADCIRC-2DDI INPUT FILE: MESH DESCRIPTION
(Bathymetry Improved Model)

The Pascagoula River Tide Model (Bathymetry Improved)

66442 40060

1 354720.1999937045 3357098.9999965732 3.6597899742

2 354635.5034249023 3357105.4407406980 1.3469199486

3 354580.4179106374 3357042.8180164169 0.9981530256

...

This portion of the input has been eliminated

...

40058 348015.7584692854 3360709.8416962442 0.1779999973

40059 348016.7911018169 3360664.7213545060 0.1779999973

40060 347988.5653508675 3360734.4038821212 0.1779999973

1 3 2 10671 1

2 3 2 3 10671

3 3 10671 3 10672

...

This portion of the input has been eliminated

...

66440 3 40052 40053 40059

66441 3 40056 40057 40060

66442 3 40060 40057 40058

1 = Number of open boundaries

99 = Total number of open boundary nodes

99 = Number of nodes for open boundary 1

10670

20306

23470

...

This portion of the input has been eliminated

...

10672

10671

1

10 = Number of land boundaries

13606 = Total number of land boundary nodes

1810 1 = Number of nodes for land boundary 1

26896

26894

28032

...

This portion of the input has been eliminated

...

10668

10669

10670

APPENDIX B.
ADCIRC-2DDI INPUT FILE: MODEL PARAMETER

Pascagoula River! 32 CHARACTER ALPHANUMERIC RUN DESCRIPTION
Cross Sections Update! 24 CHARACTER ALPHANUMERIC RUN IDENTIFICATION

1 ! NFOVER - NONFATAL ERROR OVERRIDE OPTION
0 ! NABOUT - ABBREVIATED OUTPUT OPTION PARAMETER
0 ! NSCREEN - UNIT 6 OUTPUT OPTION PARAMETER
0 ! IHOT - HOT START PARAMETER
1 ! ICS - COORDINATE SYSTEM SELECTION PARAMETER
0 ! IM - MODEL SELECTION PARAMETER
2 ! NOLIBF - BOTTOM FRICTION TERM SELECTION PARAMETER
2 ! NOLIFA - FINITE AMPLITUDE TERM SELECTION PARAMETER
1 ! NOLICA - SPATIAL DERIVATIVE CONV. SELECTION PARAMETER
1 ! NOLICAT- TIME DERIVATIVE CONV. TERM SELECTION PARAMETER
0 ! NWP - VARIABLE BOTTOM FRICTION & LATERAL VISCOSITY OPTION
0 ! NCOR - VARIABLE CORIOLIS IN SPACE OPTION PARAMETER
0 ! NTIP - TIDAL POTENTIAL OPTION PARAMETER
0 ! NWS - WIND STRESS AND BAROMETRIC PRESSURE OPTION PARAMETER
1 ! NRAMP - RAMP FUNCTION OPTION
9.81 ! G - ACCELERATION DUE TO GRAVITY - DETERMINES UNITS
0.006 ! TAU0 - WEIGHTING FACTOR IN GWCE
0.5 ! DT - TIME STEP (IN SECONDS)
0.00 ! STATIM - STARTING TIME (IN DAYS)
0.00 ! REFTIM - REFERENCE TIME (IN DAYS)
60.0 ! RNDAY - TOTAL LENGTH OF SIMULATION (IN DAYS)
20.0 ! DRAMP - DURATION OF RAMP FUNCTION (IN DAYS)
0.35 0.30 0.35 ! TIME WEIGHTING FACTORS FOR THE GWCE EQUATION
0.01 2 1 0.05 ! H0, NODEDRYMIN, NODEWETRMP, VELMIN
-88.6 30.6 ! SLAM0,SFEA0 - CENTER OF CPP PROJECTION (NOT USED IF IC
0.0025 10.0 10.0 0.33333 ! FFACTOR,HBREAK,FTHETA,FGAMMA
5.00 ! ESL - LATERAL EDDY VISCOSITY COEFFICIENT
0.0000742398 ! CORI - CORIOLIS PARAMETER
0 ! NTIF - TOTAL NUMBER OF TIDAL POTENTIAL CONSTITUENTS
23 ! NBFR - TOTAL NUMBER OF FORCING FREQUENCIES ON OPEN
BOUNDARY

STEADY ! ALPHANUMERIC DATA FOR OPEN OCEAN BOUNDARY FORCING DATA
0.0000000000000000 1.000 0.000
MN ! ALPHANUMERIC DATA FOR OPEN OCEAN BOUNDARY FORCING DATA
0.000002639203022 1.000 0.000
SM ! ALPHANUMERIC DESCRIPTION OF OPEN BOUNDARY FORCING DATA
0.000004925201824 1.000 0.000
O1 ! ALPHANUMERIC DESCRIPTION OF OPEN BOUNDARY FORCING DATA
0.000067597744150 1.000 0.000
K1 ! ALPHANUMERIC DESCRIPTION OF OPEN BOUNDARY FORCING DATA
0.000072921158360 1.000 0.000
MNS2! ALPHANUMERIC DESCRIPTION OF OPEN BOUNDARY FORCING DATA

0.000132954497700 1.000 0.000
 2MS2 ! ALPHANUMERIC DESCRIPTION OF OPEN BOUNDARY FORCING DATA
 0.000135593700700 1.000 0.000
 N2 ! ALPHANUMERIC DESCRIPTION OF OPEN BOUNDARY FORCING DATA
 0.000137879699500 1.000 0.000
 M2 ! ALPHANUMERIC DESCRIPTION OF OPEN BOUNDARY FORCING DATA
 0.000140518902500 1.000 0.000
 2MN2 ! ALPHANUMERIC DESCRIPTION OF OPEN BOUNDARY FORCING DATA
 0.000143158105500 1.000 0.000
 S2 ! ALPHANUMERIC DESCRIPTION OF OPEN BOUNDARY FORCING DATA
 0.000145444104300 1.000 0.000
 2SM2 ! ALPHANUMERIC DESCRIPTION OF OPEN BOUNDARY FORCING DATA
 0.000150369306200 1.000 0.000
 MN4 ! ALPHANUMERIC DESCRIPTION OF OPEN BOUNDARY FORCING DATA
 0.000278398602000 1.000 0.000
 M4 ! ALPHANUMERIC DESCRIPTION OF OPEN BOUNDARY FORCING DATA
 0.000281037805000 1.000 0.000
 MS4 ! ALPHANUMERIC DESCRIPTION OF OPEN BOUNDARY FORCING DATA
 0.000285963006800 1.000 0.000
 2MN6 ! ALPHANUMERIC DESCRIPTION OF OPEN BOUNDARY FORCING DATA
 0.000418917504500 1.000 0.000
 M6 ! ALPHANUMERIC DESCRIPTION OF OPEN BOUNDARY FORCING DATA
 0.000421556707500 1.000 0.000
 MSN6 ! ALPHANUMERIC DESCRIPTION OF OPEN BOUNDARY FORCING DATA
 0.000423842706300 1.000 0.000
 M8 ! ALPHANUMERIC DESCRIPTION OF OPEN BOUNDARY FORCING DATA
 0.000562075610000 1.000 0.000
 M10 ! ALPHANUMERIC DESCRIPTION OF OPEN BOUNDARY FORCING DATA
 0.000702594512500 1.000 0.000
 P1 ! ALPHANUMERIC DESCRIPTION OF OPEN BOUNDARY FORCING DATA
 0.000072522946000 1.000 0.000
 K2 ! ALPHANUMERIC DESCRIPTION OF OPEN BOUNDARY FORCING DATA
 0.000145842317200 1.000 0.000
 Q1 ! ALPHANUMERIC DESCRIPTION OF OPEN BOUNDARY FORCING DATA
 0.000064958541130 1.000 0.000
 STEADY
 0.0015468323 0.0000000000
 0.0015458046 0.0000000000
 0.0015447884 0.0000000000
 ...
This portion of the input has been eliminated
 ...
 0.0322069130 9.2633000000
 0.0322113720 9.2730000000

0.0322591020 9.2788000000
 100.0 ! ANGINN : INNER ANGLE THRESHOLD
 1 0.0 60.0 720 ! NOUTE,TOUTSE,TOUTFE,NSPOOLE:ELEV. STA. OUTPUT INFO
 12 ! TOTAL NUMBER OF ELEVATION RECORDING STATIONS
 349435.1846371370 3359533.2070351100 ! NOS Station: 8741533 Pascagoula, MS
 352611.5900435160 3357457.4420957800 ! NOS Station: 8741196 Pascagoula Point,
 Mississippi Sound, MS
 345415.3554692510 3362299.4077800800 ! USGS Station: 02480285 West Pascagoula @
 Highway 90 @ Gautier, MS
 342659.4323795410 3387590.8467565200 ! USGS Station: 02479310 Pascagoula River @
 Graham Ferry, MS
 349763.5864578980 3360598.7989462300 ! USGS Station: 02480212 Pascagoula River @
 Mile 1 @ Pascagoula, MS
 360657.7151295040 3370499.7074643100 ! USGS Station: 0248018020 Escatawpa River @
 1-10 near Orange Grove, MS
 349462.2665916600 3384537.4267534000 ! USGS Station: 02479330 Pascagoula River @
 Cumbest Bluff, MS
 1 0.0 60.0 720 ! NOUTV,TOUTSV,TOUTFV,NSPOOLV:VEL STA OUTPUT INFO
 12 ! TOTAL NUMBER OF VELOCITY RECORDING STATIONS
 349435.1846371370 3359533.2070351100 ! NOS Harmonics Station: 8741533 Pascagoula,
 MS
 ...
This portion of the input has been eliminated
 ...
 349462.2665916600 3384537.4267534000 ! USGS Water Levels Station: 02479330
 Pascagoula River @ Cumbest Bluff, MS
 1 28.0 42.0 7200 ! NOUTGE,TOUTSGE,TOUTFGE,NSPOOLGE: GLOBAL ELEV OUT
 1 28.0 42.0 7200 ! NOUTGV,TOUTSGV,TOUTFGV,NSPOOLGV : GLOBAL VEL OUT
 23 ! NHARFR - NUMBER OF CONSTI. IN HARMONIC ANALYSIS
 STEADY ! HAFNAM - ALPHA DESCRIPTOR FOR CONSTITUENT NAME
 0.0000000000000000 1.0 0.0 ! HAFREQ, HAFF, HAFAE
 MN
 0.000002639203022 1.0 0.0
 ...
This portion of the input has been eliminated
 ...
 Q1
 0.000064958541129 1.0 0.0
 30.0 60.0 600 0.0 ! THAS,THAF,NHAINC
 1 1 1 1 ! NHASE,NHASV,NHAGE
 0 8640 ! NHSTAR
 1 0 1.00E-10 25 0 ! ITITER, ISLDIA, CONVCR, ITMAX, ILUMP
 11 ! MNPROC

APPENDIX C.
TIDAL CONSTITUENTS FOR HARMONIC ANALYSIS

Table C.1 23 tidal constituents applied in ADCIRC harmonic analysis

| <i>Constituent</i> | <i>Description</i> | <i>Frequency (rad/s)</i> | <i>Degrees per solar hour</i> |
|--------------------|--|--------------------------|-------------------------------|
| STEADY | Principal water level | 0.0000000000000000 | 0.0000 |
| MN4 | Lunar monthly constituent | 0.000000420111582 | 0.5445 |
| SM | Lunisolar synodic fortnightly constituent | 0.000000783620452 | 1.0156 |
| O1 | Lunar diurnal constituent | 0.000010756574418 | 13.9405 |
| K1 | Lunar diurnal constituent | 0.000011608900776 | 15.0451 |
| MNS2 | Arising from interaction between MN and S2 | 0.000021159184779 | 27.4223 |
| 2MS2 | Variational constituent | 0.000021593421780 | 27.9851 |
| N2 | Larger lunar elliptic semi-diurnal constituent | 0.000021962189894 | 28.4630 |
| M2 | Principal lunar semi-diurnal constituent | 0.000022343772344 | 28.9575 |
| 2MN2 | Smaller lunar elliptic semi-diurnal constituent | 0.000022783610382 | 29.5276 |
| S2 | Principal solar semi-diurnal constituent | 0.000023148148148 | 30.0000 |
| 2SM2 | Shallow-water semi-diurnal constituent | 0.000023913376186 | 30.9917 |
| MN4 | Shallow-water quarter diurnal constituent | 0.000044345111395 | 57.4713 |
| M4 | Shallow-water overtides of principal lunar constituent | 0.000044687544688 | 57.9151 |
| MS4 | Shallow-water quarter diurnal constituent | 0.000045567220764 | 59.0551 |
| 2MN6 | Shallow-water twelfth diurnal constituent | 0.000066517667092 | 86.2069 |
| M6 | Shallow-water overtides of principal lunar constituent | 0.000066902162278 | 86.7052 |
| MSN6 | Arising from interaction between M2, N2 and S2 | 0.000067291128338 | 87.2093 |
| M8 | Shallow-water eighth diurnal constituent | 0.000089721504450 | 116.2791 |
| M10 | Shallow-water tenth diurnal constituent | 0.000111289173789 | 144.2308 |
| P1 | Solar diurnal constituent | 0.000011539455707 | 14.9551 |
| K2 | Lunisolar semi-diurnal constituent | 0.000025777447826 | 33.4076 |
| Q1 | Larger lunar elliptic diurnal constituent | 0.000010333994709 | 13.3929 |

Table C.2 37 tidal constituents used in the resynthesis of the historical tidal records for the NOS stations.

| <i>Constituent</i> | <i>Tidal species</i> | <i>Frequency (rad/s)</i> | <i>Degrees per solar hour</i> |
|--------------------|----------------------|--------------------------|-------------------------------|
| SA | long-period | 0.000000199106190 | 0.2580 |
| SSA | long-period | 0.000000398212870 | 0.5161 |
| MM | long-period | 0.000002639203000 | 3.4204 |
| MSF | long-period | 0.000004925201800 | 6.3831 |
| MF | long-period | 0.000005323414700 | 6.8991 |
| 2Q1 | diurnal | 0.000062319338000 | 80.7659 |
| Q1 | diurnal | 0.000064958541000 | 84.1863 |
| RHO1 | diurnal | 0.000065311745000 | 84.6440 |
| O1 | diurnal | 0.000067597744000 | 87.6067 |
| M1 | diurnal | 0.000070281955000 | 91.0854 |
| P1 | diurnal | 0.000072522946000 | 93.9897 |
| S1 | diurnal | 0.000072722052000 | 94.2478 |
| K1 | diurnal | 0.000072921158000 | 94.5058 |
| J1 | diurnal | 0.000075560361000 | 97.9262 |
| OO1 | diurnal | 0.000078244573000 | 101.4050 |
| 2N2 | semi-diurnal | 0.000135240500000 | 175.2717 |
| MU2 | semi-diurnal | 0.000135593700000 | 175.7294 |
| N2 | semi-diurnal | 0.000137879700000 | 178.6921 |
| NU2 | semi-diurnal | 0.000138232900000 | 179.1498 |
| M2 | semi-diurnal | 0.000140518900000 | 182.1125 |
| LDA2 | semi-diurnal | 0.000142804900000 | 185.0752 |
| L2 | semi-diurnal | 0.000143158110000 | 185.5329 |
| T2 | semi-diurnal | 0.000145245010000 | 188.2375 |
| S2 | semi-diurnal | 0.000145444100000 | 188.4956 |
| R2 | semi-diurnal | 0.000145643200000 | 188.7536 |
| K2 | semi-diurnal | 0.000145842320000 | 189.0116 |
| 2SM2 | semi-diurnal | 0.000150369310000 | 194.8786 |
| 2MK3 | terdiurnal | 0.000208116650000 | 269.7192 |
| M3 | terdiurnal | 0.000210778350000 | 273.1687 |
| MK3 | terdiurnal | 0.000213440060000 | 276.6183 |
| MN4 | fourth-diurnal | 0.000278398600000 | 360.8046 |
| M4 | fourth-diurnal | 0.000281037810000 | 364.2250 |

| | | | |
|-----|----------------|-------------------|----------|
| MS4 | fourth-diurnal | 0.000285963010000 | 370.6081 |
| S4 | fourth-diurnal | 0.000290888210000 | 376.9911 |
| M6 | sixth-diurnal | 0.000421556710000 | 546.3375 |
| S6 | sixth-diurnal | 0.000436332310000 | 565.4867 |
| M8 | eighth-diurnal | 0.000562075610000 | 728.4500 |

Table C.3 35 tidal constituents at the USGS stations extracted by T_TIDE

| <i>Constituent</i> | <i>Tidal species</i> | <i>Frequency (rad/s)</i> | <i>Degrees per solar hour</i> |
|--------------------|----------------------|--------------------------|-------------------------------|
| MM | long-period | 0.000002639286895 | 3.4205 |
| MSF | long-period | 0.000004925144616 | 6.3830 |
| ALP1 | diurnal | 0.000060033392149 | 77.8033 |
| 2Q1 | diurnal | 0.000062319424403 | 80.7660 |
| Q1 | diurnal | 0.000064958536765 | 84.1863 |
| O1 | diurnal | 0.000067597823660 | 87.6068 |
| NO1 | diurnal | 0.000070281965517 | 91.0854 |
| K1 | diurnal | 0.000072921077879 | 94.5057 |
| J1 | diurnal | 0.000075560364774 | 97.9262 |
| OO1 | diurnal | 0.000078244506630 | 101.4049 |
| UPS1 | diurnal | 0.000080883793525 | 104.8254 |
| EPS2 | semi-diurnal | 0.000132954470028 | 172.3090 |
| MU2 | semi-diurnal | 0.000135593756923 | 175.7295 |
| N2 | semi-diurnal | 0.000137879614644 | 178.6920 |
| M2 | semi-diurnal | 0.000140518901539 | 182.1125 |
| L2 | semi-diurnal | 0.000143158188434 | 185.5330 |
| S2 | semi-diurnal | 0.000145444046155 | 188.4955 |
| ETA2 | semi-diurnal | 0.000148481442652 | 192.4319 |
| MO3 | terdiurnal | 0.000208116725199 | 269.7193 |
| M3 | terdiurnal | 0.000210778352309 | 273.1687 |
| MK3 | terdiurnal | 0.000213439979418 | 276.6182 |
| SK3 | terdiurnal | 0.000218365298567 | 283.0014 |
| MN4 | fourth-diurnal | 0.000278398516183 | 360.8045 |
| M4 | fourth-diurnal | 0.000281037803078 | 364.2250 |
| SN4 | fourth-diurnal | 0.000283323835332 | 367.1877 |
| MS4 | fourth-diurnal | 0.000285962947694 | 370.6080 |
| S4 | fourth-diurnal | 0.000290888266843 | 376.9912 |
| 2MK5 | fifth-diurnal | 0.000353958880957 | 458.7307 |
| 2SK5 | fifth-diurnal | 0.000363809344722 | 471.4969 |
| 2MN6 | sixth-diurnal | 0.000418917592255 | 542.9172 |
| M6 | sixth-diurnal | 0.000421556704617 | 546.3375 |
| 2MS6 | sixth-diurnal | 0.000426481849233 | 552.7205 |
| 2SM6 | sixth-diurnal | 0.000431407168382 | 559.1037 |
| 3MK7 | seventh-diurnal | 0.000494477782496 | 640.8432 |
| M8 | eighth-diurnal | 0.000562075606156 | 728.4500 |

APPENDIX D.
CROSS SECTION INTERPOLATION TOOLBOX (FORTRAN CODE)

C Cross Section Interpolation Toolbox (Qing Wang, June 2008)

PROGRAM MAIN

C MAXNODE: MAX. NODE NUMBER
C NN: THE NUMBER OF NODES ON THE TOPOGRAPHIC BOUNDARY
C NA: THE NUMBER OF BATHYMETRIC POINTS ON THE CROSS SECTION
C LEFT_ARC, RIGHT_ARC, MID_ARC: THE TOPOGRAPHIC ARCS ALONG THE
CHANNEL
C DEPTH: DEPTH MATRIX OF ALL THE POINTS

C INPUT FILE: Boundary_Topo.xy; Cross_Section_profile.dat
C OUTPUT FILE: Interpolated_Scatter_Set.dat

IMPLICIT REAL*8(A-H,O-Z)
REAL*8 X_OLD, Y_OLD, XX, YY
REAL*8 DEPTH
REAL*8 LEFT_ARC, RIGHT_ARC, MID_ARC
REAL*8 X, Y
INTEGER NODE_T, NODE, NODE_NEW
CHARACTER*4 STR
CHARACTER*90 ANT*80
CHARACTER*30 INPUT

ALLOCATABLE :: NODE(:), NODE_NEW(:)
ALLOCATABLE :: X_OLD(:), Y_OLD(:), XX(:), YY(:),
& LEFT_ARC(:,2), RIGHT_ARC(:,2), MID_ARC(:,2),
& X(:,2), Y(:,2), DEPTH(:,2)

PRINT *, "ENTER THE NUMBER OF NODES ON THE TOPOGRAPHIC
BOUNDARY:"

READ (*,*) NN

PRINT *, "ENTER THE NUMBER OF BATHYMETRIC PTS ON THE CROSS
SECTION:"

READ (*,*) NA

MAXNODE=2*NN

ALLOCATE(NODE(MAXNODE), X_OLD(MAXNODE), Y_OLD(MAXNODE),
& NODE_NEW(MAXNODE), XX(MAXNODE), YY(MAXNODE),
& LEFT_ARC(NN,2), RIGHT_ARC(NN,2), MID_ARC(NN,2),
& X(NN,NA), Y(NN,NA), DEPTH(NA,2))

C----- READ SCATTER FILE "Boundary_Topo.xy" AND REFORMAT -----

C NODE_T: TOTAL NODE NUMBER
C NODE(I): THE I-TH NODE NUMBER
C NODE_NEW: NODE INDEX IN ASCENDING ORDER
C X_OLD: X COORDANATE VAULES READ FROM SMS.XY FILE
C Y_OLD: Y COORDANATE VULES READ FROM SMS.XY FILE
C XX: REARRANGED X VALUES
C YY: REARRANGED Y VAULES

OPEN (1,FILE='Boundary_Topo.xy')

DO II=1,5
READ (1,*) ANT
ENDDO

READ (1,*) STR, NODE_T

IF (NODE_T.NE.MAXNODE) THEN
PRINT *, "INCORRECT INPUT OF TOPOGRAPHIC BOUNDARY NODES.
&INTERPOLATION TERMINATED."
STOP
ENDIF

DO I=1, NODE_T
READ(1, *) NODE(I), X_OLD(I), Y_OLD(I)
ENDDO

IF(NODE(1).NE.1) THEN
DO J=1,NODE_T
NODE_NEW(J)=NODE(NODE_T-J+1)
XX(J)=X_OLD(NODE_T-J+1)
YY(J)=Y_OLD(NODE_T-J+1)
ENDDO

ELSE
DO J=1,NODE_T
NODE_NEW(J)=NODE(J)
XX(J)=X_OLD(J)
YY(J)=Y_OLD(J)
ENDDO
ENDIF

C----- END OF REFORMAT -----


```

OPEN(7,FILE='./Cross_Section_Profile.dat')
OPEN(8,FILE='./Interpolated_Scatter_Set.dat')

DO 10 I=1,NA
  READ(7,*) DEPTH(I,1), DEPTH(I,2)

  DO 20 K=1,NN
    LEFT_ARC(K,1)=XX(K)
    LEFT_ARC(K,2)=YY(K)
    RIGHT_ARC(K,1)=XX(K+NN)
    RIGHT_ARC(K,2)=YY(K+NN)
  20 CONTINUE

  CALL DEPTH_INTERP(LEFT_ARC, DEPTH(1,1), DEPTH(1,2), NN)
  CALL DEPTH_INTERP(RIGHT_ARC, DEPTH(NA,1), DEPTH(NA,2), NN)

  DO 30 I=1,NN
    DO 40 J=1,NA-2
      X(I,J)=LEFT_ARC(I,1)+(RIGHT_ARC(I,1)-LEFT_ARC(I,1))/(NA-1)*J
      Y(I,J)=LEFT_ARC(I,2)+(RIGHT_ARC(I,2)-LEFT_ARC(I,2))/(NA-1)*J
    40 CONTINUE
  30 CONTINUE

  DO 50 J=1,NA-2
    DO 60 I=1,NN
      MID_ARC(I,1)=X(I,J)
      MID_ARC(I,2)=Y(I,J)
    60 CONTINUE
    CALL DEPTH_INTERP(MID_ARC, DEPTH(J+1,1), DEPTH(J+1,2), NN)
  50 CONTINUE
END
C
C-----
C
SUBROUTINE DEPTH_INTERP(S, Z_DOWN, Z_UP, NODE )

  REAL*8 SS(NODE,3), S(NODE,2), Z_DOWN, Z_UP
  INTEGER NODE

  DO 70 I=1,NODE
    SS(I,1)=S(I,1)

```

```
      SS(I,2)=S(I,2)
      SS(I,3)=Z_DOWN+(Z_UP-Z_DOWN)/(NODE-1)*(I-1)
70  CONTINUE

      DO JJ=1, NODE
        WRITE (8,100 ) SS(JJ,1), SS(JJ,2), SS(JJ,3)
      ENDDO

100  FORMAT(E25.16E3, E25.16E3, E12.3E2)
      RETURN

      END
```

REFERENCES

- Bacopoulos, P. (2006). "Analysis, Modeling, and Simulation of the Tides in the Loxahatchee River Estuary (Southeastern Florida)." University of Central Florida, Orlando, FL. Master's Thesis.
- Bowden, K. F. (1983). *Physical oceanography of coastal waters*. Halsted Press, New York.
- Cartwright, D. E. and R. J. Taylor (1971). "New computation of the tide-generating potential." *Geophysical Journal of the Royal Astronomical Society* 298: 87-139.
- Cobb, M. and C.A. Blain (2001). "A coupled hydrodynamic-wave model for simulating wave and tidally-driven 2D circulation in inlets." *Proceedings of the 7th International Conference on Estuarine and Coastal Modeling*, New York, ASCE.
- Darwin, G. H. (1911). *The tides and kindred phenomena in the solar system*. John Murray, London, United Kingdom.
- Department of the Army; U.S. Army Corps of Engineers (2007). "Intent to prepare a draft supplemental environmental impact statement to evaluate construction of authorized improvements to the federal Pascagoula Harbor navigation project in Jackson County, MS." 38069-38070.
- Doodson, A. T. (1928). "The analysis of tidal observations." *Philosophical Transactions of the Royal Society of London* 227: 223-279.
- Droppo, Ian G. (2003). "Preserving the Pascagoula: D.G. Schueler." *Estuarine, Coastal and Shelf Science* 57(5-6): 1197-1198.
- Funakoshi, Y. (2006). "Coupling of hydrodynamic and wave models for storm tide simulations: A case study for Hurricane Floyd (1999)." University of Central Florida, Orlando, FL. Ph.D. Dissertation.
- Gallo, M. N. and S. B. Vinzon (2005). "Generation of overtides and compound tides in Amazon estuary." *Ocean Dynamics* 55(5-6): 441-448.
- Godin, G. and A. Martinez (1994). "Numerical experiments to investigate the effects of quadratic friction on the propagation of tides in a channel." *Continental Shelf Research* 14(7/8): 723-748.

- Godin, G. (1999). "The propagation of tides up rivers with special considerations on the upper Saint Lawrence River." *Coastal and Shelf Science* 48(3): 307-324.
- Godin, G. (1991). "Compact approximations to the bottom friction term for the study of tides propagating in channels." *Continental Shelf Research* 11(7): 579-589.
- Grenier, R. R. Jr., R. A. Jr. Luettich, et al. (1993). "Comparison of 2D and 3D models for computing shallow water tides in a friction-dominated tidal embayment." *Proceedings of the 3rd International Conference*, Oak Brook, IL, ASCE.
- Grenier, R. R. Jr., R. A. Luettich, et al. (1995). "A comparison of the nonlinear frictional characteristics of two-dimensional and three-dimensional models of a shallow tidal embayment." *Journal of Geophysical Research-Oceans* 100(C7): 13,719-13,735.
- Grenier, R. R. Jr., R. A. Jr. Luettich, and J. J. Westerink (1994). "Comparison of 2D and 3D models for computing shallow water tides in a friction-dominated tidal embayment." *Proceedings of the 3rd International Conference*, Oak Brook, IL, ASCE.
- Griffin, A. (2008). "Tides, as explained by Newton." *Physics Education*, March: 129-131.
- Hagen, S. C., J. J. Westerink, et al. (2000). "One-dimensional finite element grids based on a localized truncation error analysis." *International Journal for Numerical Methods in Fluids*, 32: 241-261.
- Hagen, S. C., J. J. Westerink, et al. (2001). "Two-dimensional, unstructured mesh generation for tidal models." *International Journal for Numerical Methods in Fluids* 35: 669-686.
- Hagen, S. C. and D. M Parrish (2004). "Meshing requirements for tidal modeling in the western North Atlantic." *International Journal of Computational Fluid Dynamics* 18(7): 585-595.
- Hagen, S.C., A.K. Zundel, et al. (2006). "Automatic, Unstructured Mesh Generation for Tidal Calculations in a Large Domain." *International Journal of Computational Fluid Dynamics* 20(8): 593-608.
- Hamilton, P. (1990). "Modeling Salinity and circulation for the Columbia River Estuary." *Progress in Oceanography* 25(1-4): 113-156.
- Hartel, H. (2000). "The tides - a neglected topic." *Physics Education* 35(1): 40-45.
- Hashemi, M. R., M. J. Abedini, et al. (In Press). "Tidal and surge modelling using differential quadrature: A case study in the Bristol Channel." *Coastal Engineering* In Press, Corrected Proof.

- Hendershott, M. C. (1981). "Long waves and ocean tides." *Evolution of Physical Oceanography*. Publisher. Cambridge, MA, B. A. Warren and C. Wunsch: 292-341.
- Hicks, S. D. (2006). "Understanding tides." National Oceanic and Atmospheric Administration, National Ocean Service, Silver Springs, MD.
- Horn, W. (1960). "Some recent approaches to tidal problems." *International Hydrographic Review* 37(2): 65-88.
- Hu, K., C.G. Mingham, et al. (1997). "Numerical simulation of tidal induced circulation and waves in harbours." *Proceedings of the 1997 3rd International Conference on Computer Modelling of Seas and Coastal Regions*, La Coruna, Spain.
- IPET Force - U.S. Army Corps. of Engineers (2007). "Performance evaluation of the New Orleans and Southeast Louisiana Hurricane Protection System." Vicksburg, MS.
- Ishiguro, S. (1972). "Electronic analogues in oceanography." *Oceanography and Marine Biology: An Annual Review* 10: 27-96.
- Jones, J. E. and A. M. Davies (2005). "An intercomparison between finite difference and finite element (TELEMAC) approaches to modelling west coast of Britain tides." *Ocean Dynamics* 55(3-4): 178-198.
- Jones, J. E. and Alan M. Davies (2007). "On the sensitivity of computed higher tidal harmonics to mesh size in a finite element model." *Continental Shelf Research* 27(14): 1908-1927.
- Kapoulitsas, G. M. (1985). "On the generation of tides." *European Journal of Physics* 6: 201-207.
- Kinmark, I., Ed. (1985). *The shallow water wave equations: Formulation, analysis and application*. Lecture Notes in Engineering. New York, New York, Springer-Verlag.
- Kolar, R. L., W. G. Gray, et al. (1994). "Shallow water modeling in spherical coordinates: Equation formulation, numerical implementation, and application." *Journal of Hydraulic Research* 32(1): 3-24.
- Kolar, R. L., J. J. Westerink, et al. (1994). "Aspects of non-linear simulations using shallow water models based on the wave continuity equation." *Computers and Fluids* 23(3): 523-538.
- Leendertse, J. J. (1988). "Influence of the advection term approximation on computed tidal propagation and circulation." The RAND Corporation, Santa Monica, CA.

- Lewis, G. D. and B. J. Noye, Eds. (1999). "Analysis and prediction of tide heights over tidal flats and currents involving eddies." *Modelling Coastal Sea Processes*. Singapore, World Scientific Publishing, 81-106.
- Luetlich, R. A. Jr. and J. J. Westerink (2000). "ADCIRC: A (parallel) advanced circulation model for oceanic, coastal and estuarine waters." Users manual, http://www.marine.unc.edu/C_CATS/adcirc/adcirc.htm.
- Luetlich, R.A., S.D. Carr, et al. (2002). "Semi-diurnal seiching in a shallow, micro-tidal lagoonal estuary." *Continental Shelf Research* 22: 1669-1681.
- Moore, M. J. C. and R. A. Seigel (2006). "No place to nest or bask: Effects of human disturbance on the nesting and basking habits of yellow-blotched map turtles (*Graptemys flavimaculata*)." *Biological Conservation* 130(3): 386-393.
- Mossa, J. and D. Coley (2004). "Planform change rates in rivers with and without instream and floodplain sand and gravel mining: Assessing instability in the Pascagoula River and Tributaries, Mississippi." University of Florida, Gainesville, FL.
- Munk, W. and D. Cartwright (1966). "Tidal spectroscopy and prediction." *Philosophical Transactions of the Royal Society of London* 259(553-581).
- Murray, R. R. (2003). "A sensitivity analysis for a tidally-influenced riverine system." University of Central Florida, Orlando, FL. Master's Thesis.
- Noye, B. J., J. B. Nixon, et al., Eds. (1999). "A 3D numerical model of tides and surges in coastal seas with tidal flats." *Modelling Coastal Sea Processes*. Singapore, World Scientific Publishing, 21-56.
- Oldham, M. B. Jr. and J. W. Rushing (1970). "Water resources planning for Pascagoula Basin." *Journal of the Waterways and Harbors Division, Proceedings of the American Society of Civil Engineers* 96(WW1): 65-85.
- Parrish, D. M. (2001). "Development of a tidal constituent database for the St. Johns River Water Management District." University of Central Florida, Orlando, FL. Master's Thesis.
- Parrish, D.M. and S. C. Hagen (2007). "2D, unstructured mesh generation for oceanic and coastal tidal models from a localized truncation error analysis with complex derivatives." *International Journal of Computational Fluid Dynamics* 21(7&8): 277-296.
- Pascagoula Harbor (1997). "Pascagoula Harbour, Mississippi - condition of improvement on 30 September 1997."

- Pawlowicz, R., B. Beardsley, et al. (2002). "Classical tidal harmonic analysis including error estimates in MATLAB using T_TIDE." *Computers and Geosciences* 28: 929-937.
- Pugh, D. T. (2004). *Changing sea levels: Effects of tides, weather and climate*. Cambridge University Press, Cambridge, UK.
- Reggio, M., A. Hess, et al. (2002). "3-D multiple-level simulation of free surface flows." *Journal of Hydraulic Research* 40(4): 413-425.
- Reid, R. O. (1990). Waterlevel changes, tides and storm surges. *Handbook of Coastal and Ocean Engineering*. Houston, Texas.
- Salisbury, M. B. and S. C. Hagen (2007). "The Effect of Tidal Inlets on Open Coast Storm Surge Hydrographs." *Coastal Engineering* 54: 377-391.
- Schwiderski, E. W. (1980). "On charting global ocean tides." *Reviews of Geophysics and Space Physics* 18: 243-268.
- Takahashi, N. (2008). "Study of a hurricane storm surge hindcast for the Pascagoula River in Mississippi." University of Central Florida, Orlando, FL. Master's Thesis (unpublished).
- Teubner, M. D., H. S. Najafi, et al., Eds. (1999). "Modelling tides in the Persian Gulf using dynamic nesting." *Modelling Coastal Sea Processes*. Singapore, World Scientific Publishing, 57-80.
- The Port of Pascagoula. (2008). "The history of the Port of Pascagoula." Retrieved May 13th, 2008, from <http://www.portofpascagoula.com/>.
- Tsvetsinsky, A. S., B. V. Arkhipov, et al. (1998). "Three-dimensional hydrodynamic model of tide and wind currents in the Baidaratskaya Bay of the Kara Sea." *Proceedings of the International Offshore and Polar Engineering Conference*, Montreal, Canada.
- Turnipseed, D. P. and J. B. Storm (1995). "Streamflow characteristics of the Lower Pascagoula River, Mississippi." *Proceedings of the Twentieth-fifth Mississippi Water Resources Conference*, Jackson, MS.
- U.S. Army Corps of Engineers (1968). "Pascagoula River comprehensive basin study." Mobile, Alabama.
- Veeramony, J. and C.A. Blain (2001). "Barotropic flow in the vicinity of an idealized inlet – Simulations with the ADCIRC model." Naval Research Laboratory, Washington, D.C..
- Wahr, J. M. (1981). "Body tides on elliptical, rotating, elastic and oceanless earth." *Journal of the Royal Astronomical Society* 64: 644-703.

- Walters, R. A. and R. T. Cheng (1979). "A two-dimensional hydrodynamic model of a tidal estuary." *Advances in Water Resources* 2: 177-184.
- Warner, J. C., W. R. Geyer, et al. (2005). "Numerical modeling of an estuary: A comprehensive skill assessment." *Journal of Geophysical Research-Oceans* 110(C5): 1-13.
- Westerink, J. J., C. A. Blain, et al. (1994). "ADCIRC: An advanced three-dimensional circulation model for shelves, coasts, and estuaries, II: User's manual for ADCIRC-2DDI." Technical Report DRP-92-6 , U.S. Army Corps of Engineers, Waterways Experiment Station, Vicksburg, Mississippi.
- Westerink, J. J., R. A. Jr. Luettich, et al. (1994). "Modeling tides in the western North Atlantic using unstructured graded grids." *Tellus* 46A: 178-199.
- Winant, C. D. and G. Gutierrez de Velasco (2003). "Tidal dynamics and residual circulation in a well-mixed inverse estuary." *Journal of Physical Oceanography* 33: 1365-1379.
- Wright, J. (2000). *Waves, tides and shallow-water processes*. Butterworth-Heinemann/Open University, Oxford, UK.
- Zwillinger, D. (2003). *Standard mathematical tables and formulae*. Chapman & Hall/CRC, Boca Raton, FL.